

**IMMUNOHISTOCHEMICAL, BIOCHEMICAL
AND IMAGING-MASS SPECTROMETRIC
ANALYSIS OF BRAIN TISSUES OF MICE
WITH COMBINED DEFICIENCIES OF
 β -*HEXOSAMINIDASE A*, SIALIDASE
NEU4 AND *GM2-AP***

**A Thesis Submitted to
the Graduate School of Engineering and Sciences of
İzmir Institute of Technology
in Partial Fulfillment of the Requirements for the Degree of**

DOCTOR OF PHILOSOPHY

in Molecular Biology and Genetic

**by
Zehra Kevser TİMUR**

**December 2017
İZMİR**

We approve the thesis of **Zehra Kevser TİMUR**

Examining Committee Members

Prof. Dr. Volkan SEYRENTEPE

Department of Molecular Biology and Genetics, Izmir Institute of Technology

Prof. Dr. Gülperi ÖKTEM

Department of Histology and Embryology, Ege University

Assoc. Prof. Dr. Michelle M. ADAMS

Department of Psychology, Bilkent University

Assist. Prof. Dr. Ayten NALBANT

Department of Molecular Biology and Genetics, Izmir Institute of Technology

Assist. Prof. Dr. Çiğdem TOSUN

Department of Molecular Biology and Genetics, Izmir Institute of Technology

18 December 2017

Prof. Dr. Volkan SEYRANTEPE

Supervisor, Department of Molecular Biology and Genetics
Izmir Institute of Technology

Prof. Dr. Volkan SEYRANTEPE

Head of the Department of Molecular
Biology and Genetics

Prof. Dr. Aysun SOFUOĞLU

Dean of the Graduate School of
Engineering and Sciences

ACKNOWLEDGMENTS

First of all, I would like to express my deepest regards and gratitude to my supervisor Prof. Dr. Volkan SEYRANTEPE for his encouragement, understanding, guidance, and excellent support during my graduate studies for six years.

My special thanks are to the committee members Prof. Dr. Gülperi ÖKTEM and Assist. Prof. Dr. Ayten NALBANT, for their attention, advice and contributions during the monitoring period. I am grateful also to other committee members Assoc. Prof. Dr. Michelle M. ADAMS and Assist. Prof. Dr. Çiğdem TOSUN, for their suggestions during the evaluation of studies.

I would like to thank Prof. Dr. Roger Sandhoff and Katrin Erich for the performance of the Imaging Mass Spectrometry experiment out of our samples at their laboratory in German Cancer Research Center, Heidelberg, Germany.

I would like to thank to The Scientific and Technological Research Council of Turkey (TÜBİTAK) (113T025) for financial support of the project.

I am indebted to my co-workers, Seçil Akyıldız Demir, Edanur Ateş, and Osman Yipkin Çalhan for their support and assistance during the thesis project. I am also thankful to every member of the Seyrantepe Laboratory and Molecular Biology and Genetics Department for their sincere help and kindness.

I am thankful to TÜBİTAK-BİDEB for the scholarship provided for my graduate studies.

I am deeply grateful to my husband Ömer Timur for his infinite love, unfailing understanding, motivation, encouragement and endless support throughout my doctoral years. His support was insuperable.

I thank my sister Dr. Gül Sevin Pekmezci for the English proofreading of my thesis.

At last but not least, I thank my family, my father Ökkaş Pekmezci, my mother Emine Pekmezci, my three sisters and my three brothers for their sincere love, encouragement, and support all my life.

ABSTRACT

IMMUNOHISTOCHEMICAL, BIOCHEMICAL AND IMAGING- MASS SPECTROMETRIC ANALYSIS OF BRAIN TISSUES OF MICE WITH COMBINED DEFICIENCIES OF β -HEXOSAMINIDASE A, SIALIDASE NEU4 AND GM2-AP

Gangliosides are complex glycosphingolipids derived from glucosylceramide or galactosylceramide and contain sialic acid in their carbohydrate chain. Sialidases, known also as neurominidases, are a family of glycohydrolytic enzymes functioning in the catabolism of sialoglycoconjugates by removing α -glycosidically linked sialic acid residues. Sialidase Neu4 is the lysosomal sialidase and GM₂ activator protein is the cofactor of β -Hexosaminidase a enzyme to degrade the GM₂ ganglioside. The activity of sialidase Neu4 activity against G_{D1a} and GM₂ gangliosides were significantly increased by the co-transfection with GM₂ activator protein to the cells transfected with sialidase *Neu4*. This *in vitro* study revealed that lipid-binding proteins can facilitate the glycolipid degradation rendered by sialidase *Neu4* in the lysosomes. In the concept of this study, a systematic comparison of the storage levels of gangliosides, gene expression ratios and behavioral features of new double (*Hexa*^{-/-}*GM2AP*^{-/-} and *GM2AP*^{-/-}*Neu4*^{-/-}) and triple (*Hexa*^{-/-}*GM2AP*^{-/-}*Neu4*^{-/-}) knockout mice models with the existing double (*Neu4*^{-/-}*Hexa*^{-/-}) and single (*Hexa*^{-/-}) knockout models revealed the possible involvement of the GM₂ activator protein as a cofactor of sialidase *Neu4* in the bypass mechanism in the Tay-Sachs mice, *in vivo*. Based on the increased GM₂ ganglioside level in brain and cerebellum detected by the immunohistochemical and imaging mass spectrometric analysis, we speculate that the sialidase *Neu4* functions on the degradation of GM₂ ganglioside with GM₂ activator protein, *in vivo*.

ÖZET

β -HEKZOSAMİNİDAZ A, SİALİDAZ NEU4 VE GM2-AP BİRLEŞİK EKSİKLİĞİ BULUNAN FARE BEYİN DOKULARININ İMMÜNOHİSTOKİMYASAL, BİYOKİMYASAL VE GÖRÜNTÜLÜ-KÜTLE SPEKTROMETRİK ANALİZİ

Gangliositler glukozilseramit veya galactozilseramitten türemiş ve karbonhidrat zincirlerinde sialik asit taşıyan karmaşık glukosfingolipitlerdir. Sialidazlar, nörominidazlar olarak da bilinirler, sialoglukokonjugatlardan α -glukozidik olarak bağlı sialik asit gruplarını ayırarak aktivite gösteren glikohidrolitik enzim ailesindedirler. Sialidaz Neu4 lizozomal sialidazdır ve G_{M2} aktivatör protein ise β -Hekzosaminidaz a enziminin G_{M2} gangliositini yıkmak için olan kofaktörüdür. Sialidaz Neu4'ün G_{D1a} ve G_{M2} gangliositlerine karşı olan aktivitesi sialidaz Neu4 aktarılan hücrelere G_{M2} aktivatör proteinin de birlikte aktarılması ile belirgin bir şekilde artmıştır. Bu *in vitro* çalışma lipid bağlayan proteinlerin lizozomlardan sialidaz Neu4 ile gerçekleştirilen glikolipid yıkımını kolaylaştırdığını ortaya koymuştur. Bu çalışma kapsamında, yeni ikili $Hexa^{-/-} G_{M2}AP^{-/-}$ ve $G_{M2}AP^{-/-} Neu4^{-/-}$ ve üçlü ($Hexa^{-/-} G_{M2}AP^{-/-} Neu4^{-/-}$) enzim eksikliği olan fare modellerinin, hali hazırda bulunan ikili ($Neu4^{-/-} Hexa^{-/-}$) ve tekli ($Hexa^{-/-}$) enzim eksikliği olan fare modelleriyle, gangliositlerin birikim miktarlarının, gen ifadesi oranlarının ve davranışsal özelliklerinin sistematik olarak karşılaştırılması, Tay-Sachs faresinde görülen metabolik baypas mekanizmasında G_{M2} aktivatör proteininin sialidaz Neu4'ün olası kofaktörü olarak katılmasını *in vivo* olarak ortaya çıkarmıştır. İmmunohistokimyasal ve görüntülü kütle spektrometrik analiz ile saptanan beyin ve beyincikte artan G_{M2} gangliosit miktarına bağlı olarak, sialidaz Neu4'ün *in vivo* olarak G_{M2} gangliositinin yıkımında G_{M2} aktivatör protein ile birlikte rol aldığını speküle ediyoruz.

Dedicated to my unique, eternal love Ömer TİMUR...

TABLE OF CONTENTS

LIST OF FIGURES.....	ix
LIST OF TABLES	xiv
CHAPTER 1. INTRODUCTION	1
1.1. Glycosphingolipids.....	1
1.2. Gangliosides	1
1.2.1. Biosynthesis of Gangliosides.....	2
1.2.2. Degradation of Gangliosides	3
1.2.2.1. G _{M2} Activator Protein.....	5
1.2.2.2. Sialidases	6
1.3. Lysosomal Storage Diseases	7
1.3.1. G _{M2} Gangliosidosis.....	9
1.3.2. Mice Models of G _{M2} Gangliosidosis.....	11
1.3.3. The <i>Neu4</i> ^{-/-} and <i>Hexa</i> ^{-/-} <i>Neu4</i> ^{-/-} Mice	11
1.4. The Aim of the Study	13
CHAPTER 2. MATERIALS AND METHODS	14
2.1. Animals.....	14
2.2. DNA Isolation for Genotyping.....	15
2.2.1. Genotyping of Mice for <i>Hexa</i> and <i>Neu4</i> Alleles	15
2.2.2. Genotyping of Mice for the <i>G_{M2}AP</i> Allele	16
2.3. Biochemical Analysis	17
2.3.1. Ganglioside Isolation from the Brain.....	17
2.3.1.1. Neutral and Acidic Ganglioside Isolation.....	18
2.3.1.2. Thin Layer Chromatography	19
2.3.1.3. Orcinol Staining of Plates	20
2.3.2. Analysis of urinary Oligosaccharides by Thin Layer Chromatography	20
2.3.3. Relative Gene Expression Analysis by Real-Time PCR	21
2.3.4. Enzyme Activity Assay	22

2.4. Immunohistochemical Staining for Lamp1 and G _{M2} Ganglioside	23
2.5. Imaging Mass Spectrometric Analysis	25
2.6. Behavioral Tests	26
2.6.1. Rotarod.....	27
2.6.2. Hot Plate	27
2.7. Statistical Analysis	27
 CHAPTER 3. RESULTS	 28
3.1. Genotyping of mice for <i>Hexa</i> , <i>G_{M2}AP</i> and <i>Neu4</i> alleles	28
3.2. Biochemical Analysis Results	28
3.2.1. Thin Layer Chromatography Results of Brain Gangliosides.....	29
3.2.2. Thin Layer Chromatography Results of Urinary Oligosaccharides.....	34
3.2.3. Relative Gene Expression Results	36
3.2.4. Enzyme Activity Results	39
3.3. Immunohistochemical Staining Results	40
3.4. Imaging Mass Spectrometry Results	51
3.5. Behavioral Test Results	55
3.5.1. Rotarod Test Results.....	55
3.5.2. Hot Plate Test Results.....	55
 CHAPTER 4. DISCUSSION.....	 58
 CHAPTER 5. CONCLUSION	 69
5.1. Future Studies	69
 REFERENCES	 71

LIST OF FIGURES

<u>Figure</u>	<u>Page</u>
Figure 1.1. Biosynthetic pathways of gangliosides.....	3
Figure 1.2. Degradation pathway of complex gangliosides.....	4
Figure 1.3. Activity of Neu1, Neu3 and Neu4 sialidases against G _{D1a} and G _{M2} gangliosides in the presence of saposins and GM2-activator protein.....	8
Figure 1.4. Model for the interaction of G _{M2} -activator protein with luminal lysosomal membranes in the degradation of G _{M2} ganglioside.....	10
Figure 1.5. Metabolic by-pass in the ganglioside degradation pathway in the <i>Hexa</i> deficient Tay-Sachs mice model.....	12
Figure 2.1. Illustrations of mice brain different sectioning.....	17
Figure 3.1. Genotyping of <i>Hexa</i> (A) <i>G_{M2}AP</i> (B) and <i>Neu4</i> (C) alleles by PCR analysis of tail genomic DNA.....	28
Figure 3.2. Thin layer chromatography and orcinol staining for neutral gangliosides of 3-month-old <i>WT</i> , <i>Hexa</i> ^{-/-} , <i>Neu4</i> ^{-/-} , <i>G_{M2}AP</i> ^{-/-} , <i>Hexa</i> ^{-/-} <i>Neu4</i> ^{-/-} , <i>Hexa</i> ^{-/-} <i>G_{M2}AP</i> ^{-/-} , <i>G_{M2}AP</i> ^{-/-} <i>Neu4</i> ^{-/-} and <i>Hexa</i> ^{-/-} <i>G_{M2}AP</i> ^{-/-} <i>Neu4</i> ^{-/-} mice brain tissues.....	29
Figure 3.3. Thin layer chromatography and orcinol staining for acidic gangliosides of 3-month-old <i>WT</i> , <i>Hexa</i> ^{-/-} , <i>Neu4</i> ^{-/-} , <i>G_{M2}AP</i> ^{-/-} , <i>Hexa</i> ^{-/-} <i>Neu4</i> ^{-/-} , <i>Hexa</i> ^{-/-} <i>G_{M2}AP</i> ^{-/-} , <i>G_{M2}AP</i> ^{-/-} <i>Neu4</i> ^{-/-} and <i>Hexa</i> ^{-/-} <i>G_{M2}AP</i> ^{-/-} <i>Neu4</i> ^{-/-} mice brain tissues.....	30
Figure 3.4. Thin layer chromatography and orcinol staining for neutral gangliosides of 6-month-old <i>WT</i> , <i>Hexa</i> ^{-/-} , <i>Neu4</i> ^{-/-} , <i>G_{M2}AP</i> ^{-/-} , <i>Hexa</i> ^{-/-} <i>Neu4</i> ^{-/-} , <i>Hexa</i> ^{-/-} <i>G_{M2}AP</i> ^{-/-} , <i>G_{M2}AP</i> ^{-/-} <i>Neu4</i> ^{-/-} and <i>Hexa</i> ^{-/-} <i>G_{M2}AP</i> ^{-/-} <i>Neu4</i> ^{-/-} mice brain tissues.....	30
Figure 3.5. Thin layer chromatography and orcinol staining for acidic gangliosides of 6-month-old <i>WT</i> , <i>Hexa</i> ^{-/-} , <i>Neu4</i> ^{-/-} , <i>G_{M2}AP</i> ^{-/-} , <i>Hexa</i> ^{-/-} <i>Neu4</i> ^{-/-} , <i>Hexa</i> ^{-/-} <i>G_{M2}AP</i> ^{-/-} , <i>G_{M2}AP</i> ^{-/-} <i>Neu4</i> ^{-/-} and <i>Hexa</i> ^{-/-} <i>G_{M2}AP</i> ^{-/-} <i>Neu4</i> ^{-/-} mice brain tissues.....	31
Figure 3.6. Intensity analysis of G _{A2} ganglioside from the 3- and 6-month-old <i>WT</i> , <i>Hexa</i> ^{-/-} , <i>Neu4</i> ^{-/-} , <i>G_{M2}AP</i> ^{-/-} , <i>Hexa</i> ^{-/-} <i>Neu4</i> ^{-/-} , <i>Hexa</i> ^{-/-} <i>G_{M2}AP</i> ^{-/-} , <i>G_{M2}AP</i> ^{-/-} <i>Neu4</i> ^{-/-} and <i>Hexa</i> ^{-/-} <i>G_{M2}AP</i> ^{-/-} <i>Neu4</i> ^{-/-} mice brain tissues.....	32

Figure 3.7. Intensity analysis of G _{M2} ganglioside from the 3- and 6-month-old <i>WT, Hexa^{-/-}, Neu4^{-/-}, G_{M2}AP^{-/-}, Hexa^{-/-}Neu4^{-/-}, Hexa^{-/-}G_{M2}AP^{-/-}, G_{M2}AP^{-/-}Neu4^{-/-} and Hexa^{-/-}G_{M2}AP^{-/-}Neu4^{-/-} mice brain tissues.....</i>	32
Figure 3.8. Intensity analysis of LacCer (A), G _{M1} (B), G _{M2} (C) and G _{D1a} (D) ganglioside from the 3- and 6-month-old <i>WT, Hexa^{-/-}, Neu4^{-/-}, G_{M2}AP^{-/-}, Hexa^{-/-}Neu4^{-/-}, Hexa^{-/-}G_{M2}AP^{-/-}, G_{M2}AP^{-/-}Neu4^{-/-} and Hexa^{-/-}G_{M2}AP^{-/-}Neu4^{-/-} mice brain tissues.....</i>	33
Figure 3.9. Intensity analysis of G _{D1b} (A) and G _{T1b} (B) ganglioside from 3- and 6-month-old <i>WT, Hexa^{-/-}, Neu4^{-/-}, G_{M2}AP^{-/-}, Hexa^{-/-}Neu4^{-/-}, Hexa^{-/-}G_{M2}AP^{-/-}, G_{M2}AP^{-/-}Neu4^{-/-} and Hexa^{-/-}G_{M2}AP^{-/-}Neu4^{-/-} mice brain tissues.....</i>	34
Figure 3.10. Thin layer chromatography and orcinol staining for urinary oligosaccharides of 6-month-old <i>WT, Hexa^{-/-}, Neu4^{-/-}, G_{M2}AP^{-/-}, Hexa^{-/-}Neu4^{-/-}, Hexa^{-/-}G_{M2}AP^{-/-}, G_{M2}AP^{-/-}Neu4^{-/-} and Hexa^{-/-}G_{M2}AP^{-/-}Neu4^{-/-} mice.....</i>	35
Figure 3.11. Intensity analysis of Galactose (A) and Raffinose (B) from the urines of 6-month-old <i>WT, Hexa^{-/-}, Neu4^{-/-}, G_{M2}AP^{-/-}, Hexa^{-/-}Neu4^{-/-}, Hexa^{-/-}G_{M2}AP^{-/-}, G_{M2}AP^{-/-}Neu4^{-/-} and Hexa^{-/-}G_{M2}AP^{-/-}Neu4^{-/-} mice.....</i>	35
Figure 3.12. Expression ratios of sialidase <i>Neu1</i> (A), <i>Neu2</i> (B), <i>Neu3</i> (C) and <i>Neu4</i> (D) enzyme genes in 3- and 6-month-old <i>WT, Hexa^{-/-}, Neu4^{-/-}, G_{M2}AP^{-/-}, Hexa^{-/-}Neu4^{-/-}, Hexa^{-/-}G_{M2}AP^{-/-}, G_{M2}AP^{-/-}Neu4^{-/-} and Hexa^{-/-}G_{M2}AP^{-/-}Neu4^{-/-} mice brain tissues.....</i>	36
Figure 3.13. Expression ratios of <i>β-Hexosaminidase b</i> (A), <i>G_{M2} Activator Protein (G_{M2}AP)</i> (B) and <i>β-Galactosidase</i> (C) in 3- and 6-month-old <i>WT, Hexa^{-/-}, Neu4^{-/-}, G_{M2}AP^{-/-}, Hexa^{-/-}Neu4^{-/-}, Hexa^{-/-}G_{M2}AP^{-/-}, G_{M2}AP^{-/-}Neu4^{-/-} and Hexa^{-/-}G_{M2}AP^{-/-}Neu4^{-/-} mice brain tissues.....</i>	37
Figure 3.14. Expression ratios of LacCer Synthase (B4Galt6) (A) and N-acetyl- Galactosaminyl Transferase 1 (Galgt1) (B) in 3- and 6-month-old <i>WT, Hexa^{-/-}, Neu4^{-/-}, G_{M2}AP^{-/-}, Hexa^{-/-}Neu4^{-/-}, Hexa^{-/-}G_{M2}AP^{-/-}, G_{M2}AP^{-/-}Neu4^{-/-} and Hexa^{-/-}G_{M2}AP^{-/-}Neu4^{-/-} mice brain tissues.....</i>	38

Figure 3.15. Expression ratios of G _{M3} Synthase (G _{M3} S) (A), G _{D3} Synthase (G _{D3} S) (B) and Galactosyl Transferase (B3Galt4) (C) in 3- and 6-month-old <i>WT</i> , <i>Hexa</i> ^{-/-} , <i>Neu4</i> ^{-/-} , <i>G_{M2}AP</i> ^{-/-} , <i>Hexa</i> ^{-/-} <i>Neu4</i> ^{-/-} , <i>Hexa</i> ^{-/-} <i>G_{M2}AP</i> ^{-/-} , <i>G_{M2}AP</i> ^{-/-} <i>Neu4</i> ^{-/-} and <i>Hexa</i> ^{-/-} <i>G_{M2}AP</i> ^{-/-} <i>Neu4</i> ^{-/-} mice brain tissues.....	38
Figure 3.16. Specific enzyme activity of Sialidase (A), β -Hexosaminidase <i>b</i> (B), β -Galactosidase (C) and β -Glucosidase (D) enzymes in 3- and 6-month-old <i>WT</i> , <i>Hexa</i> ^{-/-} , <i>Neu4</i> ^{-/-} , <i>G_{M2}AP</i> ^{-/-} , <i>Hexa</i> ^{-/-} <i>Neu4</i> ^{-/-} , <i>Hexa</i> ^{-/-} <i>G_{M2}AP</i> ^{-/-} , <i>G_{M2}AP</i> ^{-/-} <i>Neu4</i> ^{-/-} and <i>Hexa</i> ^{-/-} <i>G_{M2}AP</i> ^{-/-} <i>Neu4</i> ^{-/-} mice brain tissues.....	40
Figure 3.17. Immunostaining of Lamp1 and G _{M2} ganglioside in 3-month-old <i>WT</i> , <i>Hexa</i> ^{-/-} , <i>Neu4</i> ^{-/-} , <i>G_{M2}AP</i> ^{-/-} , <i>Hexa</i> ^{-/-} <i>Neu4</i> ^{-/-} , <i>Hexa</i> ^{-/-} <i>G_{M2}AP</i> ^{-/-} , <i>G_{M2}AP</i> ^{-/-} <i>Neu4</i> ^{-/-} and <i>Hexa</i> ^{-/-} <i>G_{M2}AP</i> ^{-/-} <i>Neu4</i> ^{-/-} mice brain coronal sections.....	42
Figure 3.18. Immunostaining of Lamp1 and G _{M2} ganglioside in 3-month-old <i>WT</i> , <i>Hexa</i> ^{-/-} , <i>Neu4</i> ^{-/-} , <i>G_{M2}AP</i> ^{-/-} , <i>Hexa</i> ^{-/-} <i>Neu4</i> ^{-/-} , <i>Hexa</i> ^{-/-} <i>G_{M2}AP</i> ^{-/-} , <i>G_{M2}AP</i> ^{-/-} <i>Neu4</i> ^{-/-} and <i>Hexa</i> ^{-/-} <i>G_{M2}AP</i> ^{-/-} <i>Neu4</i> ^{-/-} mice brain coronal sections, cortex region.....	43
Figure 3.19. Immunostaining of Lamp1 and G _{M2} ganglioside in 3-month-old <i>WT</i> , <i>Hexa</i> ^{-/-} , <i>Neu4</i> ^{-/-} , <i>G_{M2}AP</i> ^{-/-} , <i>Hexa</i> ^{-/-} <i>Neu4</i> ^{-/-} , <i>Hexa</i> ^{-/-} <i>G_{M2}AP</i> ^{-/-} , <i>G_{M2}AP</i> ^{-/-} <i>Neu4</i> ^{-/-} and <i>Hexa</i> ^{-/-} <i>G_{M2}AP</i> ^{-/-} <i>Neu4</i> ^{-/-} mice brain coronal sections, hippocampus region.....	44
Figure 3.20. Immunostaining of Lamp1 and G _{M2} ganglioside in 3-month-old <i>WT</i> , <i>Hexa</i> ^{-/-} , <i>Neu4</i> ^{-/-} , <i>G_{M2}AP</i> ^{-/-} , <i>Hexa</i> ^{-/-} <i>Neu4</i> ^{-/-} , <i>Hexa</i> ^{-/-} <i>G_{M2}AP</i> ^{-/-} , <i>G_{M2}AP</i> ^{-/-} <i>Neu4</i> ^{-/-} and <i>Hexa</i> ^{-/-} <i>G_{M2}AP</i> ^{-/-} <i>Neu4</i> ^{-/-} mice brain coronal sections, thalamus region.....	45
Figure 3.21. Immunostaining of Lamp1 and G _{M2} ganglioside in 6-month-old <i>WT</i> , <i>Hexa</i> ^{-/-} , <i>Neu4</i> ^{-/-} , <i>G_{M2}AP</i> ^{-/-} , <i>Hexa</i> ^{-/-} <i>Neu4</i> ^{-/-} , <i>Hexa</i> ^{-/-} <i>G_{M2}AP</i> ^{-/-} , <i>G_{M2}AP</i> ^{-/-} <i>Neu4</i> ^{-/-} and <i>Hexa</i> ^{-/-} <i>G_{M2}AP</i> ^{-/-} <i>Neu4</i> ^{-/-} mice brain coronal sections.....	46
Figure 3.22. Immunostaining of Lamp1 and G _{M2} ganglioside in 6-month-old <i>WT</i> , <i>Hexa</i> ^{-/-} , <i>Neu4</i> ^{-/-} , <i>G_{M2}AP</i> ^{-/-} , <i>Hexa</i> ^{-/-} <i>Neu4</i> ^{-/-} , <i>Hexa</i> ^{-/-} <i>G_{M2}AP</i> ^{-/-} , <i>G_{M2}AP</i> ^{-/-} <i>Neu4</i> ^{-/-} and <i>Hexa</i> ^{-/-} <i>G_{M2}AP</i> ^{-/-} <i>Neu4</i> ^{-/-} mice brain coronal sections, cortex region.....	47

Figure 3.23. Immunostaining of Lamp1 and G _{M2} ganglioside in 6-month-old <i>WT, Hexa^{-/-}, Neu4^{-/-}, G_{M2}AP^{-/-}, Hexa^{-/-}Neu4^{-/-}, Hexa^{-/-} G_{M2}AP^{-/-}, G_{M2}AP^{-/-}Neu4^{-/-} and Hexa^{-/-}G_{M2}AP^{-/-}Neu4^{-/-} mice brain coronal sections, hippocampus region.....</i>	48
Figure 3.24. Immunostaining of Lamp1 and G _{M2} ganglioside in 6-month-old <i>WT, Hexa^{-/-}, Neu4^{-/-}, G_{M2}AP^{-/-}, Hexa^{-/-}Neu4^{-/-}, Hexa^{-/-} G_{M2}AP^{-/-}, G_{M2}AP^{-/-}Neu4^{-/-} and Hexa^{-/-}G_{M2}AP^{-/-}Neu4^{-/-} mice brain coronal sections, thalamus region.....</i>	49
Figure 3.25. Intensity analysis of G _{M2} ganglioside from the 3- and 6-month-old <i>WT, Hexa^{-/-}, Neu4^{-/-}, G_{M2}AP^{-/-}, Hexa^{-/-}Neu4^{-/-}, Hexa^{-/-}G_{M2}AP^{-/-}, G_{M2}AP^{-/-}Neu4^{-/-} and Hexa^{-/-}G_{M2}AP^{-/-}Neu4^{-/-} mice brain coronal sections cortex region.....</i>	50
Figure 3.26. Intensity analysis of G _{M2} ganglioside from the 3- and 6-month-old <i>WT, Hexa^{-/-}, Neu4^{-/-}, G_{M2}AP^{-/-}, Hexa^{-/-}Neu4^{-/-}, Hexa^{-/-}G_{M2}AP^{-/-}, G_{M2}AP^{-/-}Neu4^{-/-} and Hexa^{-/-}G_{M2}AP^{-/-}Neu4^{-/-} mice brain coronal sections hippocampus region.....</i>	51
Figure 3.27. Intensity analysis of G _{M2} ganglioside from the 3- and 6-month-old <i>WT, Hexa^{-/-}, Neu4^{-/-}, G_{M2}AP^{-/-}, Hexa^{-/-}Neu4^{-/-}, Hexa^{-/-}G_{M2}AP^{-/-}, G_{M2}AP^{-/-}Neu4^{-/-} and Hexa^{-/-}G_{M2}AP^{-/-}Neu4^{-/-} mice brain coronal sections thalamus region.....</i>	52
Figure 3.28. Distribution of G _{M2} ganglioside (d36:1 and d38:1) in 3-month-old <i>Hexa^{-/-}, Neu4^{-/-}, G_{M2}AP^{-/-}, Hexa^{-/-}Neu4^{-/-}, Hexa^{-/-}G_{M2}AP^{-/-}, G_{M2}AP^{-/-}Neu4^{-/-} and Hexa^{-/-}G_{M2}AP^{-/-}Neu4^{-/-} mice brain sagittal sections.....</i>	53
Figure 3.29. Distribution of G _{M1} ganglioside (d36:1 and d38:1) in 3-month-old <i>Hexa^{-/-}, Neu4^{-/-}, G_{M2}AP^{-/-}, Hexa^{-/-}Neu4^{-/-}, Hexa^{-/-}G_{M2}AP^{-/-}, G_{M2}AP^{-/-}Neu4^{-/-} and Hexa^{-/-}G_{M2}AP^{-/-}Neu4^{-/-} mice brain sagittal sections.....</i>	53
Figure 3.30. Distribution of G _{D1} ganglioside (d36:1 and d38:1) in 3-month-old <i>Hexa^{-/-}, Neu4^{-/-}, G_{M2}AP^{-/-}, Hexa^{-/-}Neu4^{-/-}, Hexa^{-/-}G_{M2}AP^{-/-}, G_{M2}AP^{-/-}Neu4^{-/-} and Hexa^{-/-}G_{M2}AP^{-/-}Neu4^{-/-} mice brain sagittal sections.....</i>	54
Figure 3.31. Running time on rotarod of 3- and 6-month-old <i>WT, Hexa^{-/-}, Neu4^{-/-}, G_{M2}AP^{-/-}, Hexa^{-/-}Neu4^{-/-}, Hexa^{-/-}G_{M2}AP^{-/-}, G_{M2}AP^{-/-}Neu4^{-/-} and Hexa^{-/-}G_{M2}AP^{-/-}Neu4^{-/-} mice.....</i>	56

Figure 3.32. Paw licking (A), shaking (B), and jumping (C) times of 3- and 6-month-old *WT*, *Hexa*^{-/-}, *Neu4*^{-/-}, *G_{M2}AP*^{-/-}, *Hexa*^{-/-}*Neu4*^{-/-}, *Hexa*^{-/-}*G_{M2}AP*^{-/-}, *G_{M2}AP*^{-/-}*Neu4*^{-/-} and *Hexa*^{-/-}*G_{M2}AP*^{-/-}*Neu4*^{-/-} mice.....57

LIST OF TABLES

<u>Table</u>	<u>Page</u>
Table 2.1. Mice models used as parents to produce F1 and further generations to obtain single, double and triple knock-outs with wild type control.....	15
Table 2.2. Primers used for genotyping of <i>Hexa</i> and <i>Neu4</i> alleles.....	16
Table 2.3. Primers used for genotyping of <i>G_{M2}AP</i> allele.....	16
Table 2.4. Genes analyzed by the Real-Time PCR, their specific primers and the lengths of PCR products.....	22
Table 2.5. Substrates used for the enzyme activity assay.....	23
Table 2.6. Components of the reactions for enzyme activity assays.....	24

CHAPTER 1

INTRODUCTION

Sphingolipids are complex glycolipids having the core structure of sphingosine which is an 18-carbon amino alcohol with an unsaturated hydrocarbon chain¹. Sphingolipids are found in the external layer of the membrane and build cell surface by anchoring carbohydrate groups to plasma membrane².

1.1. Glycosphingolipids

Glycosphingolipids (GSLs) are sphingolipids that have ceramide as the hydrophobic lipid moiety derived from glucosylceramide (GlcCer) or galactosylceramide (GalCer). Among all of the tissues, the highest concentration of GSLs is observed to be in the central nervous system tissues³, which are essential for the development and maintenance of the nervous system⁴. In the cells, GSLs are found at the outer leaflet of plasma membrane as forming lipid raft structures, effective on various cellular processes⁵. GSLs can be neutral or acidic, depending on the absence or presence of sialic acid residue including cerebroside, globoside, and ganglioside⁶.

1.2. Gangliosides

Gangliosides are complex glycosphingolipids which contain sialic acid (SA) - also known as N-acetyl neuraminic acid (NANA), on their carbohydrate chain consisted of glucose, galactose and N-acetylgalactosamine residues. Gangliosides are widely distributed throughout body tissues. Principally, they are enriched in the grey matter and neurons in the brain⁴. They are the major components of plasma membrane, being localized at membrane microdomains, lipid rafts, in association with the other sphingolipids and cholesterol⁷. In eukaryotic cells, gangliosides compose 10-20% of total lipids along with GSLs⁶ and mainly function on signal transduction, cell adhesion, modulating growth factor/hormone receptor, antigen recognition, and protein trafficking⁶.

1.2.1. Biosynthesis of Gangliosides

The ganglioside synthesis begins in the endoplasmic reticulum, continues and completes in the Golgi apparatus. In endoplasmic reticulum, ceramide is formed by *de novo* synthesis, and the ones forming the ceramide can be used for the synthesis of many different macromolecules through various pathways⁴. For the ganglioside synthesis (Figure 1.1), the ceramide is transferred into the Golgi apparatus where each ganglioside is generated by the addition of various glucose, galactose, N-acetylgalactosamine and sialic acid residues⁵.

The synthesis of gangliosides is catalyzed by numerous glycosyltransferases and galactosyltransferases which are exclusive to each substrate. Almost all of the gangliosides are derived from lactosylceramide (except G_{M4} which is derived from galactosylceramide) in a sequential synthesis pathway. The addition of galactose into the glucosylceramide is catalyzed by Lactosylceramide synthase (B4Galt6) (Figure 1.1) forming the lactosylceramide which is the precursor of 0-series gangliosides (G_{A2}, G_{A1}, G_{M1b} and G_{D1c}). G_{M3} ganglioside is synthesized by the addition of one sialic acid residue into the lactosylceramide via the activity of G_{M3} synthase enzymes. G_{D3} and G_{T3} gangliosides are derived from the G_{M3} and G_{D3} ganglioside by the addition of one each sialic acid via the activity of G_{D3} synthase (G_{D3}S) and Sialyltransferase III (STIII) enzymes, respectively. These G_{M3}, G_{D3} and G_{T3} gangliosides are the precursors of a more complex belonging to the a-, b- and c- series, respectively. The addition of N-acetylgalactosamine residues into each precursor is catalyzed by β 1-4N-acetylgalactosaminyltransferase enzyme (Galgt1 or also known as G_{A2}/G_{M2}/G_{D2}/G_{T2} synthase) constitutes G_{A2}, G_{M2}, G_{D2}, G_{T2} gangliosides. These newly formed gangliosides are utilized for the synthesis of G_{A1}, G_{M1}, G_{D1b}, and G_{T1c} by the addition of galactose moiety via the activity of Galactosyltransferase (B3Galgt4 or G_{A1}/G_{M1}/G_{D1b}/G_{T1c} synthase). The addition of one sialic acid residue into each ganglioside is catalyzed by Sialyltransferase IV (STIV) leading to the formation of G_{M1b}, G_{D1a}, G_{T1b}, and G_{Q1c} gangliosides. Sialyltransferase V (STV) also adds one sialic acid residue into the G_{M1b}, G_{D1a}, G_{T1b}, and G_{Q1c} gangliosides; thereby synthesizes the G_{D1c}, G_{T1a}, G_{Q1b}, and G_{P1c} gangliosides which have two, three, four and five sialic acid groups, respectively, attached to their galactose subunits^{5,8}.

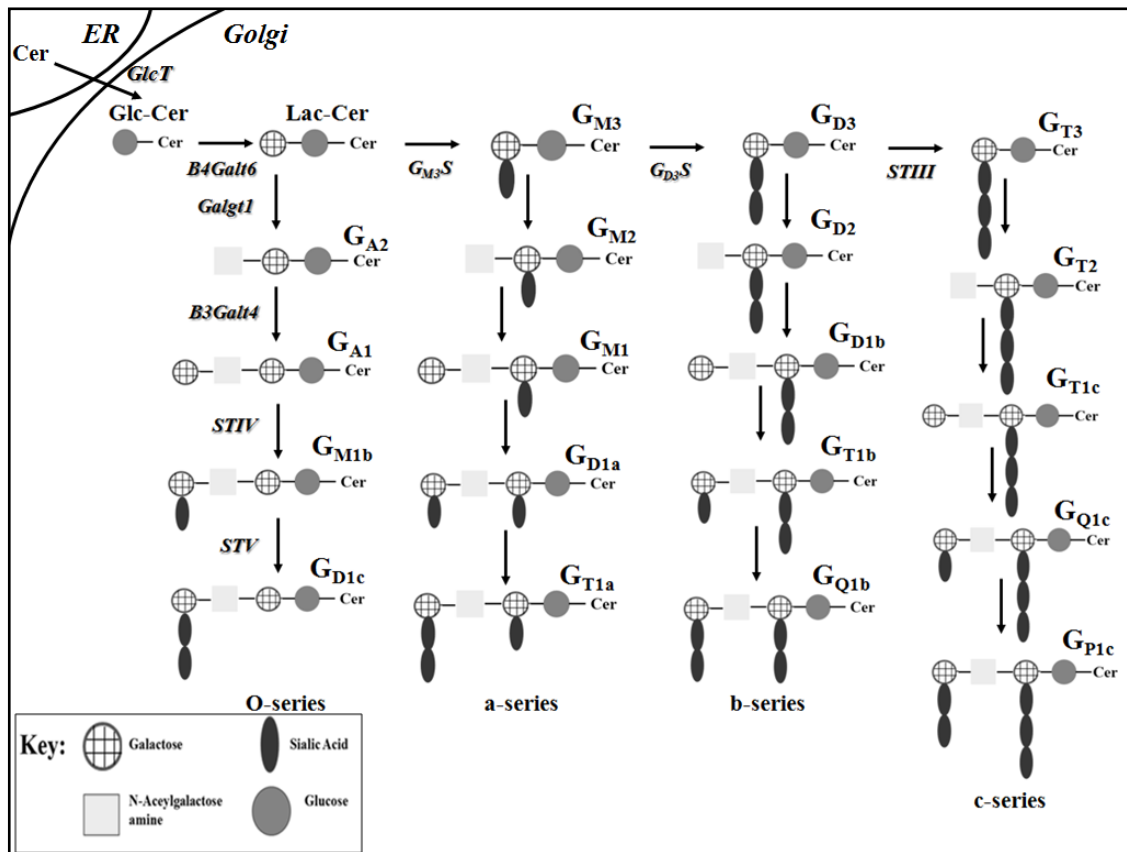


Figure 1.1. Biosynthetic pathways of gangliosides. The synthesis of gangliosides progress stepwise and are catalyzed by membranous glycosyltransferases in the ER and Golgi apparatus. The first step is the transfer of a glucose residue onto ceramide by β -glucosyltransferase (GlcCer synthase). The next step is the conversion of the glucosylceramide into lactosylceramide by the β 1,4-galactosyltransferase (LacCer synthase, B4Galt6). The transfer of sialic acid residue to LacCer is then catalyzed by the specific sialyltransferases ($G_{M3}S$, $G_{D3}S$ and STIII), all being highly specific for glycolipid substrates. LacCer, G_{M3} , G_{D3} , and G_{T3} are the precursors for O-, a-, b-, and c-series gangliosides, respectively. Further, monosaccharides can be transferred in a stepwise manner by the β 1,4-N-acetylgalactosaminyltransferase I (Galgt1) and the β 1,3-galactosyltransferase IV (B3Galt4), both acting on the four series of gangliosides. The terminal Gal residue can be further sialylated by the activity of STIV and STV enzymes.^{5,8,9}

1.2.2. Degradation of Gangliosides

A balance is found between the anabolism and catabolism of gangliosides, as can be observed in all of the biomolecular metabolisms throughout the cell. Gangliosides are transported to the acidic compartments and lysosomes of the cells by the endocytosis, being degraded via a complex mechanism involving enzymes, activator

proteins (sphingolipids activator proteins –SAPs) and negatively charged lipids². This degradation occurs by the sequential release of carbohydrate and sialic acid residues (Figure 1.2), with the stepwise activity of specific lysosomal exohydrolases and protein cofactors: β -Galactosidase (β -Gal) for the removal of galactose residues, β -Hexosaminidase a and b (*Hexa* and *Hexb*) for the removal of N-acetylgalactosamine residues and β -Glucosidase (GCase) for the removal of glucose residues functioning on different gangliosides during degradation in lysosome⁶.

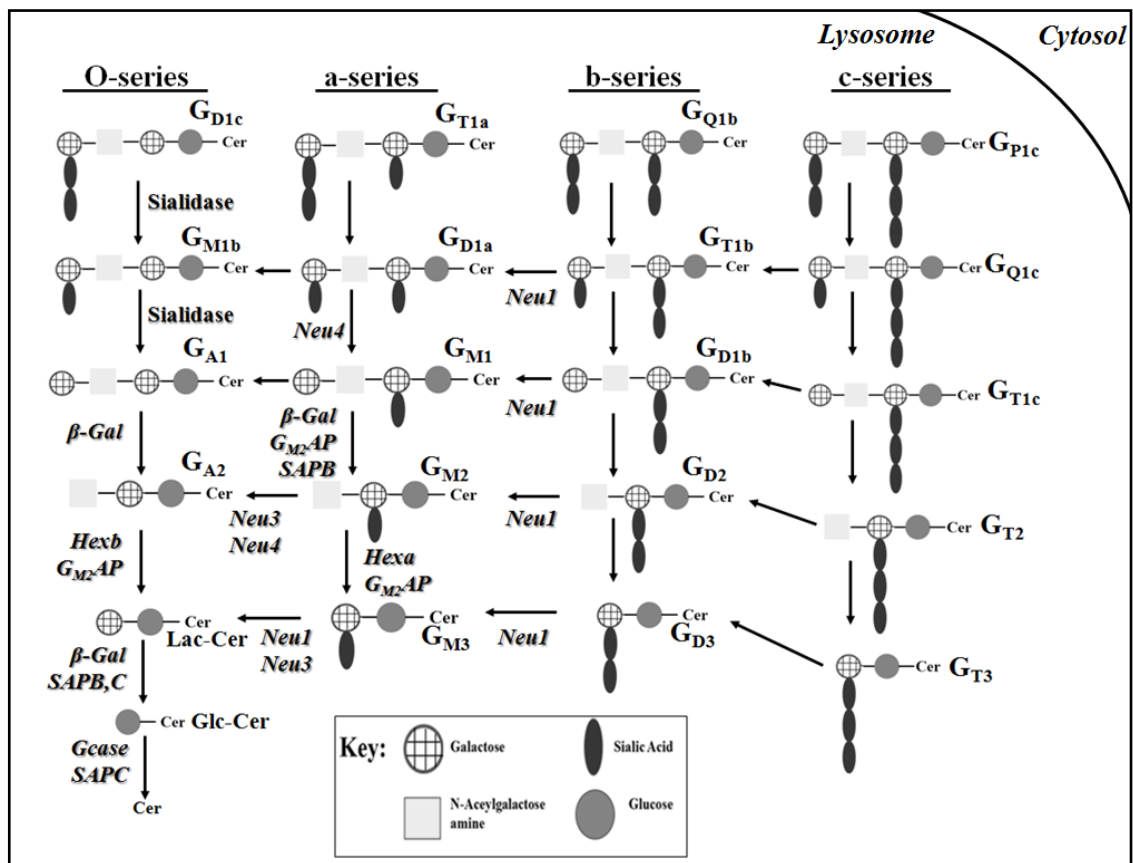


Figure 1.2. Degradation pathway of complex gangliosides. The degradation reactions are sequential and occur within the lysosomes by various hydrolases. Sialidases are responsible for the removal of sialic acid residue from different gangliosides. β -Galactosidase (β -Gal) is responsible for the degradation of galactose residues, β -Hexosaminidases are responsible for the removal of N-acetylgalactosamine residues with the help of activator proteins whereas β -Glucosidase (GCase) removes glucose residues from glucosylceramide^{6,10,11,12,13}.

The removal of sialic acid residues from different gangliosides are carried out by sialidase enzymes (features of these enzymes explained further in subtitle 1.2.3.2), since each of them has a substrate specificity¹⁴. *In vivo* studies with deficient mice models, it

is revealed that the sialidase *Neu4* has an activity against the G_{D1a} ¹⁰ and G_{M2} ¹¹ gangliosides, where the sialidase *Neu1* has an activity against all of the G_{T1b} , G_{D1b} , G_{D2} , G_{D3} and G_{M3} gangliosides¹². As indicated in a recently published study, the sialidase *Neu3* has an activity against the G_{M2} and G_{M3} gangliosides¹³ as depicted in Figure 1.2.

The anabolism and catabolism reactions of the gangliosides differ from each other in one aspect: At the anabolism of gangliosides, both substrates of glycosphingolipids and enzymes are membrane-bound; whereas at the catabolism of gangliosides, the enzymes are soluble in the lysosome. This points out to the requirement of activator proteins which have an important role in catabolism reactions, however, not in anabolism reactions². Until now, five SAPs have been determined to be encoded from two different genes: While one gene produces the G_{M2} activator protein ($G_{M2}AP$)¹⁵, the other gene produces the prosaposin protein which is further processed into four homologous proteins (SAP-A, -B, -C, -D) via the proteolytic cleavage functioning with different enzymes to degrade different molecules⁶.

1.2.2.1. G_{M2} Activator Protein

The G_{M2} activator protein is a lysosomal glycoprotein with a molecular weight of 17.6 kDa in its deglycosylated form, and it is required for the *in vivo* degradation of ganglioside G_{M2} by β -Hexosaminidase *a*¹⁶. $G_{M2}AP$ had a hydrophobic pocket which is a specific feature for the lipid carrier proteins helping them interact with lipid moieties¹⁷. Carrying negatively-charged amino acids in its structure may provide specificity to different substrates thorough the ionic binding¹⁷. *In vitro* studies, it is demonstrated that $G_{M2}AP$ can stimulate the removal of sialic acid residue from G_{M1} and G_{M2} , by not only the microbial sialidase¹⁸, but also the mammalian membrane bound sialidase (*Neu3*)¹⁹.

The G_{M2} activator protein also seems to be functioning as a cofactor of β -galactosidase enzyme in order to degrade the G_{M1} ganglioside²⁰, besides being a cofactor of β -Hexosaminidase *a* to degrade the G_{M2} ganglioside²¹. Some studies have revealed that there is a difference between the G_{M2} activator proteins of the human and of the mouse. While the human $G_{M2}AP$ has an effective role only in the degradation of G_{M2} with β -Hexosaminidase *a* enzyme, the mouse $G_{M2}AP$ has a function on the degradation of both G_{M2} and asialo- G_{M2} (G_{A2}) with the same enzyme¹⁷. Beside all of these decomposer roles occurring in lysosome, $G_{M2}AP$ has also an inhibitory effect on

phosphatidylcholine and platelet activating factor (PAF)¹⁶. *G_{M2}AP* can function as a shuffling protein for the proton pumps in the kidney IC cell cytosol at a high pH value like 7²².

1.2.2.2. Sialidases

Sialidases, known also as neurominidases, are a family of glycohydrolytic enzymes functioning in the catabolism of sialoglycoconjugates, glycoproteins, glycolipids and gangliosides by removing α -glycosidically linked sialic acid residues²³. By their activity against the sialylated biomolecules lysosomes, the sialidases are of importance for many biological processes such as the cell proliferation/differentiation, cell adhesion, clearance of plasma proteins and the modification of receptors, as well as the catabolism of gangliosides and glycoproteins¹⁴.

Mammalian sialidases are categorized differently according to their subcellular localization; cytosolic²⁴, lysosomal²⁵, plasma-membrane associated²⁶ and mitochondrial²⁷. The sialidases differ also in the substrate specificity and immunological properties^{24,26}. Mammalian sialidases are encoded by four different genes named *Neu1*, *Neu2*, *Neu3* and *Neu4*¹⁴.

Sialidase *Neu1* is the lysosomal sialidase bringing out a complex with β -galactosidase (β -Gal) and lysosomal carboxypeptidase *Cathepsin A* (*CathA*). Deficiency of the sialidase *Neu1* results in sialidosis (mucopolipidosis I) which is an autosomal recessive lysosomal storage disorder. A clinically similar disease called galactosialidosis resulting from the secondary deficiency of *Neu1* is caused by the genetic defects in *CathA* gene¹⁴.

Sialidase *Neu2* is a cytosolic protein that demonstrates activity against the glycopeptides and gangliosides, mostly found in skeletal muscles. Although its exact function is not yet to be known, it is reported in several studies that *Neu2* has a selective activity against the *G_{M3}* ganglioside¹⁴.

Sialidase *Neu3* is an integral membrane protein found in caveolae microdomains, which are a special type of lipid raft, of the plasma membrane. *Neu3* is mostly active against the *G_{M1}* and *G_{D1a}* gangliosides, de-sialylates, *G_{M2}* and *G_{M3}* gangliosides to asilo derivatives *in vitro*¹⁴ and *in vivo*¹³. *Neu3* is thought also to be involved in the modulation of ganglioside oligosaccharide chains on cell surface. These modulations of

gangliosides are important for the transformation, cell contact formation, differentiation, insulin signaling, carcinogenesis and apoptosis¹⁴.

Sialidase *Neu4* is recently identified sialidase located in the 2nd chromosome, having broad substrate specificity against the glycoproteins, oligosaccharides and sialylated glycolipids. Elimination of undigested substrates of *Neu1* and restoration of normal morphological phenotype in *Neu1* deficient sialidosis fibroblasts after the over-expression of *Neu4* also reveal that *Neu4* is active against a majority of endogenous substrates of sialidase *Neu1*²⁵. This enzyme is observed to be located both in the lysosomal lumen by the mannose 6-phosphate receptor²⁵, and the inner and outer membranes of mitochondria²⁷.

Neu4 holds two isoforms which differ from each other by the terminal amino acid residues targeting the enzyme to mitochondria. The isoforms are expressed also in a tissue-specific manner: The brain, muscle and kidney contain both of the isoforms, whereas the liver and colon contain dominantly the short form of the sialidase *Neu4*. The mitochondrial targeted long form of *Neu4* may be involved in cell apoptosis, or neural differentiation by the regulation of the apoptosis-related ganglioside, G_{D3} level¹⁴.

Sialidase *Neu4* is also known to have an activity against the gangliosides like G_{M2} *in vitro*¹⁰ and *in vivo*¹¹, G_{D1a} *in vivo*¹⁰. Beside the activity against G_{M2} ganglioside, *Neu4*-transfected cells have a tendency for the sialidase activity against G_{D1a}, G_{M3} and G_{M2} gangliosides, similar to that of the cells transfected with *Neu3* sialidase and much higher than that of the cells transfected with *Neu1* sialidase (Figure 1.3). However, this activity of sialidase *Neu4* but not *Neu3* against G_{D1a} and G_{M2} gangliosides were significantly increased by the co-transfection with sphingolipid activator proteins, saposins or G_{M2} activator protein to the cells transfected with sialidase *Neu4*. These *in vitro* studies revealed that lipid-binding proteins can facilitate the glycolipid degradation rendered by sialidase *Neu4* in the lysosomes¹⁰.

1.3. Lysosomal Storage Diseases

Gangliosides are involved in the pathology of numerous disorders such as lysosomal storage diseases. These disorders occur via the disrupted gangliosides synthesis or the break-down and also through autoimmunity against the gangliosides²⁸. Lysosomal storage diseases (LSDs) form a group of rare-inherited metabolic disorders

which result from a disruption in the lysosomal degradation pathway of biomolecules. The disruption in the lysosomal degradation may occur due to the deficiency of a specific lysosomal enzyme which has an acid hydrolysis function²⁹, a cofactor protein, a protein involved in the post-translational modification, or a protein involved in the transport of the lysosomal protein³⁰. As a consequence of the dysfunction, non-catabolized substrate of the associated enzyme/protein accumulates in lysosomes. The accumulation (or namely storage) of the substrate may cause a cellular toxicity²⁹.

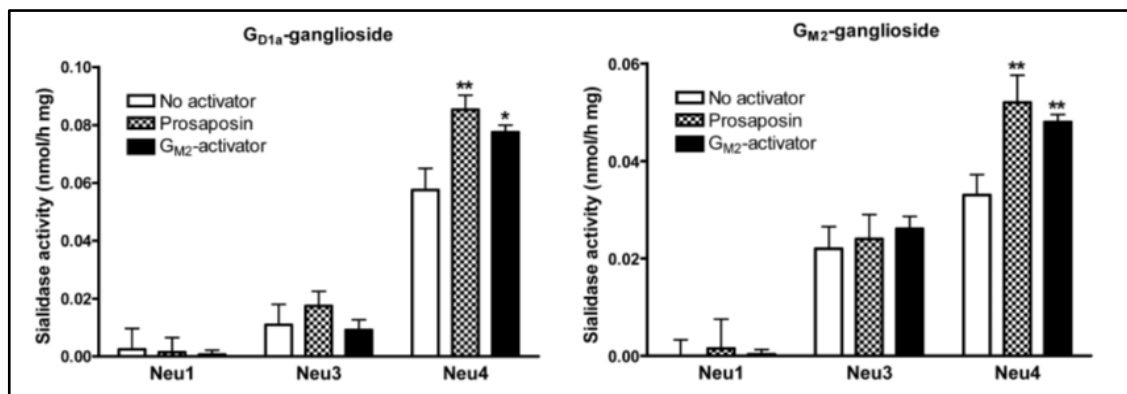


Figure 1.3. Activity of Neu1, Neu3 and Neu4 sialidases against G_{D1a} and G_{M2} gangliosides in the presence of saposins and GM2-activator protein. COS-7 cells were co-transfected as indicated with plasmids expressing a human sialidase, Neu1, Neu3 or Neu4, and a plasmid expressing G_{M2} activator protein or prosaposin, the latter being further processed in the lysosome into individual saposins A, B, C and D. The sialidase activity (nmol/h/mg protein) was measured in the cell lysates against the G_{D1a} and G_{M2} gangliosides. All transfected cells showed similar increase of sialidase activity measured with the artificial sialidase substrate, 4MU-NeuAc. Values represent means \pm S.D. of triplicate experiments. * $p < 0.05$ and ** $p < 0.01$ as compared with the cells transfected only with the Neu4 plasmid.¹⁰

In most of the cases, the storage is progressive, therefore, the disease symptoms worsen in time³¹. The storage can occur in various cell types, and affected individuals may exhibit mild or severe abnormalities, even die at early ages. The severity of the phenotype is also related to the residual activity of the responsible enzyme. A “critical threshold” of the enzyme activity which determines the storage of the substrate in lysosomes has been proposed. When the activity of the enzyme decreases below the threshold level, it cannot degrade the entire substrates, thereby the storage takes place³². In general, a lower residual activity causes an earlier age of the onset, or a more severe phenotype of the disease. The accumulated substrates make typical histochemical and ultra structural changes in the cell. These structures are characterized as vacuoles (i.e.

lysosomes) which contain non-degraded substrates (biomolecules), being the hallmarks of the storage in related disorders. The first storage bodies have been defined in Tay-Sachs disease³³.

Deficiencies of lysosomal hydrolases seen in the lysosomal storage diseases can cause secondary alterations in different degradation pathways in lysosomes. This leads to the accumulation of intermediate metabolites from glycoprotein or glycolipid degradation pathways, including free oligosaccharides (FOS) and glycoaminoacids, which may accumulate in urine.³⁴ Increases in specific urinary FOS or glycoaminoacids are often indicative of specific lysosomal disorders and can be used for diagnosis in many different diseases^{35,36}. In this manner, analysis of this possible secondary metabolite accumulation becomes important to understand disease prognosis.

1.3.1. G_{M2} Gangliosidosis

G_{M2} gangliosidosis are a group of inherited lysosomal storage disorders caused by the accumulation of ganglioside G_{M2} in the neurons of patients. The lysosomal degradation of ganglioside G_{M2} requires a catalytically active β -Hexosaminidase *a*, which consists of two subunits of α and β , along with the *Hexosaminidase a* specific glycolipid binding protein, and the *G_{M2} activator protein (G_{M2}AP)*. Inherited defects in any of the three protein components (α or β subunit, or activator protein) lead to the G_{M2} gangliosidosis³⁷.

The Tay-Sachs disease is one of the G_{M2} gangliosidosis caused by some mutations in the *HEXA* gene³⁸, encoding the α -subunit of lysosomal β -Hexosaminidase *a* (*Hexa*) enzyme. This enzyme removes the N-acetyl-galactosamine residues from the G_{M2} gangliosides converting them into G_{M3} ganglioside for a further degradation (Figure 1.2). Patients suffering from the Tay-Sachs disease are observed to have a progressive neuronal degeneration, muscle weakness, blindness and epilepsy, where the patients are to die in the second to fourth year of their life³⁹.

The Sandhoff disease is the second G_{M2} gangliosidosis disease caused by some mutations in the *HEXB* gene encoding the β subunit, having a severe phenotype due to the deficiencies of both *Hexa* (composed of both α and β subunits-heterodimer) and *Hexb* (composed of two β subunits-homodimer) enzyme activities⁴⁰.

The third type of the G_{M2} gangliosidosis is the variant AB, caused by the defects in the G_{M2} activator protein ($G_{M2}AP$), a non-enzyme protein function as a substrate specific cofactor for β -Hexosaminidase *a* enzyme to interact with the G_{M2} ganglioside. Although $G_{M2}AP$ is widely expressed in all tissues, the G_{M2} ganglioside is predominantly found in the central nervous system¹⁷, being the probable reason for why the brain is the most affected tissue among all.

The $G_{M2}AP$ functions on the G_{M2} ganglioside degradation via 3 steps: The first $G_{M2}AP$ interact with the ceramide moiety of the G_{M2} ganglioside by a non-specific hydrophobic interaction in order to produce a water-soluble complex⁴¹. It then functions on a more specific hydrophilic binding towards the oligosaccharide, with the sites interacting with both the non-reducing terminal N-acetyl-galactosamine and the sialic acid residues of the G_{M2} ganglioside⁴¹. It finally forms a strong specific interaction with the *Hexa* enzyme to let the degradation of G_{M2} ganglioside by the *Hexa* enzyme⁴¹ (Figure 1.4). The AB variant of the G_{M2} gangliosidosis has an infantile onset, and it is almost indistinguishable from the classical Tay-Sachs phenotype, clinically⁴².

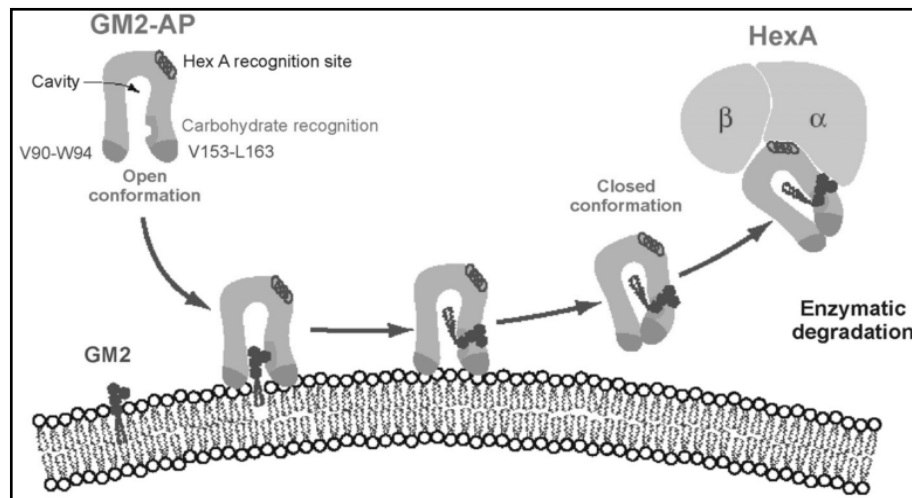


Figure 1.4. Model for the interaction of G_{M2} -activator protein with luminal lysosomal membranes in the degradation of G_{M2} ganglioside. $G_{M2}AP$ interacts with the membrane by hydrophobic loops, V90-W94 and V153-L163, into the apolar part of the membrane. G_{M2} is recognized by specific sites at the cavity. After the ceramide tail has arrived inside the activator's cavity the conformation changes to the closed form. The activator is then anchored only by the loop V90-W94. It rotates slightly, leaving the membrane and interacting with the degrading enzyme, Hexa.⁷

1.3.2. Mice Models of G_{M2} Gangliosidosis

Through the targeted disruption of the *Hexa*, *Hexb*, and *G_{M2}AP* genes, some mice models of Tay-Sachs, Sandhoff, and the AB-variant form of G_{M2} gangliosidosis have been carried out. Unlike the Tay-Sachs and Sandhoff diseases in human where the clinical phenotypes are nearly identical; they were seen to be very different in the mice. Where the Sandhoff mice (*Hexb*^{-/-}) exhibited extensive ganglioside accumulations and a severe neurological disease, the Tay-Sachs mice (*Hexa*^{-/-}) were asymptomatic. Behavioral and motor coordination of the Tay-Sachs mice (*Hexa*^{-/-}) were exact with the wild type mice (*Hexa*^{+/+}), at least during one year of life span. Only a limited accumulation of G_{M2} ganglioside and the membranous cytoplasmic bodies have been reported to be observed in the brain of the *Hexa* mice^{40,43,44}.

The AB-variant mice (*G_{M2}AP*^{-/-}) exhibited a clinical phenotype intermediate to that of the other two. The *G_{M2}AP*^{-/-} mice showed a neuronal storage, however, only in some restricted regions of the brain, similar to the asymptomatic Tay-Sachs mice (*Hexa*^{-/-}). Unlike the Tay-Sachs mice, the *G_{M2}AP*^{-/-} mice displayed a significant storage in the cerebellum, some defects in balance and coordination. There was an abnormal ganglioside storage consisted of not only G_{M2} ganglioside, but also a low amount of G_{A2} ganglioside. These results indicate a possible role of *G_{M2}AP* in the G_{A2} ganglioside degradation⁴⁵. The inequality between the mice and the human indicate that there may be some differences in the metabolic pathway of the G_{M2} ganglioside catabolizing G_{M2} ganglioside via the glycolipid G_{A2} (asialyted form of G_{M2} ganglioside), bypassing the G_{M3} routed degradation in mice⁴³. It has been proposed that activities of the sialidase(s) have a role in the bypass mechanism by removal of the sialic acid residue of G_{M2} converting them into G_{A2}, which is then further degraded by the *β-Hexosaminidase b* enzyme to lactosylceramide^{40,46} (Figure 1.5).

1.3.3. The *Neu4*^{-/-} and *Hexa*^{-/-}*Neu4*^{-/-} Mice

In the mice model with *Neu4* deficiency, the lysosomal storage was traced in lung and spleen with a microscopic investigation. In addition, an abnormal ganglioside pattern (increased G_{D1a} and decreased G_{M1} levels) in brain was demonstrated by the thin layer chromatography analysis¹⁰. To elucidate whether sialidase *Neu4* is involved in the

G_{M2} ganglioside degradation *in vivo*, a mice model has been generated previously with a combined deficiency of sialidase *Neu4* and β -Hexosaminidase *a*¹¹.

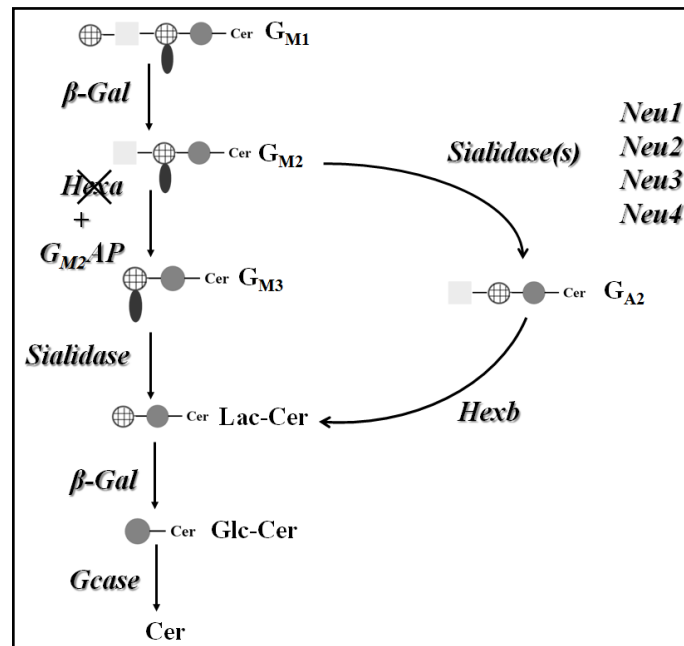


Figure 1.5. Metabolic by-pass in the ganglioside degradation pathway in the *Hexa* deficient Tay-Sachs mice model. In the deficiency of Hexa enzyme in mice, sialidase or sialidas(es) act on G_{M2} to convert it to G_{A2} , which is further degraded by Hexb to Lac-Cer. In conclusion, excessive accumulation of G_{M2} ganglioside and disease phenotype were not seen in mice.^{40,47}

The mentioned model with a targeted disruption of both *Neu4* and *Hexa* genes (*Hexa*^{-/-}*Neu4*^{-/-}) had multiple degenerating neurons in the cortex, hippocampus, and multiple layers of the cortical neurons accumulating the G_{M2} ganglioside. A significantly higher level of the G_{M2} ganglioside in lysosomes of neurons was discovered in the double knockout type of mice. Most importantly, the mice with *Hexa* and *Neu4* enzyme deficiencies had some epileptic seizures (hallmark of Tay-Sachs patients) which were not observed in the mice with a single *Hexa* enzyme deficiency. Since only 40 % of the mice with double enzyme deficiency have experienced seizures, it is postulated *Neu4* to be a modulator gene, and the sialidase *Neu4* may not be the only sialidase contributing in the metabolic bypass observed in the *Hexa*-deficient mice¹¹. Recently it was reported that sialidase *Neu2* and *Neu4* showed no differences in their relative expression levels between *WT* and *Hexa*^{-/-} mice, while the expression levels of sialidase *Neu1* and *Neu3* were increased significantly in the cerebellum, cortex, hippocampus, and thalamus of *Hexa*^{-/-} mice compared to *WT* mice¹³. In the same study

it was also demonstrated that sialidase *Neu3* is the responsible enzyme for the bypass mechanism in the Tay-Sachs mice model. *Hexa*^{-/-}*Neu3*^{-/-} mice had abnormal accumulation of G_{M2} ganglioside, exhibited progressive neurodegeneration, had ataxia, and tremors similar to Tay-Sachs patients.¹³

1.4. The Aim of the Study

Sialidase *Neu4* is recently found as being a lysosomal sialidase²⁵. Its biological involvement and function on degradation of different gangliosides were shown in different studies *in vivo*^{11,48}. Although it was previously proven that the sialidase *Neu4* had an increased degradation activity against gangliosides (G_{M2} and G_{D1a}) in the presence of *G_{M2}AP* *in vitro*¹⁰ (Figure 1.3), sialidase *Neu4*'s need to a cofactor for its degradative function *in vivo*, was unknown. Regarding the possible involvement of the G_{M2} activator protein as a cofactor of sialidase *Neu4* in the bypass mechanism in the Tay-Sachs mice (Figure 1.5), we aimed to compare the storage level of G_{M2} ganglioside between different deficient mice. By the comparison of newly created *Hexa*^{-/-}*G_{M2}AP*^{-/-}, *G_{M2}AP*^{-/-}*Neu4*^{-/-} and *Hexa*^{-/-}*G_{M2}AP*^{-/-}*Neu4*^{-/-} mice models with existing *Hexa*^{-/-}*Neu4*^{-/-} and single deficient counterparts, it was aimed to understand the biological role of the lysosomal sialidase *Neu4* in the ganglioside metabolism further. Analysis of mice might also allow us answer the involvement of *G_{M2}AP* in the degradation of other gangliosides along with *Neu4* or with the other sialidases, besides the involvement in the bypass reaction.

CHAPTER 2

MATERIALS AND METHODS

2.1. Animals

The *Hexa*^{-/-}*Neu4*^{-/-} double knock-out mouse strain was generated by Prof. Dr. Volkan Seyrantepe during his post-doctoral study, as kindly donated by Prof. Alexey V. Pshezhetsky (Centre Hospitaliere Universitaire Sainte-Justine, University of Montreal, Montreal, Quebec, Canada). The *G_{M2}AP*^{-/-} mouse strain was available at the laboratory of Prof. Dr. Roger Sandhoff (Lipid Pathobiochemistry Group, German Cancer Research Center, Heidelberg, Germany). The *G_{M2}AP*^{-/-} mice (Table 2.1) were brought from Germany to Turkey, and placed in accredited animal facility of Izmir Institute of Technology Animal Research Center. The mice were bred and housed in groups of five per cage and maintained at a constant temperature with an alternating 12-h light:dark cycle. Food and water were available ad libitum. All animal experiments were performed in accordance with the Turkish Institute of Animal Health guide for the care and use of laboratory animals. The animal studies were approved by the Institutional Animal Care and Use Committee of the Izmir Institute of Technology. Firstly, the breeding procedure was realized between the *Hexa*^{-/-}*Neu4*^{-/-} and *G_{M2}AP*^{-/-} mice in order to obtain some triple heterozygote mice. F2 generation and their offspring were inbred depending on their genotypes to produce single knock-outs (*Hexa*^{-/-}, *Neu4*^{-/-} and *G_{M2}AP*^{-/-}), double knock-outs (*Hexa*^{-/-}*G_{M2}AP*^{-/-}, *G_{M2}AP*^{-/-}*Neu4*^{-/-}) and a triple knock-out (*Hexa*^{-/-}*G_{M2}AP*^{-/-}*Neu4*^{-/-}) with the wild type group (*Hexa*^{+/+}*G_{M2}AP*^{+/+}*Neu4*^{+/+}) with the exact genetic background. All deficient mice were healthy and lived longer than 12 months. There were no significant differences in weight gain between mutant and littermate control mice. Both males and female double and triple deficient mice were fertile.

In the concept of this study, three- and six-month-old mice were analyzed in order to reveal if the accumulation of gangliosides was age-dependent. Two age groups were also used compare the features of different age groups of mice in the aspects of phenotypic, biologic and biochemical manners. For the biochemical and imaging mass

spectrometric analysis, single, double and triple knock-out mice were sacrificed with CO₂ when they reached to their targeted ages (3 or 6 months old). Their brains were removed, right and left hemispheres were separated, and they were immediately treated with liquid nitrogen, and kept frozen under -80°C.

Table 2.1. Mice models used as parents to produce F1 and further generations to obtain single, double and triple knock-outs with wild type control.

Colony	ID	Sex	Birthday	Genotype
<i>G_{M2}AP</i>	459	Female	13.05.13	<i>Neu4^{+/+} Hexa^{+/+} G_{M2}AP^{-/-}</i>
	460	Female	13.05.13	<i>Neu4^{+/+} Hexa^{+/+} G_{M2}AP^{-/-}</i>
	450	Male	26.04.13	<i>Neu4^{+/+} Hexa^{+/+} G_{M2}AP^{-/-}</i>
	451	Male	26.04.13	<i>Neu4^{+/+} Hexa^{+/+} G_{M2}AP^{-/-}</i>
<i>HexaNeu4</i>		Female & Male	Different aged	<i>Neu4^{-/-} Hexa^{-/-} G_{M2}AP^{+/+}</i>

2.2. DNA Isolation for Genotyping

The genotypes of mice were determined from the genomic DNA extracted from mice's tails when weaned from their parents at the age of 1 month. Isolation of the genomic DNA was carried out by the following steps⁴⁹. The tails taken from mice were put in Eppendorf tubes in which 500µl of lysis buffer (consist of 10% 1M Tris pH 7.6, 2.5% 0.2M EDTA, 20% SDS, 4% 5M NaCl) and 12µl of Proteinase K (from 25µg/µl solution) were added. Samples were incubated overnight in the incubator shaker at 55°C at 70 rpm. On the following day, the samples were centrifuged at 14.000rpm for 10 minutes. The supernatant was transferred into a new Eppendorf tube, and an equal volume of 100% isopropanol was added into each sample. DNAs were collected by a tip, and transferred into a new Eppendorf containing 500µl of 70% ethanol. After 1 minute of a centrifugation at 14.000rpm, the supernatant was removed, and the remaining ethanol was completely air-dried for 10 minutes. DNAs were dissolved in 200µl of distilled water, and incubated at 55°C for 1 hour.

2.2.1. Genotyping of Mice for *Hexa* and *Neu4* Alleles

Isolated genomic DNAs were used in PCR for the detection of wild type and mutant allele of *Hexa* and *Neu4* separately, using the genotyping primers designed previously¹¹. The PCR performed with ~100ng of genomic DNA in the 25µl of a

reaction mix containing 0.4 μ M of each forward primer, 0.8 μ M of reverse primer (Table 2.2), 0.4mM of each dNTPs, 1.5 unit of Taq polymerase (Geneaid, New Taipei City, Taiwan), 1.5mM of MgCl₂, and a PCR buffer containing 4% DMSO. The conditions for PCR were as in the following: 1 cycle of 3 minutes at 95°C; 30 cycles of 45 seconds at 95°C, 45 seconds at 60°C, and 45 seconds at 72°C; and 1 cycle of 5 minutes at 72°C.

Table 2.2. Primers used for genotyping of *Hexa* and *Neu4* alleles¹¹

Gene	Primer Name	Primer sequence	Product size
<i>Hexa</i>	<i>Hexa</i> -F	GGCCAGATACAATCATACAG	WT allele; 420bp KO allele; 210bp
	<i>Hexa</i> -R	CTGTCCACATACTCTCCCCACAT	
	PGK-F	CACCAAAGAAGGGAGCCGGT	
<i>Neu4</i>	<i>Neu4</i> -F	CTCTTCTTCATTGCCGTGCT	WT allele; 465bp KO allele; 635bp
	<i>Neu4</i> -R	GACAAGGAGAGCCTCTGGTG	
	Neo-F	GCCGAATATCATGGTGGAAA	

2.2.2. Genotyping of Mice for the *G_{M2}AP* Allele

The *G_{M2}AP*^{-/-} mice were obtained by a 1kb of deletion in *G_{M2}AP* gene that consists of an entire exon 3, entire intron 3, and a part of the exon 4⁴⁵. Depending on the mentioned deletion, some knock-out and wild type allele specific primers was designed (Table 3) for genotyping *G_{M2}AP* in one reaction as multiplex-PCR. The PCR performed with ~100ng of genomic DNA in the 50 μ l of reaction mix containing 0.6 μ M of the forward primer, 0.3 μ M of the reverse primer from each (Table 2.3), 0.4mM of every dNTP, 1.25 units of Taq polymerase (Geneaid, New Taipei City, Taiwan), 1.5mM of MgCl₂, and a PCR buffer specified for the enzyme. The conditions for the PCR were as in the following: 1 cycle of 3 minutes at 94°C; 30 cycles of 30 seconds at 94°C, 30 seconds at 60°C, and 75 seconds at 72°C; and 1 cycle of 7 minutes at 72°C.

Table 2.3. Primers used for genotyping of *G_{M2}AP* allele

Gene	Primer Name	Primer Sequence	Product Size
<i>G_{M2}AP</i>	WT-F	TATGTGCCAGTGAATCGGGC	WT; 930bp KO; 1100bp
	WT-R	CAGCTGCCTAGCTGTTCTACA	
	KO-R	GATGCCTGCTTGCCGAATATC	

2.3. Biochemical Analysis

In the concept of biochemical analyses, brain was used as illustrated in Figure 2.1B, the acidic and neutral ganglioside isolation, the analysis of isolated gangliosides with the thin layer chromatography, a relative gene expression analysis by the real-time PCR, the enzyme activity analysis, and the urinary oligosaccharides analysis with the thin layer chromatography, were performed in order to analyze the artificially-formed deficient mice in different aspects.

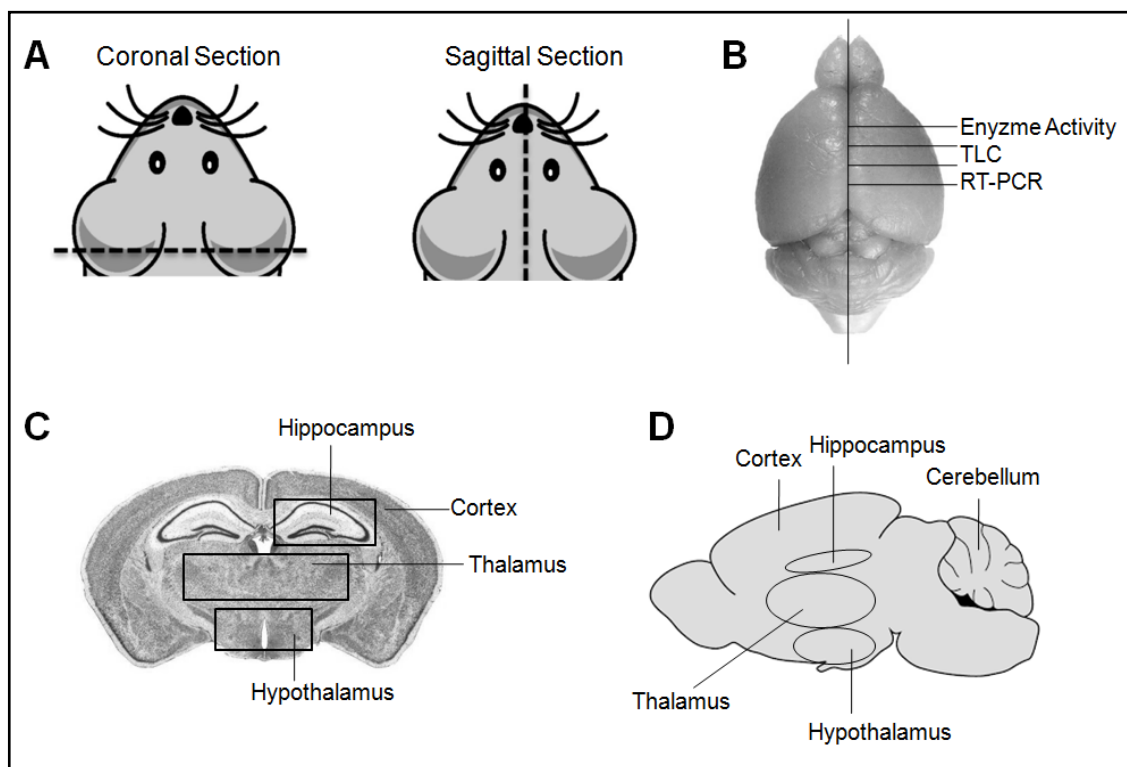


Figure 2.1. Illustrations of mice brain different sectioning (A)⁵⁰, regions used for biochemical analysis from mice brain (B), specific regions of brain in coronal (C)^{51,52}, and sagittal sections (D)

2.3.1. Ganglioside Isolation from the Brain

The acidic and neutral ganglioside isolations and the thin layer chromatography analysis were performed with 3- and 6-month-old mice brains according to the optimized protocol described below.

2.3.1.1. Neutral and Acidic Ganglioside Isolation

25mg of brain tissue from each genotyped mouse (8 samples in total) was homogenized in 2ml of dH₂O using the ultra turax homogenizer (IKA T10, Sigma, Darmstadt, Germany) for 30 seconds at 6000rpm in a borosilicate glass tube. The homogenized samples were sonicated (Bandelin-sonopuls, Berlin, Germany) for 3 minutes. The samples were then dried with a N₂ flow in the Reacti-Therm Heating module (Thermo, Massachusetts, USA) by 55°C of water in order to speed up the evaporation. After the entire water was evaporated, the extraction was performed with 3ml of 100% acetone. The samples were given a vortex and centrifuged at 2000rpm for 5 minutes. The supernatants containing phospholipids and other small membrane lipids were removed. This extraction step was repeated twice. Each pellet was washed with a 1.5ml of chloroform:methanol:water (10:10:1) solution, centrifuged at 2000 rpm for 5 minutes, and then the supernatant was collected in a new neutral glass tube with glass Pasteur pipettes. This step was repeated twice, and each time the supernatant was collected in the same glass tube for each. Afterwards, 2ml of a chloroform:methanol:water (30:60:8) solution was added into the pellets, and the samples were given a vortex. The centrifugation was performed at 2000rpm for 5 minutes, and the supernatant was collected in the same tube mentioned for the previous step. This procedure was repeated twice. At the end of this step, the collected supernatant contained both acidic and neutral gangliosides together. In order to separate the neutral and acidic gangliosides, DEAE Sephadex A-25 was used. The DEAE Sephadex A-25 ion exchange columns were prepared freshly before the usage⁵³. For this purpose, 10ml of chloroform: methanol:0.8M sodium acetate (30:60:8) was added into 1gr of DEAE Sephadex A-25 resin (GE Health Care, Little Chalfont, United Kingdom). After the incubation at room temperature for 5 minutes, a centrifugation was performed at 2000rpm for 1 minute. The solution was removed, and washing of the resin with the same solution was repeated thrice. The resin was incubated overnight with 10ml of chloroform: methanol:0.8M sodium acetate (30:60:8). On the following day, the supernatant was removed and the resin was washed with 10ml of chloroform:methanol:water (30:60:8) thrice so that it was ready to be used. Before loading the resin into the Pasteur pipette, the tips of the pipettes were closed with glass woolen order to make the separation of acidic and neutral ganglioside in the columns.

The resin was loaded into Pasteur pipettes, and the lengths of columns were calibrated for 2cm. Before loading the samples, the columns were washed with 1ml of chloroform:methanol:water (10:10:1) solution, and 1ml of chloroform:methanol:water (30:60:8) solution, then located in new empty neutral glass tubes. The total ganglioside samples obtained were loaded in the columns, and the liquid through was collected as neutral gangliosides. The columns were washed with 4ml of 100% methanol, and then collected as neutral ganglioside. The eluted samples were evaporated with a N₂ flow in the Reacti-Therm Heating module (Thermo, Massachusetts, USA) in 55°C of water, and kept at +4°C for maximum one or two days until the analysis. Before separating the acidic gangliosides from the columns, each column was placed in a new neutral glass tube, being washed with 5ml of 500mM potassium acetate in methanol. The eluted solution contained acidic gangliosides, where the desalting process of the acidic gangliosides was carried out by the Supelclean LC-18 column (Supelco, Sigma, Darmstadt, Germany). The LC-18 columns were placed in the Chromabond Vacuum manifold (Macherey-Nagel, Düren, Germany) which was fixed to 5Hg. For the equilibration, each column was washed with 2ml of methanol, and then with 2ml of 500mM potassium acetate in methanol solution. The collected acidic gangliosides were loaded in the LC-18 columns, and the liquid flow through was discarded. The columns were washed with 10ml of distilled water. New neutral glass tubes were placed under the columns, and the samples were eluted with 4ml of methanol and 4ml of chloroform:methanol (1:1) under low vacuum (<5 Hg). The eluted samples were evaporated with a N₂ flow in the Reacti-Therm Heating module (Thermo, Massachusetts, USA) in 55°C water, and kept at +4°C for maximum one or two days until the analysis.

2.3.1.2. Thin Layer Chromatography

Thin Layer Chromatography (TLC) method was used in order to separate gangliosides based on their structures and weights. 20cm x 20cm silica TLC plates (Merck, New Jersey, USA) were incubated at 100°C oven for 30 minutes to evaporate humidity if there was any. Chloroform:methanol: 0.2% CaCl₂(30:65:8) was used as the running solution, and the TLC tank (Camag, Muttenz, Switzerland) containing this solution was prepared 2 hour 15 minutes before running for equilibrium. The samples

were loaded on silica plates automatically with the Linomat 5 (Camag, Muttentz, Switzerland) machine. N₂-dried samples were resolved in 100µl of chloroform:methanol:water (10:10:1) solution and 30µl of sample were loaded on the TLC plate. Both neutral and acidic gangliosides ran under the exact conditions in separate plates that were put into TLC tank and ran for 10 cm.

2.3.1.3. Orcinol Staining of Plates

Orcinol (Sigma, Darmstadt, Germany) stain was prepared fresh before usage. 0.04g orcinol was solved in 10ml of 25% sulfuric acid in TLC sprayer (Sigma, Darmstadt, Germany), and left at room temperature for cooling. The plates were dyed with orcinol, and incubated on TLC plate heater (Camag, Muttentz, Switzerland) at 120°C until all of the bands became visible⁴⁹. After staining, the gangliosides were identified by a comparison with brain ganglioside standards (Avanti Polar Lipids, Alabaster, Alabama, USA). The plates were then scanned with the HP scanner system, and the band intensities were analyzed by the ImageJ program.

2.3.2. Analysis of Urinary Oligosaccharides by Thin Layer Chromatography

Urines from mice were collected with the help of metabolic cages (Techniplast). The cages were cleaned, water and food were provided. The mice (6 months old) were placed in the metabolic cages for 16-hour (overnight) urine collection. The collected urine samples were kept in freezer at -80°C until they were analyzed. The creatine in urine was used as a normalization measure, and the concentration of creatine in each urine sample was measured by the creatine assay kit (BioVision, Milpitas, California, USA) according to the manufacturer's instructions to equalize creatine levels in different samples. 500ng of creatine-containing urine samples were loaded to 20 cm x 20 cm silica TLC plates (Merck, New Jersey, USA) with glass pipette tips (Blaubrand, Merck, New Jersey, USA) after 1,5 µg of sugar standards (D+ Lactose Monohydrate, D+ Mannose, D+ Glucose, Sucrose, D+ Xylose and D+ Raffinose Pentahidrat (Sigma-Aldrich, Darmstadt, Germany)) were loaded to plates. The plates were run on butanol:water:acetic acid (50:25:25) solution for 5 hours, after the solution was incubated in TLC chamber for 3 hours. The plates were dyed with orcinol prepared in

the same manner for the gangliosides, and incubated on the TLC plate heater (Camag, Muttenz, Switzerland) at 120°C until all of the bands became apparent. The plates were scanned with the HP scanner system, and the band intensities were analyzed by the ImageJ program.

2.3.3. Relative Gene Expression Analysis by Real-Time PCR

Relative expression analyses were performed for two groups of genes: The first one was the degradation of enzymes/proteins, and the second one was the synthesis of enzymes. In the degradation group were 7 genes analyzed: sialidase *Neu1*, *Neu2*, *Neu3*, *Neu4*, *Hexb*, *G_{M2} activator protein (G_{M2}AP)*, and *β-Galactosidase (β-Gal)*. In the synthesis group were 5 genes analyzed using primers: *lactosyl ceramide synthase (B4Galt6)*, *N-acetyl-galactosaminyl transferase 1 (Galgt1)*, *G_{M3} ganglioside synthase (G_{M3}S)*, *G_{D3} ganglioside synthase (G_{D3}S)*, and *galactosyltransferase (B3Galt4)* (Table 2.4). The glyceraldehyde-3-phosphate dehydrogenase (*GAPDH*) gene was utilized as the internal control of the experiment. 50 mg of tissue from 3- and 6-month-old mice brains were used for the RNA isolation via Trizol Reagent (Geneaid, New Taipei City, Taiwan) according to the manufacturer's instructions. RNAs were used in order to produce cDNAs. 50ng/μl of cDNA was synthesized by the High-Capacity cDNA Reverse Transcription kit (Applied Biosystems, California, USA) according to manufacturer's instructions.

cDNAs were controlled by a normal PCR utilizing the *GAPDH* gene primers. The Real-Time PCR were optimized thanks to the LightCycler 96 machine (Roche, Basel, Switzerland) with 75ng of cDNA in the 20μl of reaction mix containing 0.4μM of primer pair and 1X LightCycler 480 SYBR Green I Master Mix (Roche, Basel, Switzerland). The conditions of PCR were as in the following: 1 cycle of 10 minutes at 95°C; 45 cycles of 20 seconds at 95°C, 15 seconds at 61°C, and 22 seconds at 72°C. The values were read after each cycle. In the end, the amplification melting analysis was performed under the following conditions: 30 seconds at 95°C, 10 seconds at 60°C, then continuous reading while the temperature increased to 99°C, in order to detect the primer dimers if there were any. The threshold cycle changes (ΔC_t) denote the difference in Ct for the gene of interest based on the Ct level of housekeeping genes. Expression of each gene was normalized using the expression of housekeeping gene.

Data from each genotype was obtained according to the comparative threshold (Δ CT) method.

Table 2.4. Genes analyzed by the Real-Time PCR, their specific primers and the lengths of PCR products

Gene	Primer	Primer Sequence	PCR product length
<i>Sialidase Neu1</i> ⁵⁴	Forward	TCATCGCCATGAGGAGGTCCA	431bp
	Reverse	AAAGGGAATGCCGCTCACTCCA	
<i>Sialidase Neu2</i> ⁵⁴	Forward	CGCAGAGTTGATTGTCCTGA	429bp
	Reverse	TTCTGAGCAGGGTGCAGTTTCC	
<i>Sialidase Neu3</i> ⁵⁴	Forward	CTCAGTCAGAGATGAGGATGCT	416bp
	Reverse	GTGAGACATAGTAGGCATAGGC	
<i>Sialidase Neu4</i> ⁵⁴	Forward	AGGAGAACGGTGTCTTCCAGA	339bp
	Reverse	GTTCTTGCCAGTGGCGATTGTC	
<i>Hexosaminidase b</i> ⁵⁴	Forward	AGTGCAGATCCTTCCCTAGT	412bp
	Reverse	ATCCGGACATCGTTTGGTGT	
<i>G_{M2} Activator Protein</i>	Forward	GCTGGCTTCTGGGTCAAGAT	193bp
	Reverse	GCACTGTGAAGTTGCTCGTG	
<i>β-Galactosidase</i>	Forward	TTTCTGGGGACCGTGATGTG	432bp
	Reverse	AATCCACTGTGGCGTACAGG	
<i>LacCer Synthase (B4Galt6)</i>	Forward	CACCTGATTCCGATGCTCCA	410bp
	Reverse	CCTTCTGGCCGGGTACATT	
<i>N-acetyl-Galactosaminyl Transferase 1 (Galgt1)</i> ⁵⁵	Forward	TCAGGATCAAGGAGCAAGTG	124bp
	Reverse	AAGGCTTTAGTGAGGTCAACC	
<i>G_{M3} Synthase</i> ⁵⁵	Forward	AATGCACTATGTGGACCCTG	133bp
	Reverse	GTTGATGCTGTACCTGTCCCTC	
<i>G_{D3} Synthase</i> ⁵⁵	Forward	CGATAATTCCACGTACTCCCTC	193bp
	Reverse	TTTGGAACCGACATCTCTGG	
<i>Galactosyl Transferase (B3Galt4)</i>	Forward	GGCAGTGCCCCTTCTGTATT	407bp
	Reverse	GTGCAGTCCTCTCCCATTC	
<i>Glyceraldehyde-3-Phosphate Dehydrogenase (GAPDH)</i> ⁵⁴	Forward	CCCCTTCATTGACCTCAACTAC	347bp
	Reverse	ATGCATTGCTGACAATCTTGAG	

2.3.4. Enzyme Activity Assay

Specific activities of *Sialidase*, *β-Hexosaminidase b*, *β-Galactosidase* and *β-Glucosidase* enzymes were measured by the brain tissues of 3- and 6-month-old deficient mice to analyze if these enzymes were affected by the deficiency of *Neu4*, *Hexa* and/or *G_{M2}AP*. The substrates for these enzymes (Table 2.5.) are fluorescently tagged with 4-Methylumbelliferyl (4-MU). 4-MU was digested from the substrate by the activity of each enzyme during reaction. The released 4-MU concentration was calculated depending on the standard curve by spectrofluorophotometer (Shimadzu, Kyoto, Japan) in the emission wavelength of 365 nanometers and the excision wavelength of 445 nanometers.

Table 2.5. Substrates used for the enzyme activity assay

Enzyme	Substrate
<i>Sialidase</i>	2'-(4-Methylumbelliferyl)- α -D-N-acetylneuraminic acid (Sigma 69587)
β - <i>Galactosidase</i>	4-Methylumbelliferyl β -D-galactopyranoside (Sigma M1633)
β - <i>Glucosidase</i>	4-Methylumbelliferyl β -D-glucopyranoside (Sigma M3633)
β - <i>Hexosaminidase b</i>	4-Methylumbelliferyl N-acetyl- β -D-glucosaminide (Sigma M2133)

25mg of brain tissue was homogenized with the pellet pestle hand homogenizer in 100 μ l of distilled water, and sonicated in a water bath for 3 minutes. For the β -Hexosaminidase enzyme reaction, 20 μ l of the homogenate was diluted in 1/5 ratio with 0.1 M sodium citrate pH4.3. In order to measure only the β -Hexosaminidase *b* enzyme activity, these diluted homogenates were incubated at 55°C for 3 hours before the setting reaction. For the reaction of other enzymes, 20 μ l of the homogenate was diluted in 1/10 ratio with 0.5M sodium acetate pH4.5 which was used directly. The reactions were prepared as summarized in the Table 2.6.

Protein concentrations of the samples were measured by the Bradford Reagent (Sigma, Cat No B6916, Darmstadt, Germany). For this purpose, 5 μ l of homogenates were diluted with their buffer in 1/4 ratio. 5 μ l of the sample was incubated for 10 minutes at room temperature under dark with 250 μ l of Bradford reagent. The absorbance of each was measured by the micro plate reader spectrophotometer (Biorad iMark, Hercules, California, USA) at 595nanometer of wavelength. The protein concentration was calculated depending on the BSA standard curve formed out of the known concentrated bovine serum albumin protein. Enzyme activity is expressed as the conversion of 1nmol of substrate per hour. To calculate the specific enzyme activity, the formulation in the following was used for each sample.²⁵

Enzyme Activity (nmol/hour/ml) = Concentration of 4-MU x (Last volume/Sample volume) x (1/time in hour)

Specific Enzyme Activity (nmol/mg protein/hour) = Enzyme activity / protein concentration

2.4. Immunohistochemical Staining for Lamp1 and G_{M2} Ganglioside

For the immunohistochemical analysis, the mice were anesthetized at their 3rd and 6th. The transcardiac perfusion was initiated with the serum physiologic (0.9 %

NaCl) followed by 4% paraformaldehyde in 1X PBS. The brain tissues were removed and placed in the same fixative overnight at +4°C, then treated sequentially with 10%, 20% sucrose for 2 hours, and 30% sucrose in PBS for overnight at +4°C. The brains were embedded in OCT (Sakura) in embedding modules, and kept at -80°C until they were used.

Table 2.6. Components of the reactions for enzyme activity assays

<i>Sialidase</i>	
Blank	Sample
50µl substrate	50µl substrate
40µl 0.5M sodium acetate buffer (pH4.5)	40µl 0.5M sodium acetate buffer (pH4.5)
10µl dH ₂ O	10µl sample
30 minutes incubation at 37°C	
3.9ml 0.2M glycine buffer (pH10.8) to stop reaction	
<i>β-Hexosaminidase b</i>	
Blank	Sample
75µl substrate	75µl substrate
25µl dH ₂ O	25µl sample
30 minutes incubation at 37°C	
3.9ml 0.2M glycine buffer (pH10.8) to stop reaction	
<i>β-Galactosidase</i>	
Blank	Sample
25µl substrate	25µl substrate
50µl 0.1M NaCl	50µl 0.1M NaCl
25µl dH ₂ O	25µl sample
10 minutes incubation at 37°C	
3.9ml 0.2M glycine buffer (pH10.8) to stop reaction	
<i>β-Glucosidase</i>	
Blank	Sample
50µl substrate	50µl substrate
40µl 0.5M sodium acetate buffer (pH4.5)	40µl 0.5M sodium acetate buffer (pH4.5)
10µl dH ₂ O	10µl sample
30 minutes incubation at 37°C	
3.9ml 0.2M glycine buffer (pH10.8) to stop reaction	

10 µm of coronal sections (Figure2.1) were taken from each brain by Leica Cryostat (CM1850-UV, Leica, Wetzlar, Germany) at -20°C. Lamp1, lysosomal marker protein and the G_{M2} ganglioside were immunostained from the slides containing exact brain regions. Firstly, the slides were kept on ice for 30 minutes and washed with 1X PBS for 10 minutes in chalet. They were then incubated in 100% acetone for 15 minutes and washed with 1X PBS for 5 minutes for two times. The edges of the brains were marked with liquid blocker PAP pen (Sigma, Darmstadt, Germany) not to allow the solution leak away. Blocking was carried out with a blocking solution (0.3 M Glycine,

40% BSA -in mg, 10% normal goat serum in 1X PBS) in a dark and humidified chamber, at room temperature for 1 hour. 1° antibody mixture prepared in blocking solution (1:500 Lamp1 1° antibody (Cat No ab24170, Abcam, Cambridge, United Kingdom) (Lamp1 is the lysosomal associated membrane protein 1, and it was used in staining as a lysosome marker.) and 1:500 G_{M2} ganglioside 1° antibody (KM966, commercially not available⁵⁶, produced in KYOWA Hakko Kirin Co., Japan. It was kindly donated by Dr. Shigeyuki Yamano in the concept of maternal transfer agreement.) was added into each brain, and the slides were incubated overnight in a dark and humidified chamber at +4°C. The following day, the slides were washed with 1X PBS for 5 minutes in a chalet for three times. 2° antibody mixture prepared in blocking solution (1:500 Lamp1 2° antibody (Cat No ab175471 Alexa Flour 568, red, Abcam, Cambridge, United Kingdom) and G_{M2} ganglioside 2° antibody (Cat No SA5-10118 Dylight 488, green, Thermo, Massachusetts, USA)) was added to each brain, and the incubation was carried out in a dark and humidified chamber at room temperature for 1 hour. The slides were washed with 1X PBS for 5 minutes in a chalet for four times. After the slides were dried with KimWipes (KimTech, Irving, Texas, USA), the mounting medium with Dapi (Cat No ab104139, Abcam, Cambridge, United Kingdom) was added into mount cells and stained their nucleus. 5 minutes later, the lam was put on the slides, and each was fixed with a nail polish. The slides were kept at +4°C for maximum 2 days, until when the cortex, hippocampus and thalamus regions of brains were photographed on fluorescent Microscopy (BX53, Olympus, Tokyo, Japan) with same light intensity specifically determined for each filter (Dapi, red and green filters) by the help of negative controls. Intensity of G_{M2} ganglioside in each region, cortex, hippocampus and thalamus was determined by ImageJ program.

2.5. Imaging Mass Spectrometric Analysis

Imaging mass spectrometry is a promising method that can be used to determine the distribution and relative abundance of specific molecules in biological samples such as histological slices of tissues by desorbing compounds from specific locations on the sample surface. The resulting ions can be separated and analyzed by mass spectrometry to provide a full mass spectrum from each location⁵⁷. When single, double and triple knock-out mice turned 3 months old, they were sacrificed with CO₂. Their brains were

removed; right and left hemispheres were separated, and immediately treated with liquid nitrogen and kept frozen under -80°C until they were needed.

The samples were sent to the laboratory of Prof. Dr. Roger Sandhoff (Heidelberg, Germany) conserved with dry ice, and they were studied there according to the protocol explained in the following¹³. The frozen brains were mounted onto a metal chuck with a frozen section compound, and $10\ \mu\text{m}$ of sagittal sections (Figure 2.1) were taken with Leica cryostat (Leica, Wetzlar, Germany). The cryosections were thaw mounted onto the precooled conductive indium tin oxide (ITO) slides. Before the application of the matrix, the ITO slides were desiccated overnight under the vacuum at room temperature. A $5\ \text{mg/mL}$ of phenyl-cyano-cinnamamide (SiChem, Bremen, Germany) solution in acetonitrile/water (90:10 v/v) was applied on the tissue sections by spray coating using the following parameters of the SunCollect device (SunChrom, Friedrichsdorf, Germany). First, the three initial matrix layers were applied using the flow rates of $10\ \mu\text{L/min}$, $15\ \mu\text{L/min}$, and $20\ \mu\text{L/min}$ followed by six layers at $25\ \mu\text{L/min}$ with a velocity of $1000\ \text{mm/min}$ to ensure a homogeneous matrix layer on the tissue slides. MALDI imaging mass spectrometry (MALDI-IMS) was performed in a negative linear mode in the m/z range of 900–2600 using an Autoflex Speed TOF/TOF with a 2000 Hz modulated Nd:YAG laser (355 nm) and the FlexImaging 4.0 software (Bruker Daltonics, Massachusetts, USA). Prior to the analysis, the acquisition method was calibrated using the total ganglioside porcine brain extract (Avanti Polar Lipids, Alabaster, Alabama, USA). 200 laser shots in total were accumulated per raster spot with a laser width of $100\ \mu\text{m}$. In addition, the baseline subtraction was performed, and the images were visualized after the total ion current (TIC)-normalization¹³.

2.6. Behavioral Tests

Two different tests were performed in order to observe if the changes in the ganglioside pattern could affect the neurons in the brain. The motor neurons and their function were examined under the Rotarod test, and the sensory neurons were tested with the hot plate technique.

2.6.1. Rotarod

An accelerating Rotarod (Pan-Lab Harvard Aparatus, Barcelona, Spain) was used to test the motor coordination ability of the mice. They (5-8 from each group) were first trained at 4rpm on a 5 line Rotarod unit, and then tested using an accelerated mode from 4 to 40 rpm over 5 minutes. Three trials were performed and the duration to stay on the rod of each animal was recorded¹¹.

2.6.2. Hot Plate

A Hot/Cold Plate (IITC Life Science, Woodland Hills, USA) was used to test the pain sensitivity of the mice. After the plate was heated to 55°C, the mice (5-8 from each group) were put on a plate (10cmx20cm) surrounded by 30cm height plexiglass enclosure. The moments when they exhibited the behaviors of paw licking, shaking and jumping were noted. 300 seconds of duration was set as the cut-off time. The mice which did not jump were taken out being scored as 301^{45,58}.

Since mice are able to learn that the experimenter will take them out once they jump at the first trial, this test can be useful only one time for each animal. The second trial will not prove a correct response to the heat since the mice do not exhibit the licking behavior, but jump immediately instead, right after they are put on the hot plate.

2.7. Statistical Analyses

P-values between the data sets were determined by the 2-way-Anova analysis, since there are two age groups and 8 different genotypes, via GraphPad. The significance was defined as $p < 0.05$ (* $p < 0.05$, ** $p < 0.005$, *** $p < 0.001$, **** $p < 0.0001$). The data were reported as means \pm SE.

CHAPTER 3

RESULTS

3.1. Genotyping of mice for *Hexa*, *G_{M2AP}* and *Neu4* alleles

PCRs performed for the detection of wild type and mutant allele of *Neu4*, *Hexa* and *G_{M2AP}* genes separately, according to the amplified bands, the mice were labeled as +/+, +/- or -/- for the genes of *Hexa* (Figure 3.1A), *G_{M2AP}* (Figure 3.1B) and *Neu4* (Figure 3.2C).

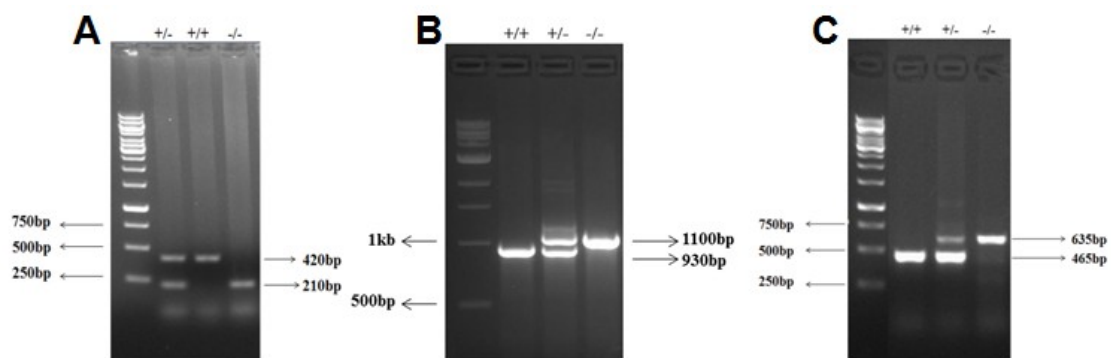


Figure 3.1. Genotyping of *Hexa* (A) *G_{M2AP}* (B) and *Neu4* (C) alleles by PCR analysis of tail genomic DNA. (A) *Hexa* allele-specific PCR amplifying 420 and 210bp fragments in heterozygous (+/-) mutants, a 420bp fragment in wild type (+/+) mice, and 210bp fragment in homozygous (-/-) HexA deficient animals. (B) *G_{M2AP}* allele-specific PCR amplifying a 930bp fragment in wild-type (+/+) mice, 930 and 1100bp fragments in heterozygous (+/-) mutants and 1100bp fragment in homozygous (-/-) *G_{M2AP}* deficient animals. (C) *Neu4* allele-specific PCR amplifying a 465bp fragment in wild-type (+/+) mice, 465 and 635bp fragments in heterozygous (+/-) mutants and 635bp fragment in homozygous (-/-) *Neu4* deficient animals.

3.2. Biochemical Analysis Results

In the concept of biochemical analysis, gangliosides from the brain and oligosaccharides from the urine were analyzed by the thin layer chromatography. The

relative gene expressions in the brain tissue and enzyme activity measurement were performed, as well.

3.2.1 Thin Layer Chromatography Results of Brain Gangliosides

The 3- and 6-month-old wildtype (*WT*), *Hexa* deficient (*Hexa*^{-/-}), *Neu4* deficient (*Neu4*^{-/-}), *G_{M2}AP* deficient (*G_{M2}AP*^{-/-}), *Hexa* and *Neu4* deficient (*Hexa*^{-/-}*Neu4*^{-/-}), *Hexa* and *G_{M2}AP* deficient (*Hexa*^{-/-}*G_{M2}AP*^{-/-}), *G_{M2}AP* and *Neu4* deficient (*G_{M2}AP*^{-/-}*Neu4*^{-/-}), and *Hexa*, *G_{M2}AP* and *Neu4* deficient (*Hexa*^{-/-}*G_{M2}AP*^{-/-}*Neu4*^{-/-}) mice samples were used in order to analyze the neutral (Figure 3.2 and Figure 3.4) and acidic (Figure 3.3 and Figure 3.5) ganglioside with the TLC analysis. In the neutral gangliosides, only *G_{A2}* ganglioside; and in the acidic gangliosides, LacCer, *GM1*, *G_{M2}*, *GD1a*, *GD1b* and *GT1b* gangliosides could be analyzed by the chromatography method.

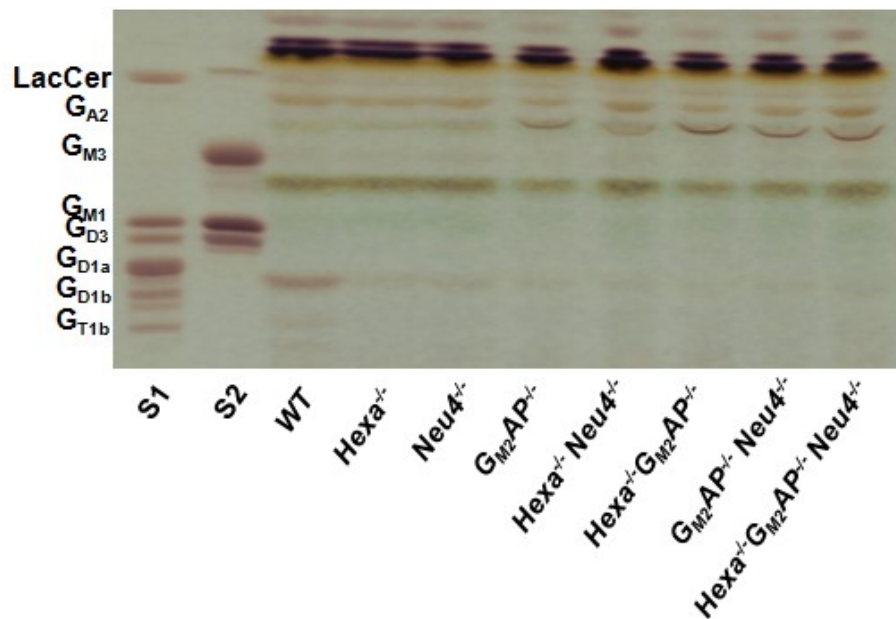


Figure 3.2. Thin layer chromatography and orcinol staining for neutral gangliosides of 3-month-old *WT*, *Hexa*^{-/-}, *Neu4*^{-/-}, *G_{M2}AP*^{-/-}, *Hexa*^{-/-}*Neu4*^{-/-}, *Hexa*^{-/-}*G_{M2}AP*^{-/-}, *G_{M2}AP*^{-/-}*Neu4*^{-/-} and *Hexa*^{-/-}*G_{M2}AP*^{-/-}*Neu4*^{-/-} mice brain tissues (S1, total ganglioside standard; S2, mixed ganglioside standard, *G_{M3}*, *G_{M1}* and *G_{D3}*)

The intensities of each band from two age groups and eight genotypes were analyzed by the ImageJ program, and the plots were obtained for the neutral (Figure 3.6) and acidic gangliosides (Figure 3.7, 3.8 and 3.9).

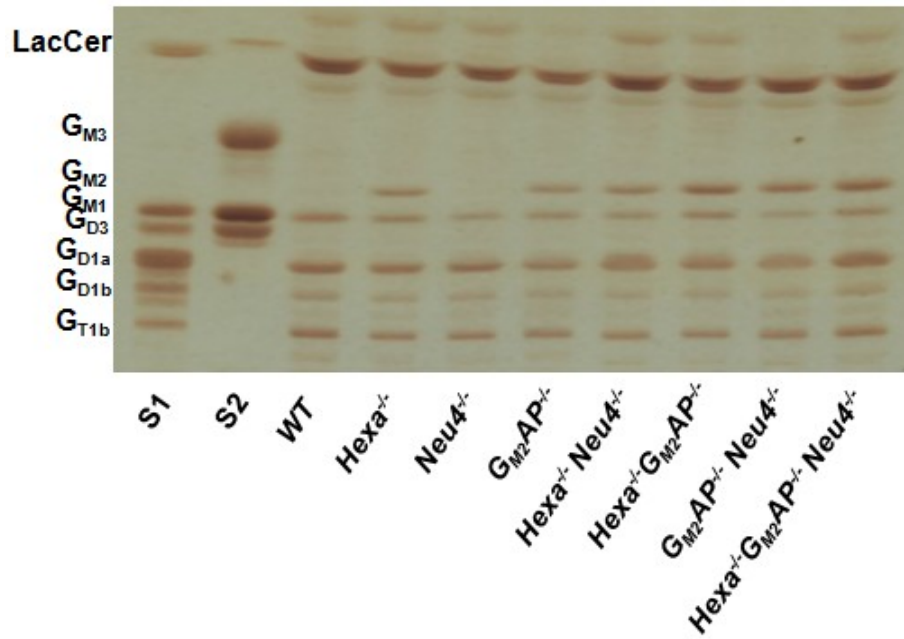


Figure 3.3. Thin layer chromatography and orcinol staining for acidic gangliosides of 3-month-old *WT*, *Hexa*^{-/-}, *Neu4*^{-/-}, *GM2AP*^{-/-}, *Hexa*^{-/-}*Neu4*^{-/-}, *Hexa*^{-/-}*GM2AP*^{-/-}, *GM2AP*^{-/-}*Neu4*^{-/-} and *Hexa*^{-/-}*GM2AP*^{-/-}*Neu4*^{-/-} mice brain tissues (S1, total ganglioside standard; S2, mixed ganglioside standard, *G*_{M3}, *G*_{M1} and *G*_{D3})

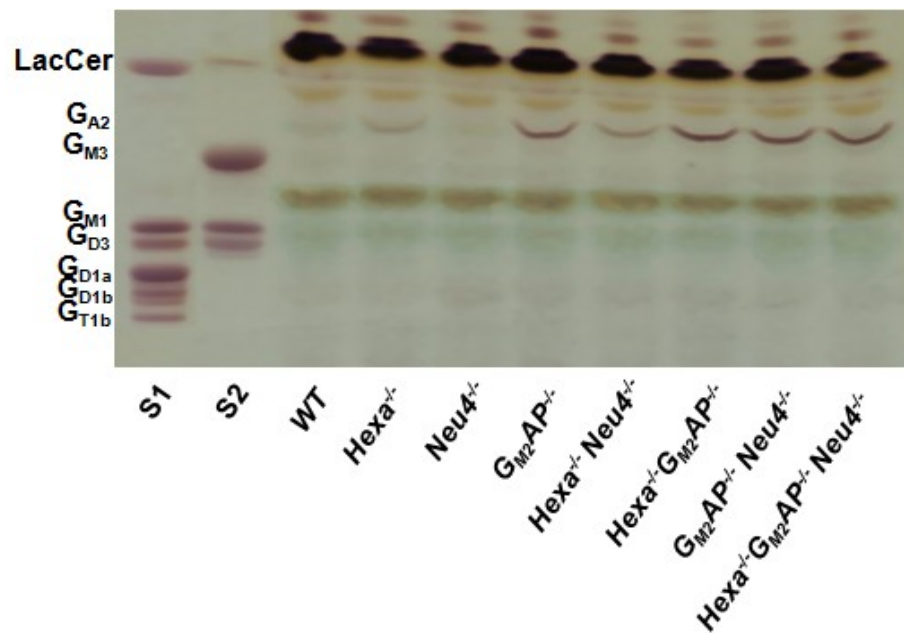


Figure 3.4. Thin layer chromatography and orcinol staining for neutral gangliosides of 6-month-old *WT*, *Hexa*^{-/-}, *Neu4*^{-/-}, *GM2AP*^{-/-}, *Hexa*^{-/-}*Neu4*^{-/-}, *Hexa*^{-/-}*GM2AP*^{-/-}, *GM2AP*^{-/-}*Neu4*^{-/-} and *Hexa*^{-/-}*GM2AP*^{-/-}*Neu4*^{-/-} mice brain tissues (S1, total ganglioside standard; S2, mixed ganglioside standard, *G*_{M3}, *G*_{M1} and *G*_{D3})

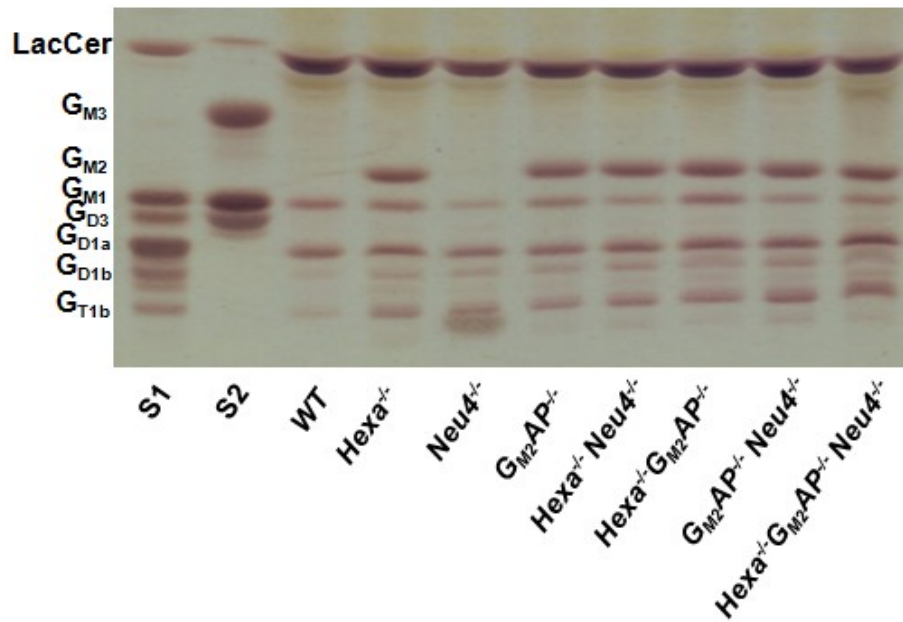


Figure 3.5. Thin layer chromatography and orcinol staining for acidic gangliosides of 6-month-old *WT*, *Hexa*^{-/-}, *Neu4*^{-/-}, *GM2AP*^{-/-}, *Hexa*^{-/-}*Neu4*^{-/-}, *Hexa*^{-/-}*GM2AP*^{-/-}, *GM2AP*^{-/-}*Neu4*^{-/-} and *Hexa*^{-/-}*GM2AP*^{-/-}*Neu4*^{-/-} mice brain tissues (S1, total ganglioside standard; S2, mixed ganglioside standard, *GM3*, *GM1* and *GD3*)

The *G_{A2}* ganglioside is one of the neutral ganglioside since it does not have a sialic acid residue. It is also one of the intermediate molecules formed by sialidases via the removal of sialic acid from *GM2* ganglioside. Therefore, its accumulation is of importance in order to figure out the functions of sialidases on the ganglioside degradation.

As depicted in Figure 3.6, the *G_{A2}* ganglioside was accumulated in *Hexa*^{-/-}, *GM2AP*^{-/-}, *Hexa*^{-/-}*Neu4*^{-/-}, *Hexa*^{-/-}*GM2AP*^{-/-}, *GM2AP*^{-/-}*Neu4*^{-/-} and *Hexa*^{-/-}*GM2AP*^{-/-}*Neu4*^{-/-} mice. *GM2AP*^{-/-}, *Hexa*^{-/-}*GM2AP*^{-/-} and *GM2AP*^{-/-}*Neu4*^{-/-} also exhibited significant increases in the level of *G_{A2}* ganglioside in the 6-month-old group compared to the 3-month-old ones, implying the presence of a progressive accumulation. When the deficiencies of *Hexa*^{-/-} and *GM2AP*^{-/-} combined in the double deficient mice model (*Hexa*^{-/-}*GM2AP*^{-/-}), the accumulation of *G_{A2}* ganglioside was increased 1.8 time in the 3-month-old, and 1.5 time in the 6-month-old groups compared to the *GM2AP*^{-/-} mice (Figure 3.6). 3-month-old *Hexa*^{-/-}*GM2AP*^{-/-}*Neu4*^{-/-} mice had a close level of the *G_{A2}* ganglioside which decreased at their 6th month for 0.78 times compared to the *Hexa*^{-/-}*GM2AP*^{-/-} mice (Figure 3.6), while the *GM2AP*^{-/-}*Neu4*^{-/-} mice had a slightly higher level of the *G_{A2}* ganglioside relative to the 3-month-old *GM2AP*^{-/-} mice for 1.14 times, and 6-month-old mice for 1.15 times.

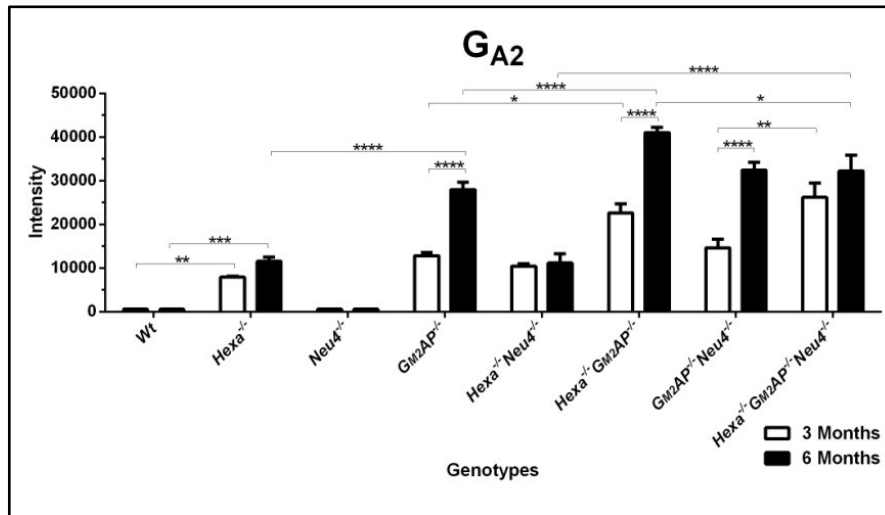


Figure 3.6. Intensity analysis of G_{A2} ganglioside from the 3- and 6-month-old *WT*, *Hexa*^{-/-}, *Neu4*^{-/-}, *G_{M2}AP*^{-/-}, *Hexa*^{-/-}*Neu4*^{-/-}, *Hexa*^{-/-}*G_{M2}AP*^{-/-}, *G_{M2}AP*^{-/-}*Neu4*^{-/-} and *Hexa*^{-/-}*G_{M2}AP*^{-/-}*Neu4*^{-/-} mice brain tissues (n=4) (*p<0.05, **p<0.005, ***p<0.001, ****p<0.0001) (Intensity of band was determined by ImageJ and p-values were determined by 2-way-Anova analysis via GraphPad. Data were reported as means ± SE.)

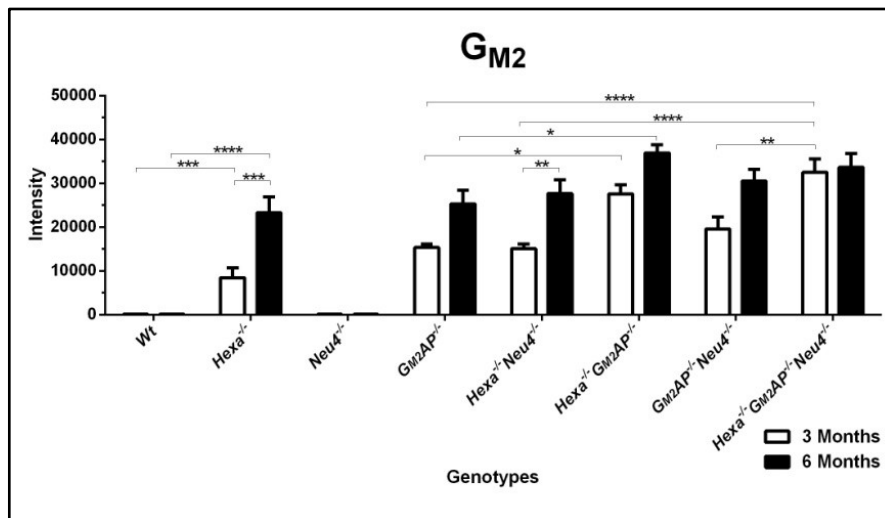


Figure 3.7. Intensity analysis of G_{M2} ganglioside from the 3- and 6-month-old *WT*, *Hexa*^{-/-}, *Neu4*^{-/-}, *G_{M2}AP*^{-/-}, *Hexa*^{-/-}*Neu4*^{-/-}, *Hexa*^{-/-}*G_{M2}AP*^{-/-}, *G_{M2}AP*^{-/-}*Neu4*^{-/-} and *Hexa*^{-/-}*G_{M2}AP*^{-/-}*Neu4*^{-/-} mice brain tissues (n=4) (*p<0.05, **p<0.005, ***p<0.001, ****p<0.0001) (Intensity of band was determined by ImageJ and p-values were determined by 2-way-Anova analysis via GraphPad. Data were reported as means ± SE.)

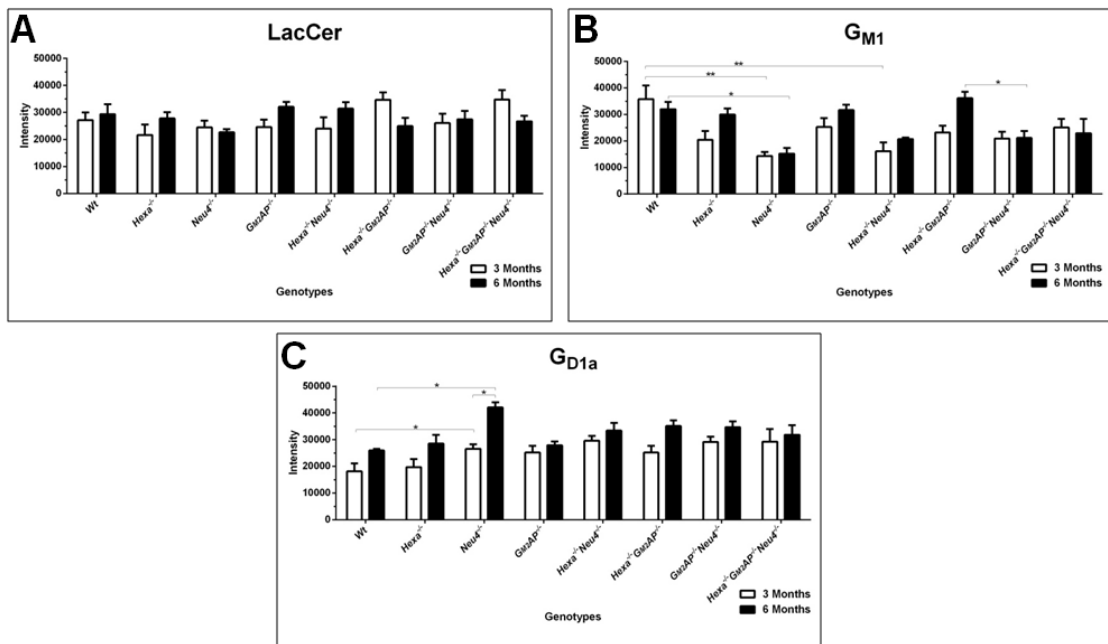


Figure 3.8. Intensity analysis of LacCer (A), GM₁ (B), GM₂ (C) and GD_{1a} (D) ganglioside from the 3- and 6-month-old WT, *Hexa*^{-/-}, *Neu4*^{-/-}, *GM2AP*^{-/-}, *Hexa*^{-/-}*Neu4*^{-/-}, *Hexa*^{-/-}*GM2AP*^{-/-}, *GM2AP*^{-/-}*Neu4*^{-/-} and *Hexa*^{-/-}*GM2AP*^{-/-}*Neu4*^{-/-} mice brain tissues (n=4) (*p<0.05, **p<0.005) (Intensity of each band was determined by ImageJ and p-values were determined by 2-way-Anova analysis via GraphPad. Data were reported as means ± SE.)

LacCer (Figure 3.8A) and GD_{1b} (Figure 3.9A), GT_{1b} (Figure 3.9B) gangliosides did not exhibit a difference in both age groups and in all of the genotypes.

The intensity of GM₁ ganglioside was decreased in *Hexa*^{-/-}*Neu4*^{-/-} and *GM2AP*^{-/-}*Neu4*^{-/-} mice, in addition to the *Neu4*^{-/-} mice in both 3- and 6-month-old groups (Figure 3.8B).

The GM₂ ganglioside were significantly increased in *Hexa*^{-/-}, *GM2AP*^{-/-}, *Hexa*^{-/-}*Neu4*^{-/-}, *Hexa*^{-/-}*GM2AP*^{-/-}, *GM2AP*^{-/-}*Neu4*^{-/-} and *Hexa*^{-/-}*GM2AP*^{-/-}*Neu4*^{-/-} compared to the wild type in an age-dependent manner (Figure 3.7). Besides, the *GM2AP*^{-/-}*Neu4*^{-/-} mice compared to *GM2AP*^{-/-}, and the *Hexa*^{-/-}*GM2AP*^{-/-}*Neu4*^{-/-} mice compared to the *Hexa*^{-/-}*GM2AP*^{-/-} ones did not demonstrate a significant increase in the GM₂ ganglioside level (Figure 3.7).

As indicated previously¹⁰, the GD_{1a} ganglioside exhibits a significant increase in the *Neu4*^{-/-} mice compared to the wild type in both ages (Figure 3.8C). However, this increase was not significant in the other double and triple deficient mice.

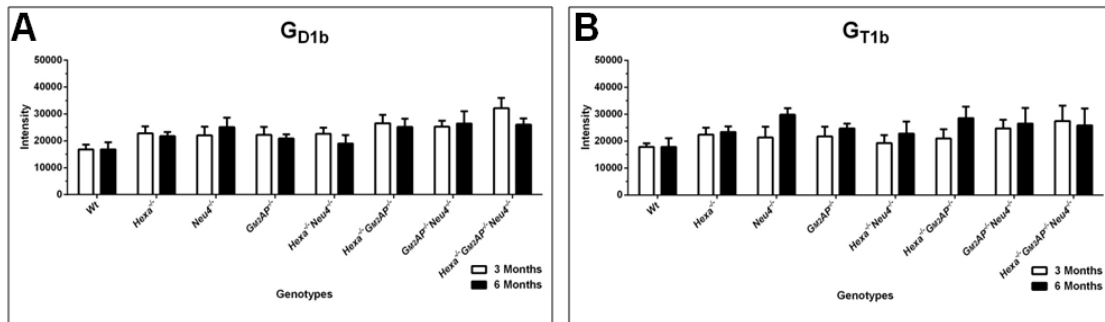


Figure 3.9. Intensity analysis of G_{D1b} (A) and G_{T1b} (B) ganglioside from 3- and 6-month-old WT , $Hexa^{-/-}$, $Neu4^{-/-}$, $G_{M2AP}^{-/-}$, $Hexa^{-/-}Neu4^{-/-}$, $Hexa^{-/-}G_{M2AP}^{-/-}$, $G_{M2AP}^{-/-}Neu4^{-/-}$ and $Hexa^{-/-}G_{M2AP}^{-/-}Neu4^{-/-}$ mice brain tissues (n=4) (Intensity of each band was determined by ImageJ and p-values were determined by 2-way-Anova analysis via GraphPad. No significant change was observed. Data were reported as means \pm SE.)

3.2.2. Thin Layer Chromatography Results of Urinary Oligosaccharides

The urine analysis with the chromatography was performed in order to reveal if sugars were affected by the deficiency of different enzymes. An alteration was noticed in the content of oligosaccharides in the urine in the double and triple deficient mice (Figure 3.10).

The intensity analysis could only be performed for the galactose and raffinose bands appeared in the chromatography. The galactose was observed to decrease in the $Hexa^{-/-}$ and $Neu4^{-/-}$ mice, similar to those in the $G_{M2AP}^{-/-}$, $Hexa^{-/-}Neu4^{-/-}$, $Hexa^{-/-}G_{M2AP}^{-/-}$ mice, slightly increased in the $G_{M2AP}^{-/-}Neu4^{-/-}$ mice, and significantly increased in the $Hexa^{-/-}G_{M2AP}^{-/-}Neu4^{-/-}$ mice urine, compared to the wild type mice (Figure 3.11A).

The raffinose is the heaviest oligosaccharide analyzed, and different from the galactose, its intensity was decreased not only in the $Hexa^{-/-}$ and $Neu4^{-/-}$ mice, but in the $Hexa^{-/-}G_{M2AP}^{-/-}$ and $G_{M2AP}^{-/-}Neu4^{-/-}$ mice, also. The accumulation of raffinose was not traced in any other deficient mice and $G_{M2AP}^{-/-}$, $Hexa^{-/-}Neu4^{-/-}$, and the $Hexa^{-/-}G_{M2AP}^{-/-}Neu4^{-/-}$ mice had a close amount of raffinose to the wild type mice (Figure 3.11B).

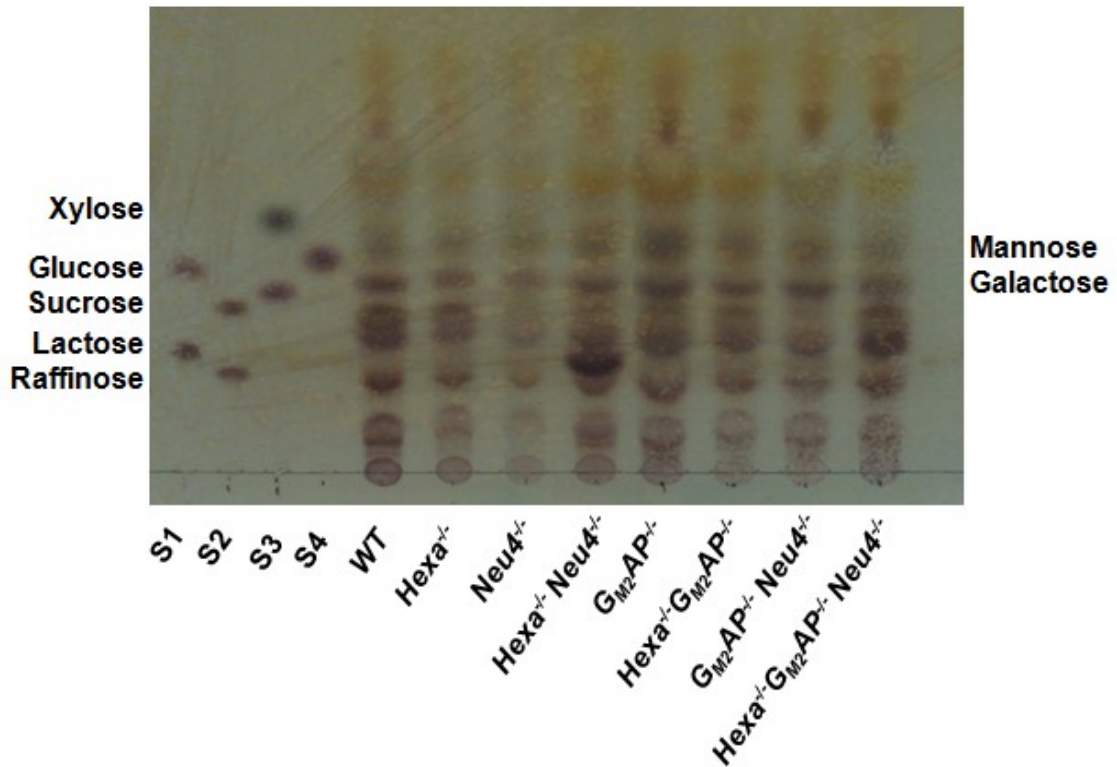


Figure 3.10. Thin layer chromatography and orcinol staining for urinary oligosaccharides of 6-month-old *WT*, *Hexa*^{-/-}, *Neu4*^{-/-}, *GM2AP*^{-/-}, *Hexa*^{-/-}*Neu4*^{-/-}, *Hexa*^{-/-}*GM2AP*^{-/-}, *GM2AP*^{-/-}*Neu4*^{-/-} and *Hexa*^{-/-}*GM2AP*^{-/-}*Neu4*^{-/-} mice (S1; Glucose and Lactose, S2; Sucrose and Raffinose, S3; Xylose and Galactose and S4; Mannose)

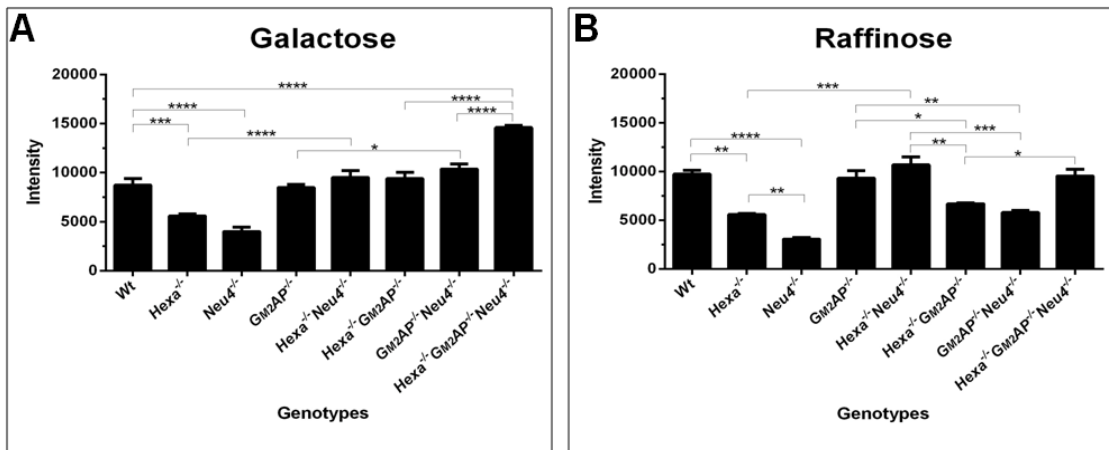


Figure 3.11. Intensity analysis of Galactose (A) and Raffinose (B) from the urines of 6-month-old *WT*, *Hexa*^{-/-}, *Neu4*^{-/-}, *GM2AP*^{-/-}, *Hexa*^{-/-}*Neu4*^{-/-}, *Hexa*^{-/-}*GM2AP*^{-/-}, *GM2AP*^{-/-}*Neu4*^{-/-} and *Hexa*^{-/-}*GM2AP*^{-/-}*Neu4*^{-/-} mice (n=2) (*p<0.05, **p<0.005, ***p<0.001, ****p<0.0001) (Intensity of each band was determined by ImageJ and p-values were determined by 2-way-Anova analysis via GraphPad. Data were reported as means ± SE.)

3.2.3. Relative Gene Expression Results

The gene expression analysis was performed in order to observe the possible change in the ganglioside degradation and/or synthesis enzymes' gene expression. For this purpose, seven degradation enzymes and five synthesis enzymes were examined.

In the expression ratio analysis of sialidases; *Neu1*, *Neu3* and *Neu4* had similar levels in the single, double and triple deficient mice compared to the wild type (Figure 3.12A, C, and D). Beside these three sialidase, the sialidase *Neu2* had significantly different ratios between different genotypes (Figure 3.12B). The *Neu2* expression was noted to be significantly increased in the 3-month-old *G_{M2}AP^{-/-}* and *Hexa^{-/-}G_{M2}AP^{-/-}* mice compared to the exact aged *Hexa^{-/-}* mice, significantly increasing in 6-month-old *Neu4^{-/-}* mice compared to the 3-month-old *Neu4^{-/-}* mice (Figure 3.12B).

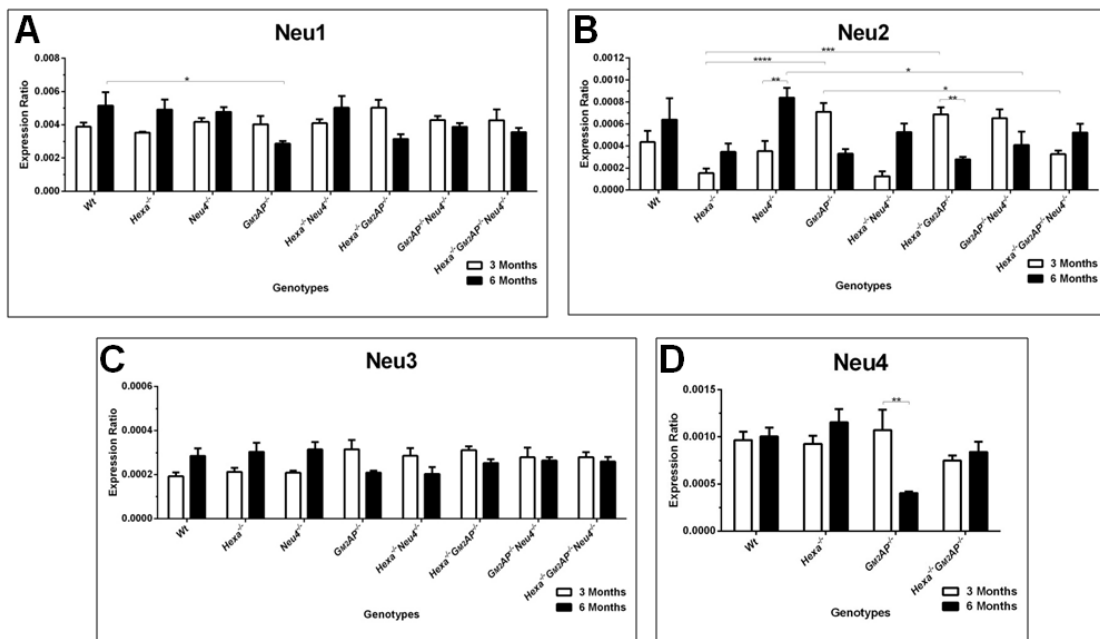


Figure 3.12. Expression ratios of sialidase *Neu1* (A), *Neu2* (B), *Neu3* (C) and *Neu4* (D) enzyme genes in 3- and 6-month-old *WT*, *Hexa^{-/-}*, *Neu4^{-/-}*, *G_{M2}AP^{-/-}*, *Hexa^{-/-}Neu4^{-/-}*, *Hexa^{-/-}G_{M2}AP^{-/-}*, *G_{M2}AP^{-/-}Neu4^{-/-}* and *Hexa^{-/-}G_{M2}AP^{-/-}Neu4^{-/-}* mice brain tissues (n=3) (*p<0.05, **p<0.005, ***p<0.001, ****p<0.0001) (Expression ratios were determined by Δ CT method, p-values were determined by 2-way-Anova analysis via GraphPad. Data were reported as means \pm SE.)

The expression levels of the β -Hexosaminidase band *G_{M2}AP* genes in the single, double and triple deficient mice did not change significantly compared to the wild type

(Figure 3.13A, B). However, the β -Galactosidase was significantly decreased in 6-month-old $G_{M2AP}^{-/-}$ and $Hexa^{-/-}G_{M2AP}^{-/-}$ mice compared to 6-month-old $Hexa^{-/-}$ mice (Figure 3.13C). Likewise, the β -Galactosidase expression levels in 6-month-old $G_{M2AP}^{-/-}$, $Hexa^{-/-}G_{M2AP}^{-/-}$ and $Neu4^{-/-}G_{M2AP}^{-/-}$ mice were decreased compared to the 3-month-old counterparts (Figure 3.13C).

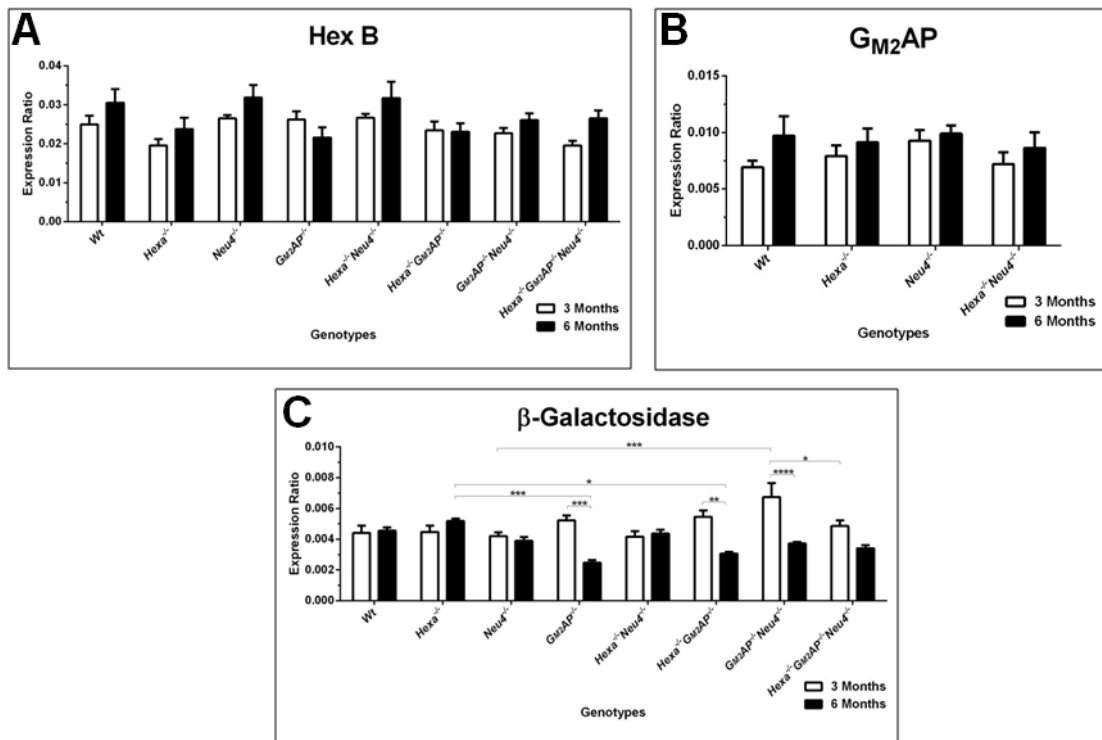


Figure 3.13. Expression ratios of β -Hexosaminidase *b* (A), G_{M2} Activator Protein (G_{M2AP}) (B) and β -Galactosidase (C) in 3- and 6-month-old WT, $Hexa^{-/-}$, $Neu4^{-/-}$, $G_{M2AP}^{-/-}$, $Hexa^{-/-}Neu4^{-/-}$, $Hexa^{-/-}G_{M2AP}^{-/-}$, $G_{M2AP}^{-/-}Neu4^{-/-}$ and $Hexa^{-/-}G_{M2AP}^{-/-}Neu4^{-/-}$ mice brain tissues (n=3) (*p<0.05, **p<0.005, ***p<0.001, ****p<0.0001) (Expression ratios were determined by Δ CT method, p-values were determined by 2-way-Anova analysis via GraphPad. Data were reported as means \pm SE.)

Between the synthesis enzymes analyzed, LacCer Synthase (B4Galt6) was significantly decreased in 6-month-old $Hexa^{-/-}G_{M2AP}^{-/-}Neu4^{-/-}$ group compared to the 3-month-old $Hexa^{-/-}G_{M2AP}^{-/-}Neu4^{-/-}$ mice (Figure 3.14A). The Galgt1 enzyme expression level was similar in all the mice in both ages (3.14B).

The G_{M3S} expression level was increased in 6-month-old $G_{M2AP}^{-/-}Neu4^{-/-}$ mice compared to 6-month-old $Neu4^{-/-}$ mice (Figure 3.15A). Similarly, the G_{D3S} expression level was increased in 3-month-old $G_{M2AP}^{-/-}$ mice compared to the wild type mice,

where it was decreased in 6-month-old $G_{M2AP}^{-/-}$ mice compared to 3-month-old $G_{M2AP}^{-/-}$ mice (Figure 3.15B).

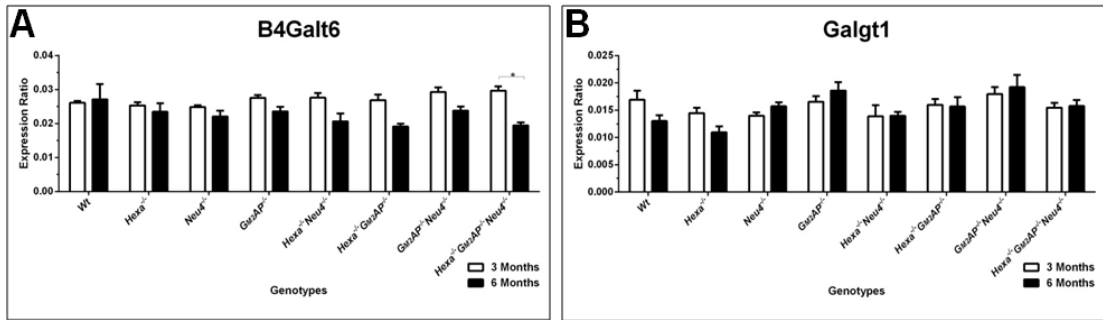


Figure 3.14. Expression ratios of LacCer Synthase (B4Galt6) (A) and N-acetyl-Galactosaminyl Transferase 1 (Galgt1) (B) in 3- and 6-month-old WT , $Hexa^{-/-}$, $Neu4^{-/-}$, $G_{M2AP}^{-/-}$, $Hexa^{-/-}Neu4^{-/-}$, $Hexa^{-/-}G_{M2AP}^{-/-}$, $G_{M2AP}^{-/-}Neu4^{-/-}$ and $Hexa^{-/-}G_{M2AP}^{-/-}Neu4^{-/-}$ mice brain tissues (n=3) (*p<0.05) (Expression ratios were determined by ΔCT method, p-values were determined by 2-way-Anova analysis via GraphPad. Data were reported as means \pm SE.)

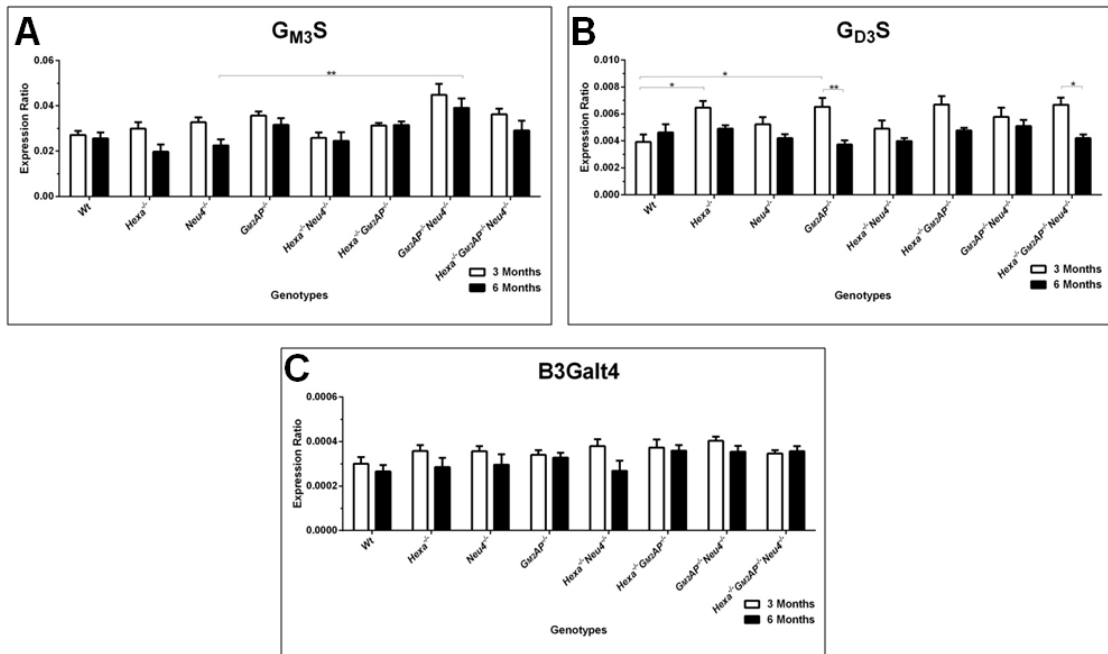


Figure 3.15. Expression ratios of G_{M3} Synthase ($G_{M3}S$) (A), G_{D3} Synthase ($G_{D3}S$) (B) and Galactosyl Transferase (B3Galt4) (C) in 3- and 6-month-old WT , $Hexa^{-/-}$, $Neu4^{-/-}$, $G_{M2AP}^{-/-}$, $Hexa^{-/-}Neu4^{-/-}$, $Hexa^{-/-}G_{M2AP}^{-/-}$, $G_{M2AP}^{-/-}Neu4^{-/-}$ and $Hexa^{-/-}G_{M2AP}^{-/-}Neu4^{-/-}$ mice brain tissue (n=3) (*p<0.05, **p<0.005) (Expression ratios were determined by ΔCT method, p-values were determined by 2-way-Anova analysis via GraphPad. Data were reported as means \pm SE.)

The B3Galt4 expression ratio as well did not exhibit a difference between the genotypes and the ages such as the Galgt1 enzyme expression (Figure 3.15C).

3.2.4. Enzyme Activity Results

The analysis of different enzyme activities in the single, double and triple deficient mice revealed the presence of an altered activity of each enzyme in different mice groups (Figure 3.16). This alteration might be a result of the affected lysosomal environment by the accumulated gangliosides. Since each deficient mouse had a different ganglioside profile, activities of the analyzed enzymes might be affected by this situation in different manners.

The sialidase enzyme activity in the *Hexa*^{-/-}, *Neu4*^{-/-} and *G_{M2}AP*^{-/-} mice were similar to the control group, however, it was increased in the *Hexa*^{-/-}*G_{M2}AP*^{-/-}, *G_{M2}AP*^{-/-}*Neu4*^{-/-} and *Hexa*^{-/-}*G_{M2}AP*^{-/-}*Neu4*^{-/-} mice (Figure 3.16A). The increase discovered in these mice might be a result of the sialidase need for the degradation of accumulated ganglioside with the help of *G_{M2}AP* as a collaborator to render its duty.

The β -Hexosaminidase *b* enzyme is the isomer of the *Hexa* enzyme, and the deficiency results in the Sandhoff disease⁴⁰. The β -Hexosaminidase *b* enzyme activity increased in 3-month-old *Hexa*^{-/-} and *Hexa*^{-/-}*Neu4*^{-/-} mice, whereas it decreased when they reached 6-month-old (Figure 3.16B). At their sixth months, the *Hexa*^{-/-}*G_{M2}AP*^{-/-}*Neu4*^{-/-} mice had an increased activity of the β -Hexosaminidase *b* enzyme compared to the 3-month-old counterpart, which might depend on the deficiency of *G_{M2}AP* in the triple deficient mice, since the same profile was observed in the *G_{M2}AP*^{-/-} mice (Figure 3.16B).

The β -Galactosidase enzyme normally degrades the *G_{M1}* ganglioside, and the deficiency of this enzyme results in the *G_{M1}*gangliosidosis³¹. The activity analysis demonstrated that there was a slight but not a significant decrease in the activity of this enzyme in the *Neu4*^{-/-}, *G_{M2}AP*^{-/-}, double and triple deficient mice compared to the wild type and *Hexa*^{-/-} mice (Figure 3.16C). A decreased *G_{M1}* ganglioside depending on the deficiency of *Neu4* might be a reason of the low enzyme activity in the mice that do not have the *Neu4* enzyme.

β -Glucosidase is the enzyme which degrade the glucosides such as glucocerebroside (glucosylceramide) in the lysosomes, being the deficiency result in

another lysosomal storage disorder, the Gaucher disease³¹. The activity of this enzyme exhibited a significant increase in the 3-month-old mice group. The *Hexa*^{-/-}*G_{M2}AP*^{-/-}*Neu4*^{-/-}, *Hexa*^{-/-}*G_{M2}AP*^{-/-} and *G_{M2}AP*^{-/-}*Neu4*^{-/-} mice had two times of an increase compared to the *Hexa*^{-/-}*Neu4*^{-/-} and *G_{M2}AP*^{-/-} mice, and four times compared to the *Hexa*^{-/-} and *Neu4*^{-/-} mice (Figure 3.16D).

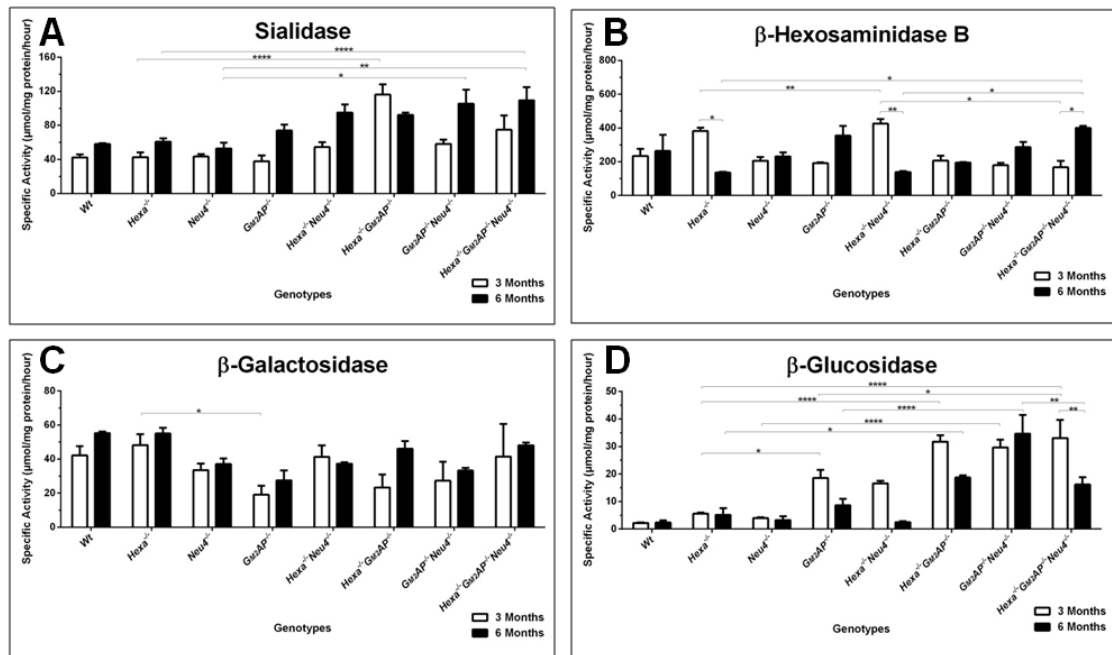


Figure 3.16. Specific enzyme activity of Sialidase (A), β -Hexosaminidase b (B), β -Galactosidase (C) and β -Glucosidase (D) enzymes in 3- and 6-month-old *WT*, *Hexa*^{-/-}, *Neu4*^{-/-}, *G_{M2}AP*^{-/-}, *Hexa*^{-/-}*Neu4*^{-/-}, *Hexa*^{-/-}*G_{M2}AP*^{-/-}, *G_{M2}AP*^{-/-}*Neu4*^{-/-} and *Hexa*^{-/-}*G_{M2}AP*^{-/-}*Neu4*^{-/-} mice brain tissues (n=3) (*p<0.05, **p<0.005, ****p<0.0001) (Specific enzyme activity of each was calculated depending on the released fluorescence molecule concentration after incubation and protein concentration of each sample. p-values were determined by 2-way-Anova analysis via GraphPad. Data were reported as means \pm SE.)

3.3. Immunohistochemical Staining Results

Accumulation of the *G_{M2}* ganglioside in brain cells was further studied by the immunohistochemistry utilizing the human-mouse chimeric monoclonal antibody from paraformaldehyde fixed brain tissue coronal sections. This antibody has been shown to be exclusive to the *G_{M2}* ganglioside, and it is non-reactive toward the *G_{A2}*, *G_{M3}*, *G_{D1a,b}* and *G_{D2a,b}* gangliosides¹¹. Lamp1 was used to show if accumulation takes place in lysosome or not.

The cortex, hippocampus and thalamus regions of 3- and 6-month-old mice were examined to detect the age dependence of the accumulations in the brain. The images were first taken under microscopy with a four times of a magnification in order to demonstrate the regions of cortex (C) and hippocampus (H) of 3-month-old (Figure 3.17) and 6-month-old mice (Figure 3.21), then with ten times of a magnification to specifically detect accumulation in a region specific manner of cortex, hippocampus and thalamus region. Intensity analysis performed by ImageJ showed the differences of G_{M2} level in cortex (Figure 3.25), hippocampus (Figure 3.26) and thalamus regions (Figure 3.27) of all genotyped mice at 3- and 6-month-old.

In addition to the cortex region which was photographed previously¹², the *WT* and *Neu4*^{-/-} mice did not have an accumulation of the G_{M2} ganglioside in their hippocampus (Figure 3.19, 3.23 and 3.26) and thalamus (Figure 3.20, 3.24, and 3.27) regions at both ages considered. In the cortex region of *G_{M2}AP*^{-/-} mice brain, it was observed that the accumulation of G_{M2} ganglioside was slightly higher than the *Hexa*^{-/-} mice cortex region for 3-month-old group (Figure 3.18). This difference was increased when the mice turn 6 months old (Figure 3.22) since the *G_{M2}AP*^{-/-} mice had an increased level of G_{M2} ganglioside compared to their 3-month-old counterparts, and the 6-month-old *Hexa*^{-/-} mice. For the 3-month-old *Hexa*^{-/-}*Neu4*^{-/-}, *Hexa*^{-/-}*G_{M2}AP*^{-/-}, *G_{M2}AP*^{-/-}*Neu4*^{-/-} and *Hexa*^{-/-}*G_{M2}AP*^{-/-}*Neu4*^{-/-} mice, it can be noted that all of them had a similar level of G_{M2} ganglioside accumulation (Figure 3.18), whereas in the *Hexa*^{-/-}*G_{M2}AP*^{-/-} and *Hexa*^{-/-}*G_{M2}AP*^{-/-}*Neu4*^{-/-} mice, the accumulation increased with time. These two mice groups had a higher level of G_{M2} ganglioside when they were 6 months old (Figure 3.22).

In the hippocampus region, the G_{M2} ganglioside accumulation did not change between the 6- and 3-month-old groups for the *Hexa*^{-/-} mice (Figure 3.19 and 3.23). It slightly increased for the *G_{M2}AP*^{-/-} mice (Figure 3.19 and 3.23) and prominently increased for the *Hexa*^{-/-}*Neu4*^{-/-}, *Hexa*^{-/-}*G_{M2}AP*^{-/-}, *G_{M2}AP*^{-/-}*Neu4*^{-/-} and *Hexa*^{-/-}*G_{M2}AP*^{-/-}*Neu4*^{-/-} mice (Figure 3.19 and 3.23).

In the thalamus region of brain, the *Hexa*^{-/-} and *G_{M2}AP*^{-/-} mice had a low level of accumulation compared to the double and triple deficient mice at both ages. However, the accumulation of G_{M2} ganglioside increased in time, and the 6-month-old *Hexa*^{-/-} and *G_{M2}AP*^{-/-} mice had a higher level of G_{M2} ganglioside than their 3-month-old counterparts (Figure 3.20 and 3.24).

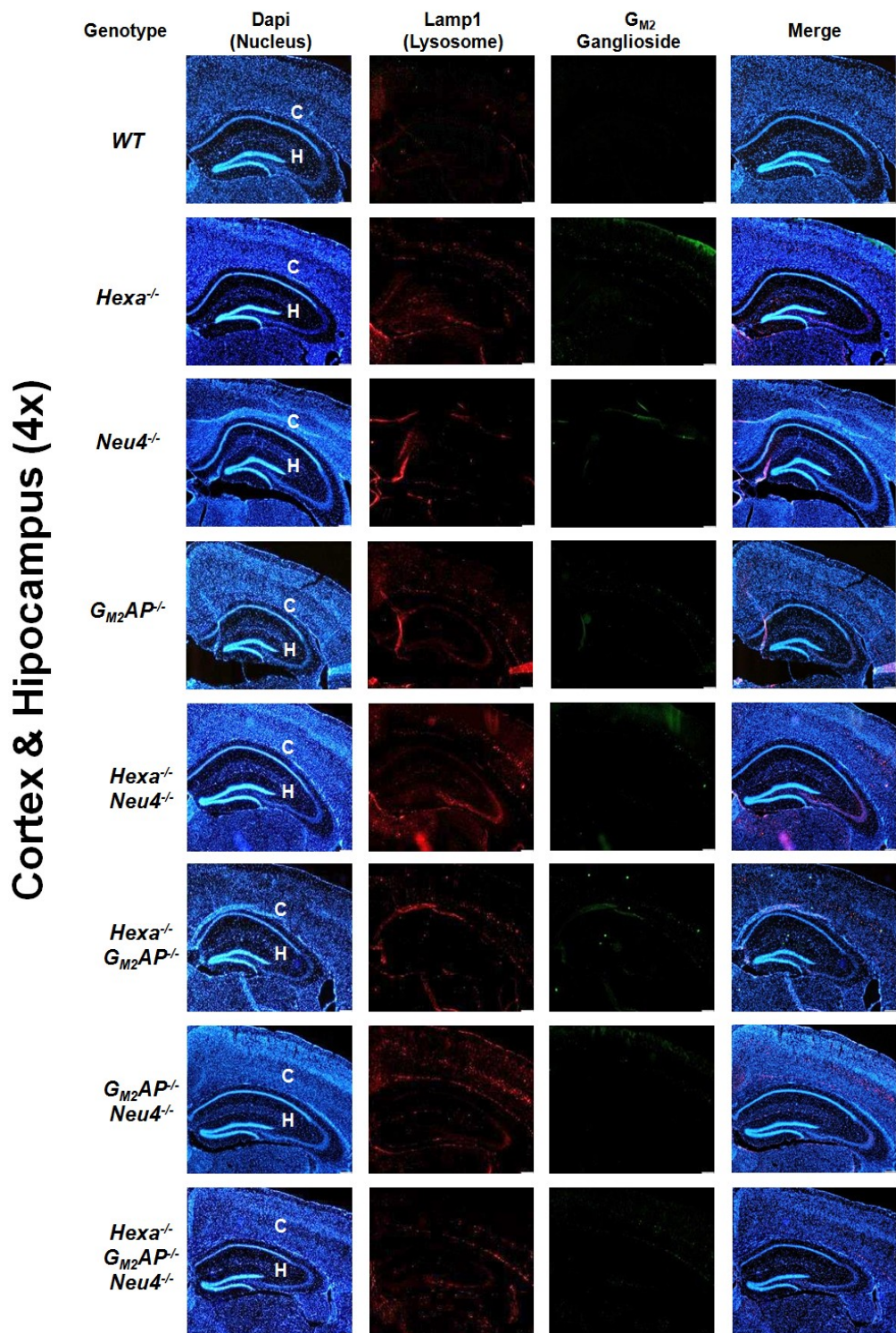


Figure 3.17. Immunostaining of Lamp1 and G_{M2} ganglioside in 3-month-old *WT*, *Hexa*^{-/-}, *Neu4*^{-/-}, *G_{M2AP}*^{-/-}, *Hexa*^{-/-}*Neu4*^{-/-}, *Hexa*^{-/-}*G_{M2AP}*^{-/-}, *G_{M2AP}*^{-/-}*Neu4*^{-/-} and *Hexa*^{-/-}*G_{M2AP}*^{-/-}*Neu4*^{-/-} mice brain coronal sections, cortex (C) and hippocampus (H) regions. (Magnification is 4x, scale bar is for 200μm.) (Images from each genotype were taken under same light intensity that only differs depending on the filter type, Dapi, red or green filters. Then 3 images were merged by modular imaging software platform (cellSens) that is specific to fluorescence microscope Olympus BX53.)

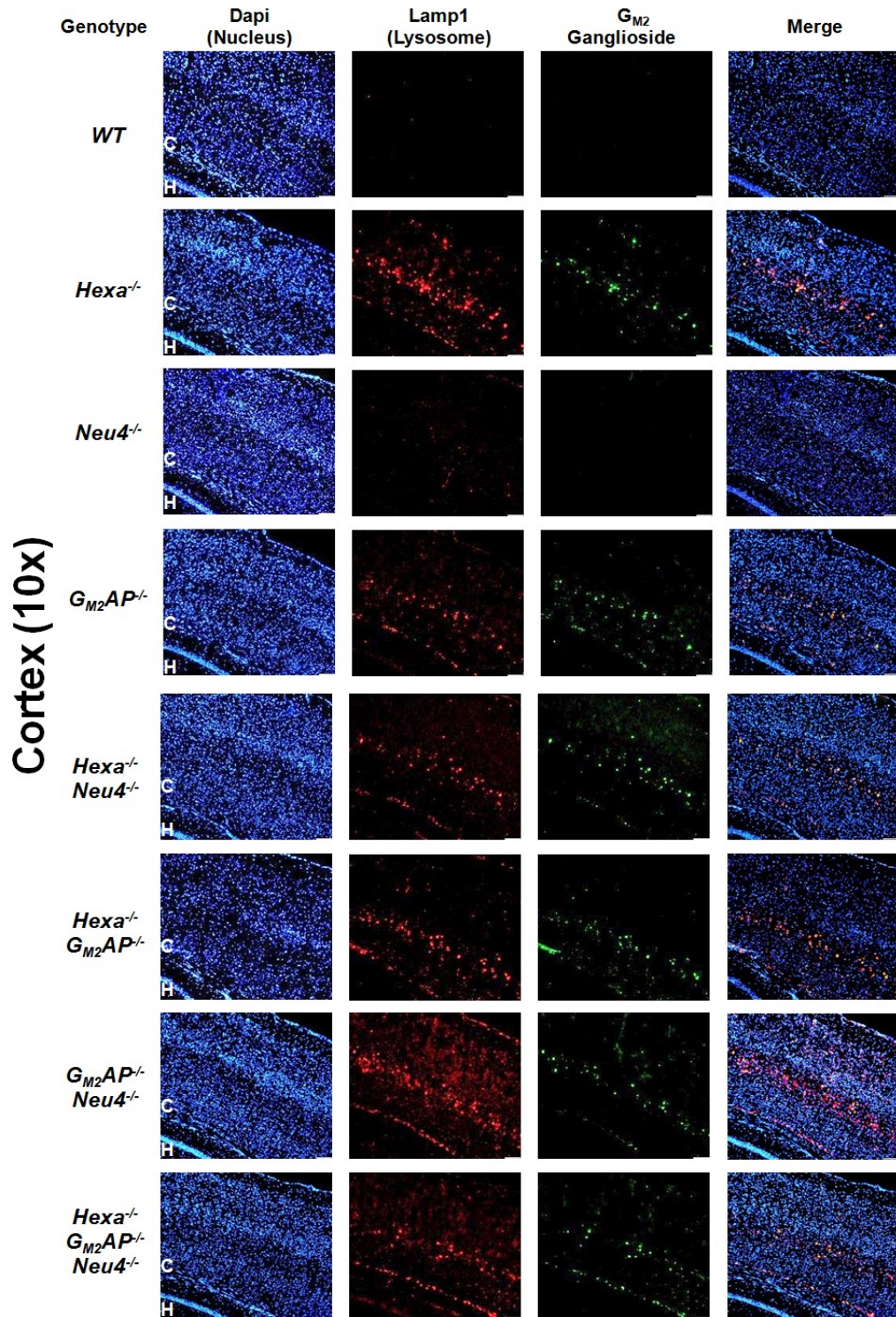


Figure 3.18. Immunostaining of Lamp1 and G_{M2} ganglioside in 3-month-old *WT*, *Hexa^{-/-}*, *Neu4^{-/-}*, *G_{M2}AP^{-/-}*, *Hexa^{-/-}Neu4^{-/-}*, *Hexa^{-/-} G_{M2}AP^{-/-}*, *G_{M2}AP^{-/-}Neu4^{-/-}* and *Hexa^{-/-}G_{M2}AP^{-/-}Neu4^{-/-}* mice brain coronal sections, cortex region. (Magnification is 10x, scale bar is for 100μm.) (Images from each genotype were taken under same light intensity that only differs depending on the filter type, Dapi, red or green filters. Then 3 images were merged by modular imaging software platform (cellSens) that is specific to fluorescence microscope Olympus BX53.)

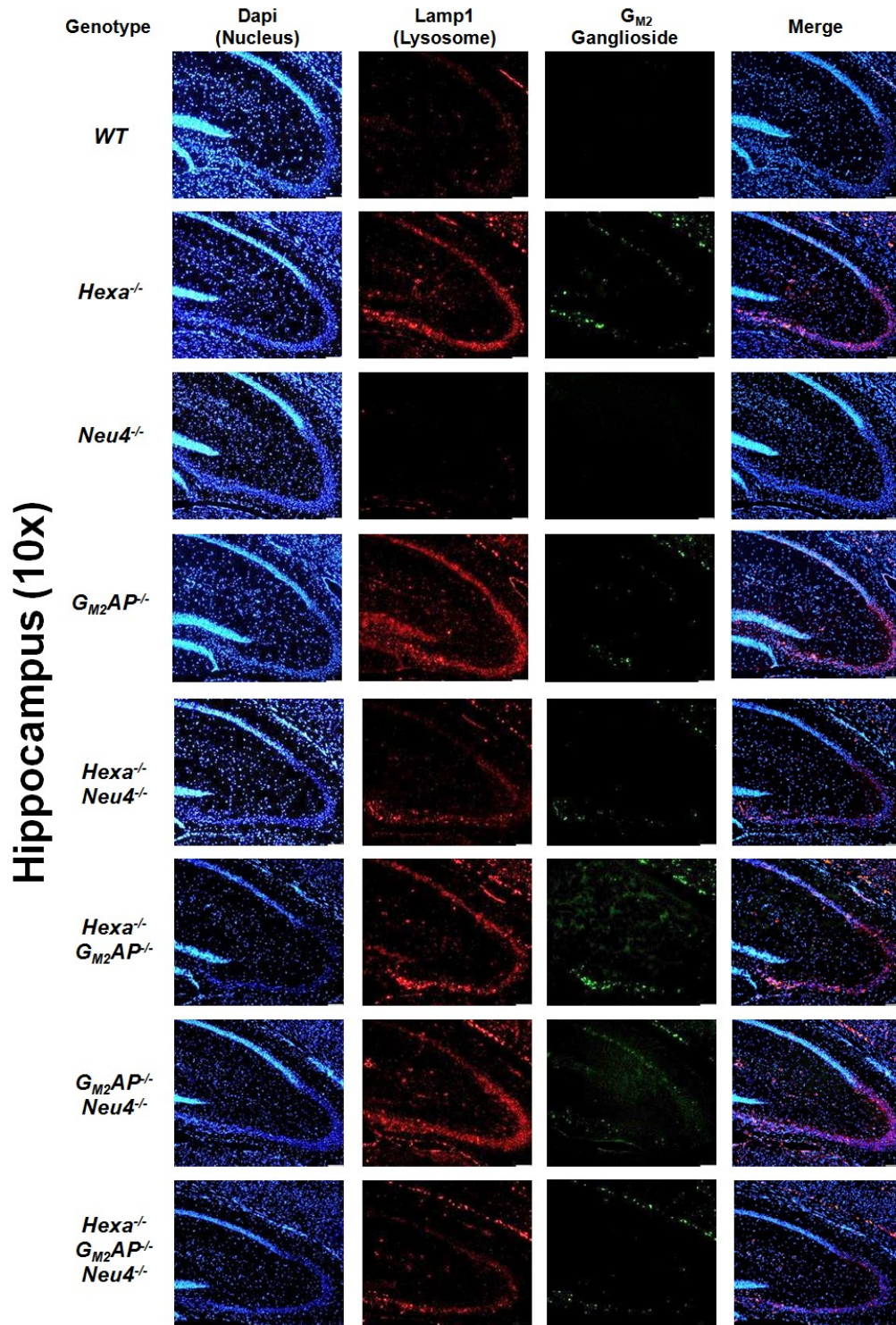


Figure 3.19. Immunostaining of Lamp1 and G_{M2} ganglioside in 3-month-old *WT*, *Hexa*^{-/-}, *Neu4*^{-/-}, *G_{M2}AP*^{-/-}, *Hexa*^{-/-}*Neu4*^{-/-}, *Hexa*^{-/-}*G_{M2}AP*^{-/-}, *G_{M2}AP*^{-/-}*Neu4*^{-/-} and *Hexa*^{-/-}*G_{M2}AP*^{-/-}*Neu4*^{-/-} mice brain coronal sections, hippocampus region. (Magnification is 10x, scale bar is for 100μm.) (Images from each genotype were taken under same light intensity that only differs depending on the filter type, Dapi, red or green filters. Then 3 images were merged by modular imaging software platform (cellSens) that is specific to fluorescence microscope Olympus BX53.)

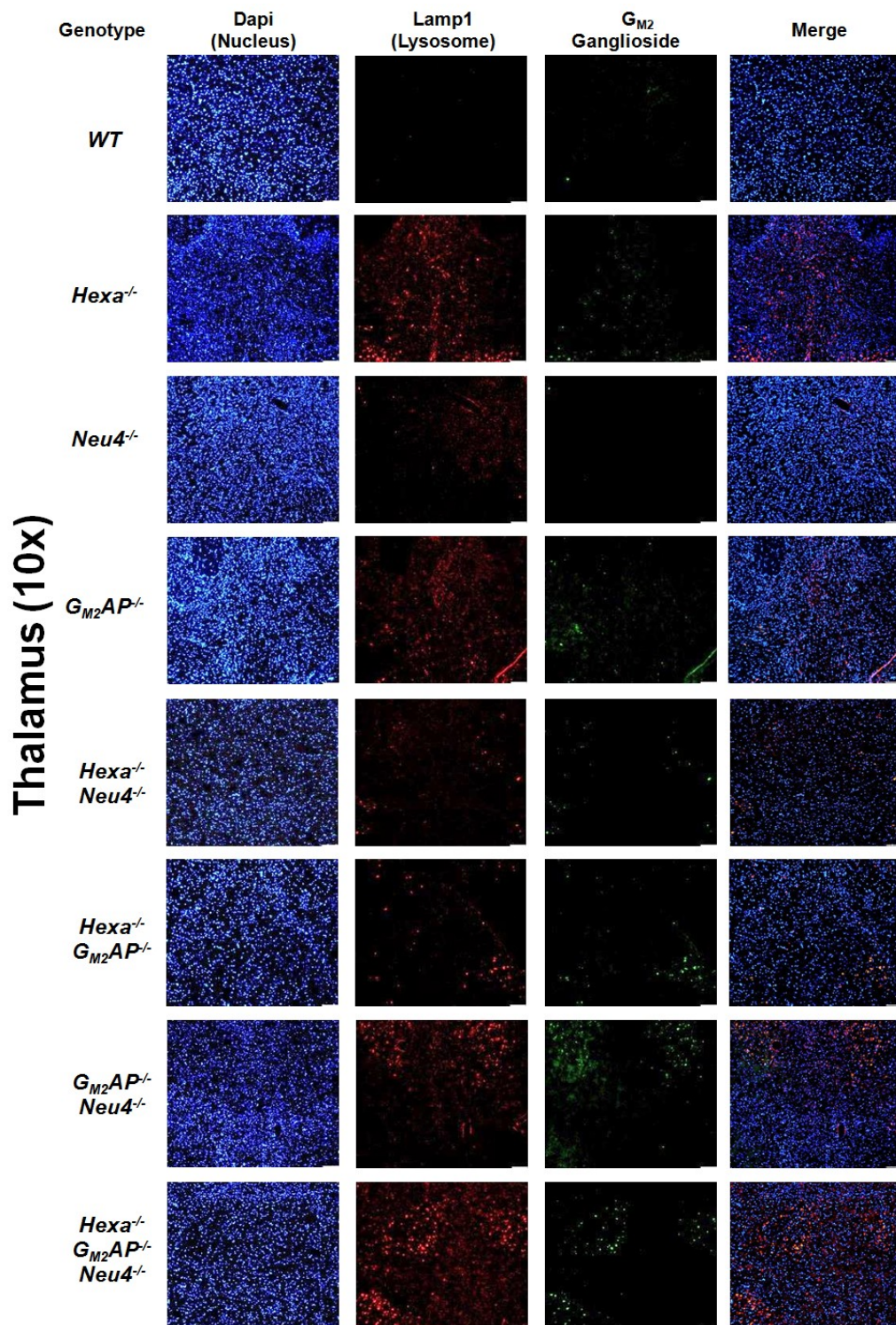


Figure 3.20. Immunostaining of Lamp1 and G_{M2} ganglioside in 3-month-old *WT*, *Hexa*^{-/-}, *Neu4*^{-/-}, *G_{M2}AP*^{-/-}, *Hexa*^{-/-}*Neu4*^{-/-}, *Hexa*^{-/-}*G_{M2}AP*^{-/-}, *G_{M2}AP*^{-/-}*Neu4*^{-/-} and *Hexa*^{-/-}*G_{M2}AP*^{-/-}*Neu4*^{-/-} mice brain coronal sections, thalamus region. (Magnification is 10x, scale bar is for 100μm.) (Images from each genotype were taken under same light intensity that only differs depending on the filter type, Dapi, red or green filters. Then 3 images were merged by modular imaging software platform (cellSens) that is specific to fluorescence microscope Olympus BX53.)

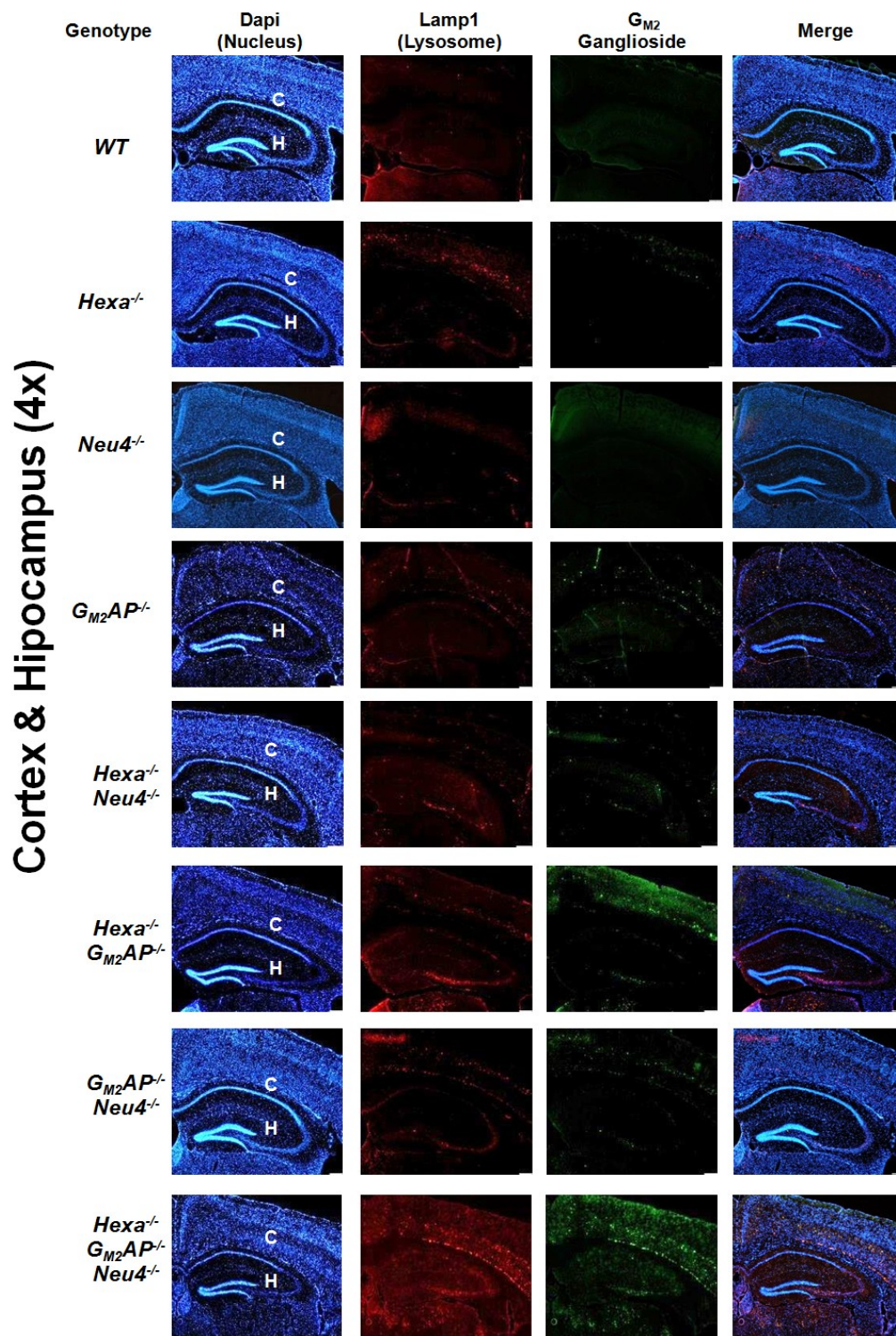


Figure 3.21. Immunostaining of Lamp1 and G_{M2} ganglioside in 6-month-old *WT*, *Hexa*^{-/-}, *Neu4*^{-/-}, *G_{M2}AP*^{-/-}, *Hexa*^{-/-}*Neu4*^{-/-}, *Hexa*^{-/-}*G_{M2}AP*^{-/-}, *G_{M2}AP*^{-/-}*Neu4*^{-/-} and *Hexa*^{-/-}*G_{M2}AP*^{-/-}*Neu4*^{-/-} mice brain coronal sections, cortex (C) and hippocampus (H) regions. (Magnification is 4x, scale bar is for 200μm.) (Images from each genotype were taken under same light intensity that only differs depending on the filter type, Dapi, red or green filters. Then 3 images were merged by modular imaging software platform (cellSens) that is specific to fluorescence microscope Olympus BX53.)

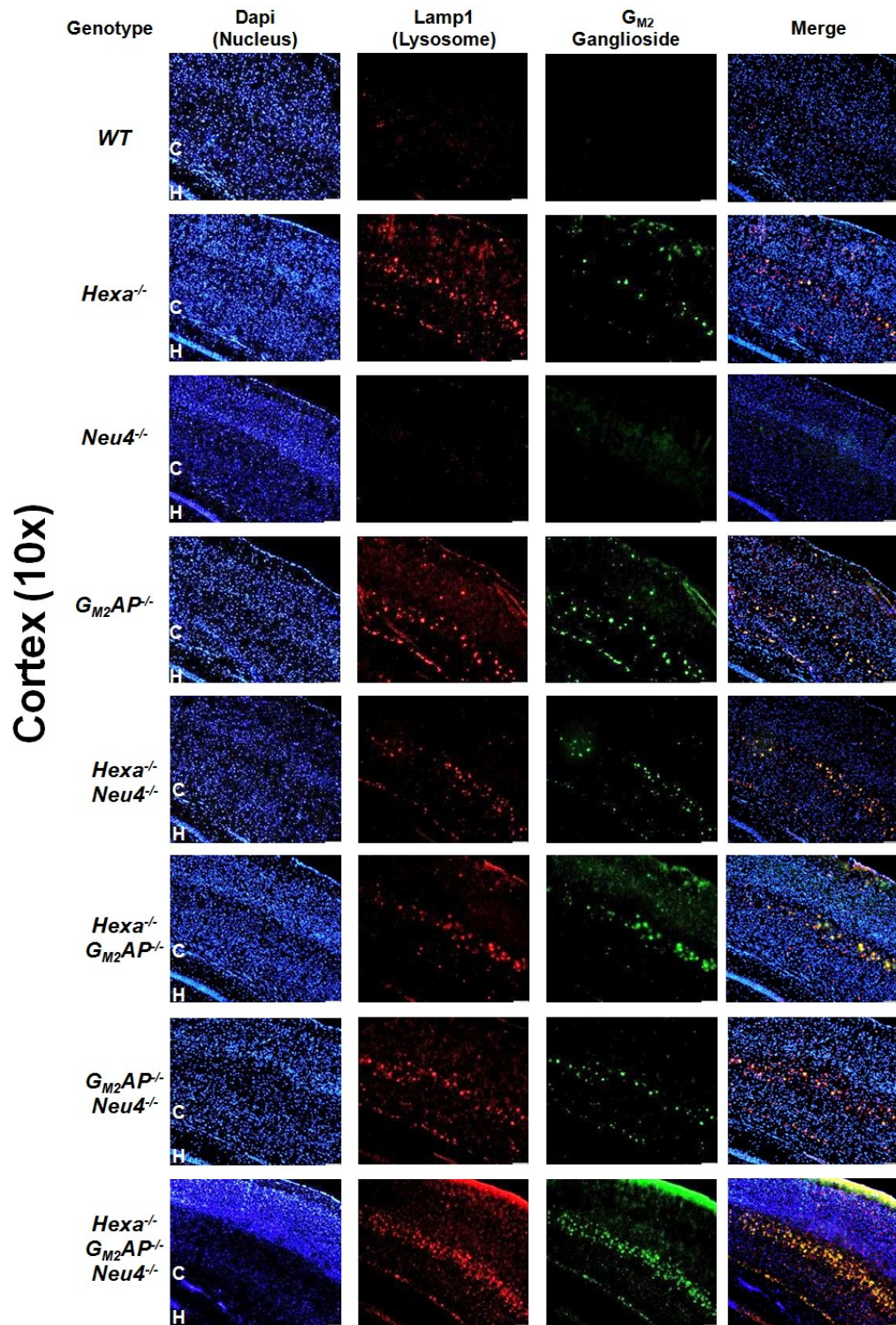


Figure 3.22. Immunostaining of Lamp1 and G_{M2} ganglioside in 6-month-old *WT*, *Hexa*^{-/-}, *Neu4*^{-/-}, *G_{M2AP}*^{-/-}, *Hexa*^{-/-}*Neu4*^{-/-}, *Hexa*^{-/-}*G_{M2AP}*^{-/-}, *G_{M2AP}*^{-/-}*Neu4*^{-/-} and *Hexa*^{-/-}*G_{M2AP}*^{-/-}*Neu4*^{-/-} mice brain coronal sections, cortex region. (Magnification is 10x, scale bar is for 100μm.) (Images from each genotype were taken under same light intensity that only differs depending on the filter type, Dapi, red or green filters. Then 3 images were merged by modular imaging software platform (cellSens) that is specific to fluorescence microscope Olympus BX53.)

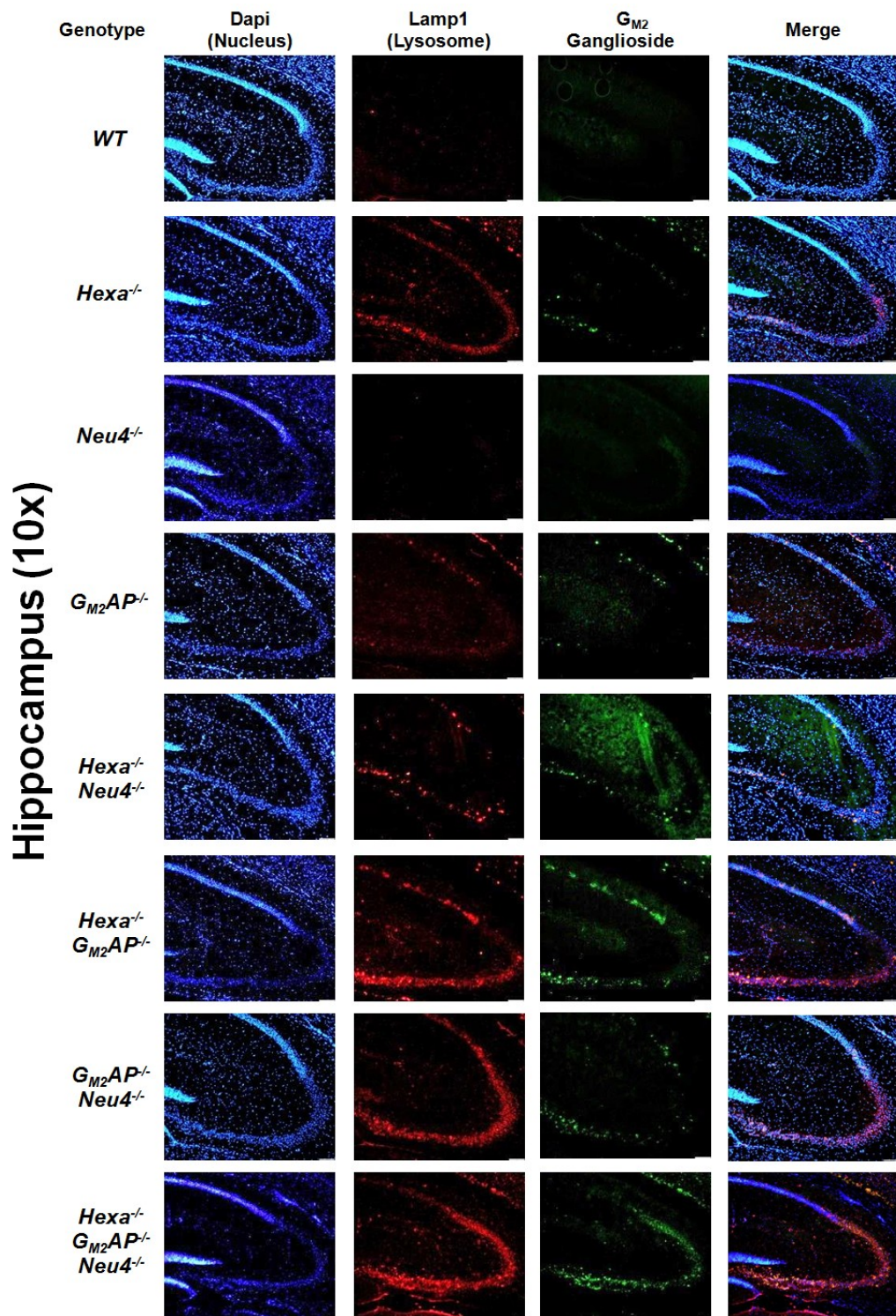


Figure 3.23. Immunostaining of Lamp1 and G_{M2} ganglioside in 6-month-old *WT*, *Hexa*^{-/-}, *Neu4*^{-/-}, *G_{M2}AP*^{-/-}, *Hexa*^{-/-}*Neu4*^{-/-}, *Hexa*^{-/-}*G_{M2}AP*^{-/-}, *G_{M2}AP*^{-/-}*Neu4*^{-/-} and *Hexa*^{-/-}*G_{M2}AP*^{-/-}*Neu4*^{-/-} mice brain coronal sections, hippocampus region. (Magnification is 10x, scale bar is for 100μm.) (Images from each genotype were taken under same light intensity that only differs depending on the filter type, Dapi, red or green filters. Then 3 images were merged by modular imaging software platform (cellSens) that is specific to fluorescence microscope Olympus BX53.)

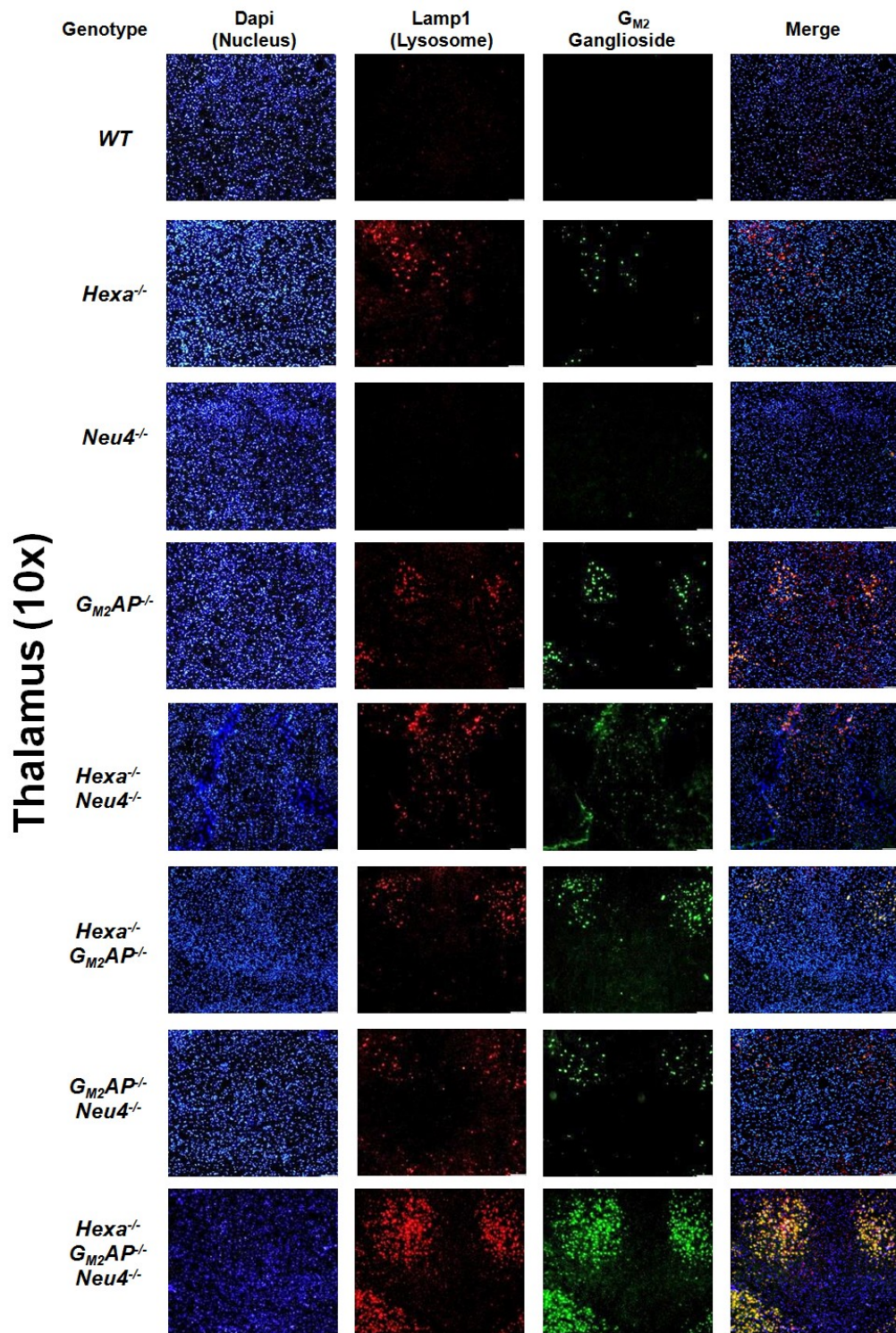


Figure 3.24. Immunostaining of Lamp1 and G_{M2} ganglioside in 6-month-old *WT*, *Hexa*^{-/-}, *Neu4*^{-/-}, *G_{M2}AP*^{-/-}, *Hexa*^{-/-}*Neu4*^{-/-}, *Hexa*^{-/-}*G_{M2}AP*^{-/-}, *G_{M2}AP*^{-/-}*Neu4*^{-/-} and *Hexa*^{-/-}*G_{M2}AP*^{-/-}*Neu4*^{-/-} mice brain coronal sections, thalamus region. (Magnification is 10x, scale bar is for 100μm.) (Images from each genotype were taken under same light intensity that only differs depending on the filter type, Dapi, red or green filters. Then 3 images were merged by modular imaging software platform (cellSens) that is specific to fluorescence microscope Olympus BX53.)

A similar case was observed in the *Hexa*^{-/-}*Neu4*^{-/-}, *Hexa*^{-/-}*G_{M2}AP*^{-/-}, *G_{M2}AP*^{-/-}*Neu4*^{-/-} and *Hexa*^{-/-}*G_{M2}AP*^{-/-}*Neu4*^{-/-} mice where these double and triple mice models had an increased accumulation of G_{M2} ganglioside when they were 6 months old compared to their 3-month-old counterparts (Figure 3.20 and 3.24). An excessive accumulation of the G_{M2} ganglioside was observed in the 6-month-old *Hexa*^{-/-}*G_{M2}AP*^{-/-}*Neu4*^{-/-} mice, and this accumulation affected almost the entire thalamus regions with highly bright three cellular groups (Figure 3.24).

Intensity analysis for cortex region of two age grouped of 8 different genotyped mice revealed that 3-month-old group similar G_{M2} ganglioside level but differently increased by age in all brains cortex region (Figure 3.25). *G_{M2}AP*^{-/-}*Neu4*^{-/-} mice had a 1.3 times increase compared to *G_{M2}AP*^{-/-} and *Hexa*^{-/-}*G_{M2}AP*^{-/-}*Neu4*^{-/-} mice 1.2 times increase compared to *Hexa*^{-/-}*G_{M2}AP*^{-/-} at the age of 6 months.

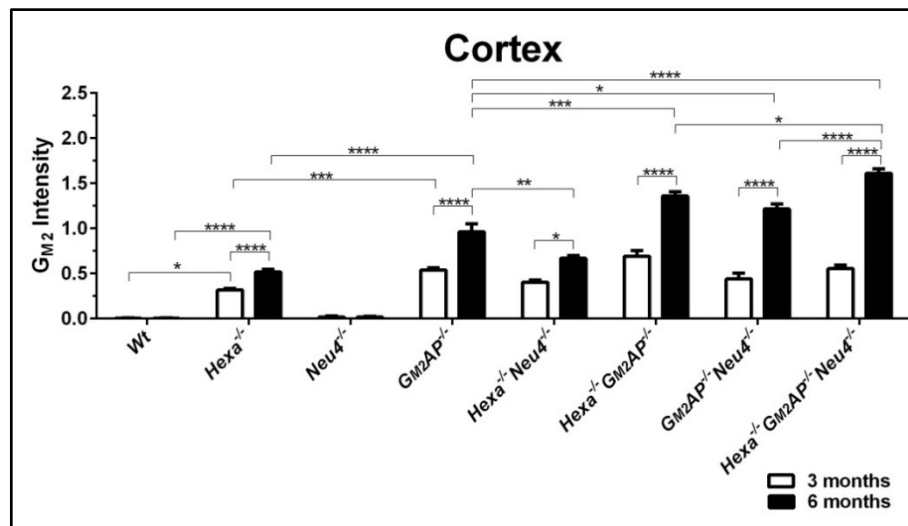


Figure 3.25. Intensity analysis of G_{M2} ganglioside from the 3- and 6-month-old *WT*, *Hexa*^{-/-}, *Neu4*^{-/-}, *G_{M2}AP*^{-/-}, *Hexa*^{-/-}*Neu4*^{-/-}, *Hexa*^{-/-}*G_{M2}AP*^{-/-}, *G_{M2}AP*^{-/-}*Neu4*^{-/-} and *Hexa*^{-/-}*G_{M2}AP*^{-/-}*Neu4*^{-/-} mice brain coronal sections cortex region. (n=2) (*p<0.05, **p<0.005, ***p<0.001, ****p<0.0001) (Intensity was determined by ImageJ and p-values were determined by 2-way-Anova analysis via GraphPad. Data were reported as means ± SE.)

3-month-old group had a similar G_{M2} ganglioside level in hippocampus of different mice brain and this was increased when mice got older (Figure 3.26). *G_{M2}AP*^{-/-}*Neu4*^{-/-} mice had a 1.5 times increase compared to *G_{M2}AP*^{-/-} and *Hexa*^{-/-}*G_{M2}AP*^{-/-}*Neu4*^{-/-} mice 1.2 times increase compared to *Hexa*^{-/-}*G_{M2}AP*^{-/-} at the age of 6 months.

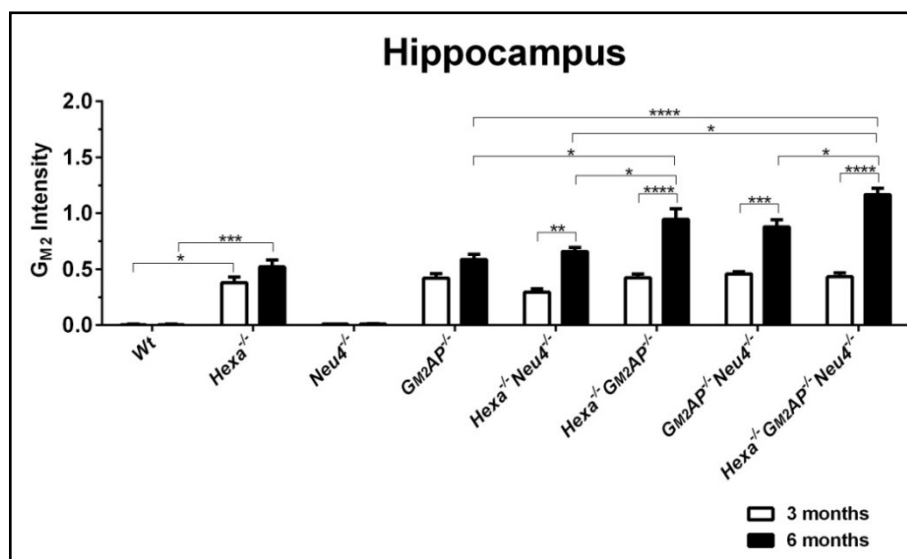


Figure 3.26. Intensity analysis of G_{M2} ganglioside from the 3- and 6-month-old *WT*, *Hexa*^{-/-}, *Neu4*^{-/-}, *GM2AP*^{-/-}, *Hexa*^{-/-}*Neu4*^{-/-}, *Hexa*^{-/-}*GM2AP*^{-/-}, *GM2AP*^{-/-}*Neu4*^{-/-} and *Hexa*^{-/-}*GM2AP*^{-/-}*Neu4*^{-/-} mice brain coronal sections hippocampus region. (n=2) (*p<0.05, **p<0.005, ***p<0.001, ****p<0.0001) (Intensity was determined by ImageJ and p-values were determined by 2-way-Anova analysis via GraphPad. Data were reported as means \pm SE.)

The most significant alteration in the level of G_{M2} ganglioside was observed in thalamus region in the double (*Hexa*^{-/-}*GM2AP*^{-/-} and *GM2AP*^{-/-}*Neu4*^{-/-}) and triple deficient mice (Figure 3.27). *GM2AP*^{-/-}*Neu4*^{-/-} mice had a 2.6 times increase compared to *GM2AP*^{-/-} and *Hexa*^{-/-}*GM2AP*^{-/-}*Neu4*^{-/-} mice 8 times increase compared to *Hexa*^{-/-}*GM2AP*^{-/-} at the age of 6 months.

3.4. Imaging Mass Spectrometry Results

This analysis could be performed for only 3-month-old mice group because of high cost. In addition to thin layer chromatography and immunohistochemical analysis, the absence of G_{M2} ganglioside was confirmed by this method in *Neu4*^{-/-} brain (Figure 3.28). The analysis of the sagittal mouse brain sections (Figure 2.1) by MALDI-IMS demonstrated that the accumulation of G_{M2} ganglioside was not only in the cortex, hippocampus and thalamus regions in the *Hexa*^{-/-} and *Hexa*^{-/-}*Neu4*^{-/-} mice, but in the forebrains of each mouse also with a high concentration in the *Hexa*^{-/-}*Neu4*^{-/-} mice compared to the *Hexa*^{-/-} mice only for $G_{M2}(d36:1)$ and not for $G_{M2}(d38:1)$ (Figure 3.25).

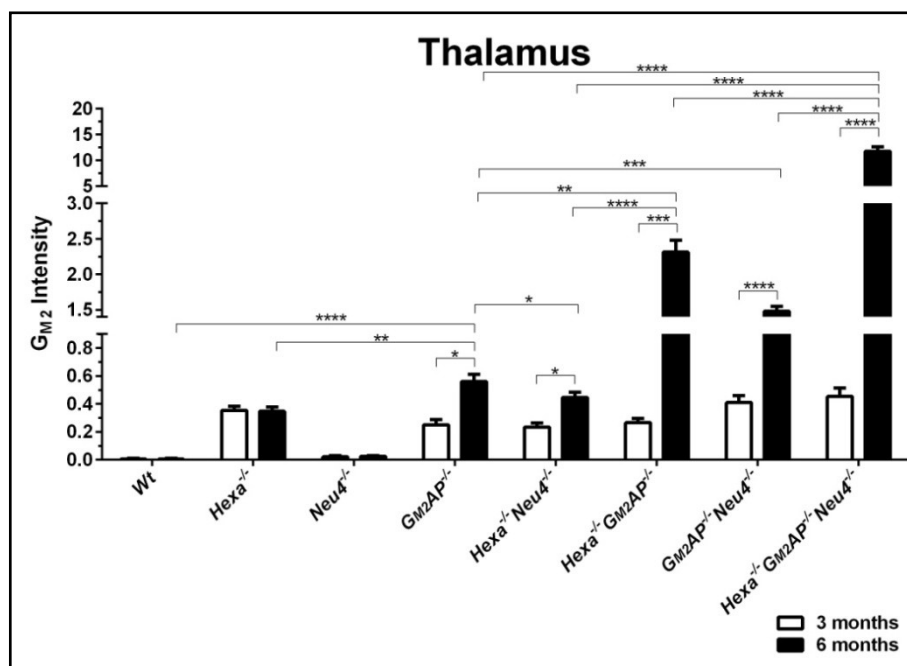


Figure 3.27. Intensity analysis of G_{M2} ganglioside from the 3- and 6-month-old *WT*, *Hexa*^{-/-}, *Neu4*^{-/-}, *G_{M2}AP*^{-/-}, *Hexa*^{-/-}*Neu4*^{-/-}, *Hexa*^{-/-}*G_{M2}AP*^{-/-}, *G_{M2}AP*^{-/-}*Neu4*^{-/-} and *Hexa*^{-/-}*G_{M2}AP*^{-/-}*Neu4*^{-/-} mice brain coronal sections thalamus region. (n=2) (*p<0.05, **p<0.005, ***p<0.001, ****p<0.0001) (Intensity was determined by ImageJ and p-values were determined by 2-way-Anova analysis via GraphPad. Data were reported as means ± SE.)

The *G_{M2}AP*^{-/-} mice had a higher concentration of G_{M2} ganglioside compared to the *Hexa*^{-/-} mice along the brain regions for both types of G_{M2} (d36:1) and G_{M2} (d38:1). The distribution of the two subgroups was different, and the G_{M2} (d36:1) ganglioside had a higher concentration in hypothalamus, and cerebellum while G_{M2} (d38:1) had a higher concentration at the thalamus region (Figure 3.28).

In the brains of *Hexa*^{-/-}*G_{M2}AP*^{-/-}, it was observed that the G_{M2} (d36:1) ganglioside and G_{M2} (d38:1) ganglioside distribution was also different from each other. The level of G_{M2} (d36:1) ganglioside was higher than that of the G_{M2} (d38:1) ganglioside when the brain was considered as a whole. The *G_{M2}AP*^{-/-}*Neu4*^{-/-} mice had a low level of G_{M2} (d38:1) ganglioside compared to the *G_{M2}AP*^{-/-} mice. Although the G_{M2} (d36:1) ganglioside level was similar with the *G_{M2}AP*^{-/-} mice in the *G_{M2}AP*^{-/-}*Neu4*^{-/-} mice, the distribution of this ganglioside was different in the *G_{M2}AP*^{-/-}*Neu4*^{-/-} mice than the *G_{M2}AP*^{-/-} mice (Figure 3.28). A higher concentration of G_{M2} (d36:1) ganglioside was observed in the *Hexa*^{-/-}*G_{M2}AP*^{-/-}*Neu4*^{-/-} mice with an accumulation in the olfactory bulbs, hypothalamus and cerebellum regions while the G_{M2} (d38:1) ganglioside was accumulated mostly in the cerebellums of mice (Figure 3.28).

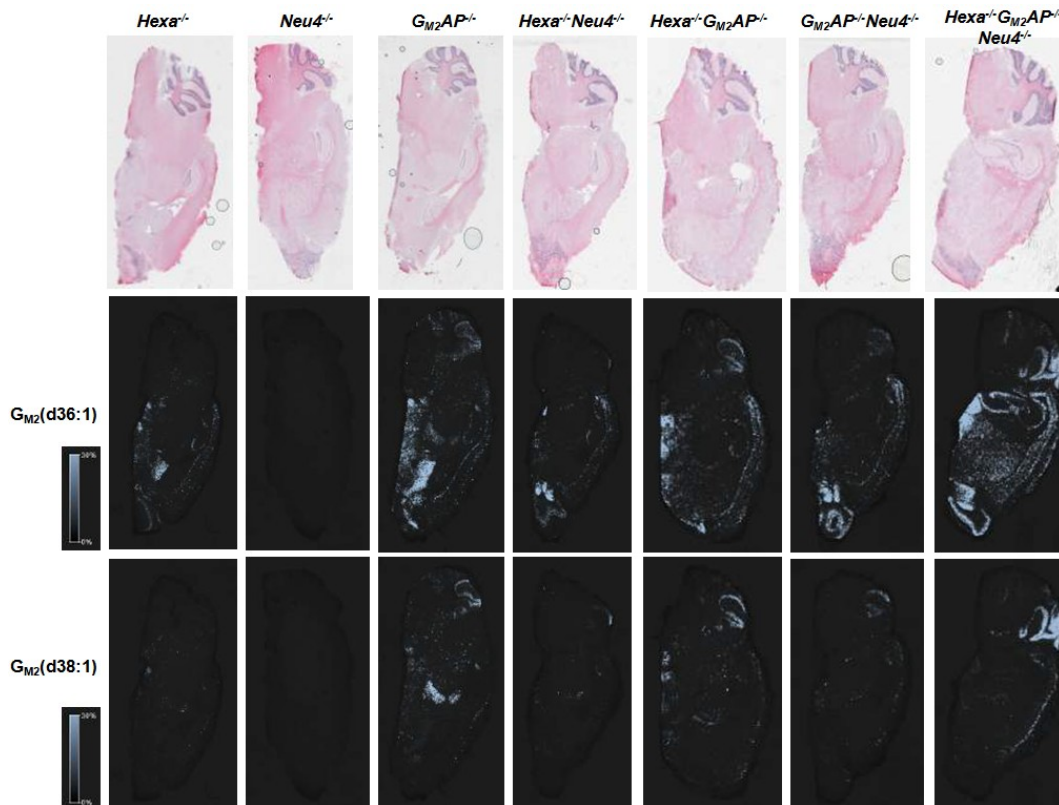


Figure 3.28. Distribution of G_{M2} ganglioside (d36:1 and d38:1) in 3-month-old $Hexa^{-/-}$, $Neu4^{-/-}$, $G_{M2AP}^{-/-}$, $Hexa^{-/-}Neu4^{-/-}$, $Hexa^{-/-}G_{M2AP}^{-/-}$, $G_{M2AP}^{-/-}Neu4^{-/-}$ and $Hexa^{-/-}G_{M2AP}^{-/-}Neu4^{-/-}$ mice brain sagittal sections. Data was obtained by imaging mass spectrometric analysis performed by Katrin Erich, from mice brains which were sent to Prof. Dr. Roger Sandhoff's laboratory (German Cancer Research Center, Heidelberg, Germany).

G_{M1} ganglioside (d36:1) and (d38:1) were detected for all the mice analyzed. A higher concentration was observed in the $G_{M2AP}^{-/-}$ mice for both of the subgroups throughout the brains with a differentiated distribution (Figure 3.29). The G_{M1} ganglioside (d36:1) was not detectable at a very low level in the cerebellum of $Neu4^{-/-}$ mice.

The third and the last ganglioside analyzed by MALDI-IMS was the G_{D1} ganglioside. It was observed that the accumulation of G_{D1} (d38:1) ganglioside was much higher in $G_{M2AP}^{-/-}$ relative to the $Hexa^{-/-}$, and higher in $Hexa^{-/-}$ compared to the other mice brains (Figure 3.30). The distributions and the concentrations were similar for G_{D1} (d38:1) ganglioside in the brains of $Neu4^{-/-}$, $Hexa^{-/-}Neu4^{-/-}$ and $Hexa^{-/-}G_{M2AP}^{-/-}Neu4^{-/-}$ mice (Figure 3.30). The $Hexa^{-/-}$, $G_{M2AP}^{-/-}$, $Hexa^{-/-}G_{M2AP}^{-/-}$ and $G_{M2AP}^{-/-}Neu4^{-/-}$ mice

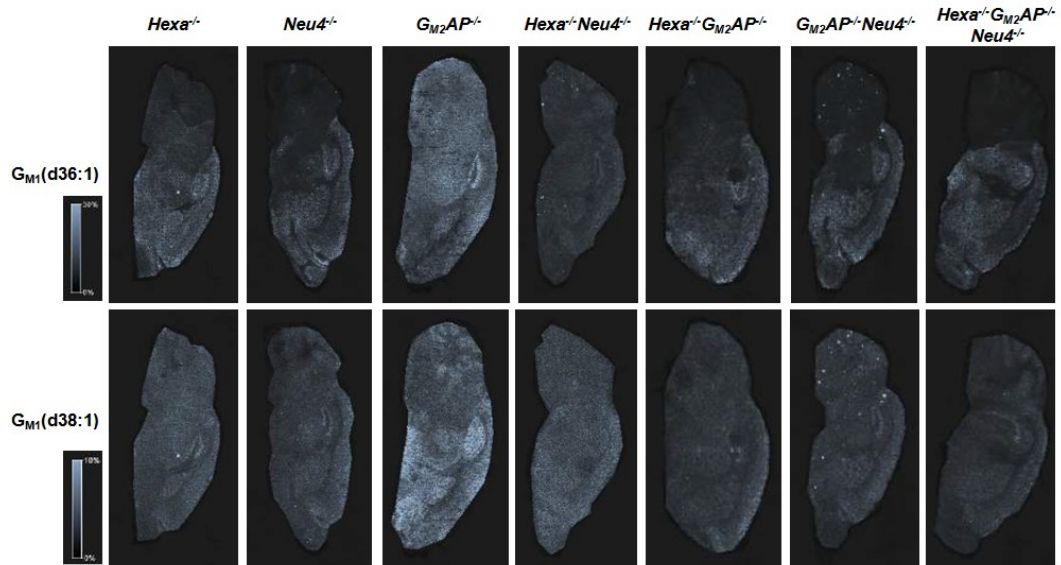


Figure 3.29. Distribution of G_{M1} ganglioside (d36:1 and d38:1) in 3-month-old $Hexa^{-/-}$, $Neu4^{-/-}$, $G_{M2AP}^{-/-}$, $Hexa^{-/-}Neu4^{-/-}$, $Hexa^{-/-}G_{M2AP}^{-/-}$, $G_{M2AP}^{-/-}Neu4^{-/-}$ and $Hexa^{-/-}G_{M2AP}^{-/-}Neu4^{-/-}$ mice brain sagittal sections. Data was obtained by imaging mass spectrometric analysis performed by Katrin Erich, from mice brains which were sent to Prof. Dr. Roger Sandhoff's laboratory (German Cancer Research Center, Heidelberg, Germany).

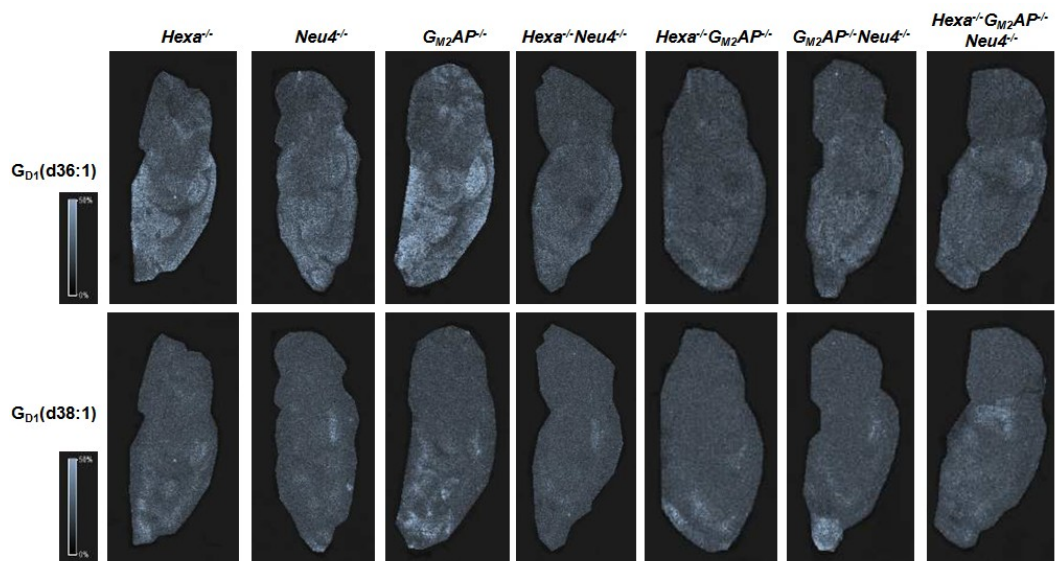


Figure 3.30. Distribution of G_{D1} ganglioside (d36:1 and d38:1) in 3-month-old $Hexa^{-/-}$, $Neu4^{-/-}$, $G_{M2AP}^{-/-}$, $Hexa^{-/-}Neu4^{-/-}$, $Hexa^{-/-}G_{M2AP}^{-/-}$, $G_{M2AP}^{-/-}Neu4^{-/-}$ and $Hexa^{-/-}G_{M2AP}^{-/-}Neu4^{-/-}$ mice brain sagittal sections. Data was obtained by imaging mass spectrometric analysis performed by Katrin Erich, from mice brains which were sent to Prof. Dr. Roger Sandhoff's laboratory (German Cancer Research Center, Heidelberg, Germany).

had a higher level of G_{D1}(d38:1) ganglioside in their olfactory bulbs compared to the other mice, with a higher distribution throughout the septum and hypothalamus regions in the *G_{M2AP}^{-/-}* mice brains (Figure 3.30).

3.5. Behavioral Test Results

3.5.1. Rotarod Test Results

The Rotarod test was performed in order to analyze if the accumulated gangliosides in brain influence the motor coordination of mice. The results from the 3- and 6-month-old mice demonstrated that all of the knock-out mice could run less than the wild type mice on an accelerating rotating rod (Figure 3.31). Although the *Hexa*^{-/-}, *Neu4*^{-/-} and *Hexa*^{-/-}*Neu4*^{-/-} mice ran for a similar duration in both ages examined, it was observed that the *G_{M2AP}^{-/-}*, *Hexa*^{-/-}*G_{M2AP}^{-/-}* and *Hexa*^{-/-}*G_{M2AP}^{-/-}**Neu4*^{-/-} mice had a reduced running duration over the 6-month-old group compared to their 3-month-old counterparts.

Two females from the 6-month-old *Hexa*^{-/-}*G_{M2AP}^{-/-}* (n=8) group, one male from the 3-month-old *Hexa*^{-/-}*G_{M2AP}^{-/-}**Neu4*^{-/-} (n=4) group, and one female and one male from 6-month-old *Hexa*^{-/-}*G_{M2AP}^{-/-}**Neu4*^{-/-} (n=4) group could not stand still on the rotating rod during the test experiment. The reduced duration on the accelerating rotating rod indicates that those mice had a reduced motor coordination depending on the accumulated gangliosides in their brain cortex (Figure 3.18 and 3.22).

3.5.2. Hot Plate Test Results

The pain resulted by different stimuli such as tissue damage or high/low temperature is called nociceptive pain, and the hot plate test is utilized in order to examine the thermal pain sensitivity of differently genotyped mice⁵⁹.

Gangliosides are found on the outer leaflet of the cell membrane, and they have many different functions on normal physiological and pathological conditions by the regulation of cellular signaling⁵. Gangliosides are also thought to have possible functions on feeling the pain and responding to the pain that include the activation of pain receptors and signal transduction between the tissue and brain cells⁵⁸.

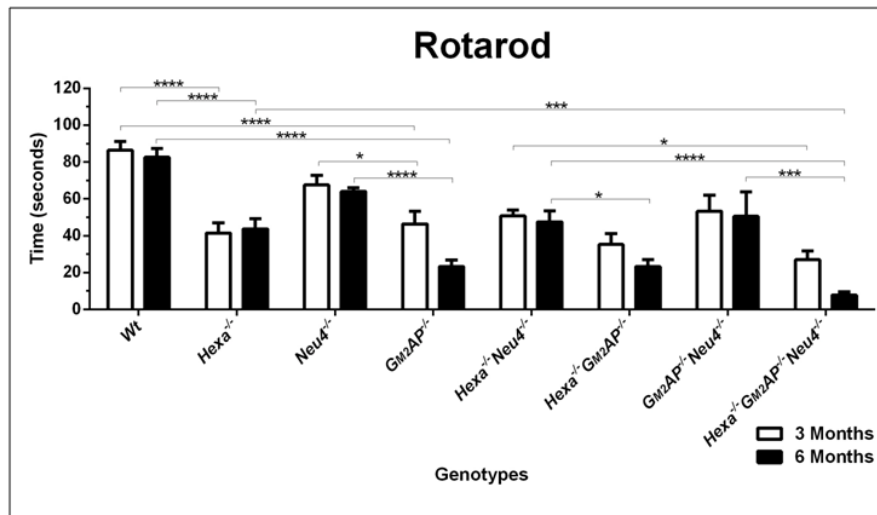


Figure 3.31. Running time on rotarod of 3- and 6-month-old *WT*, *Hexa*^{-/-}, *Neu4*^{-/-}, *GM2AP*^{-/-}, *Hexa*^{-/-}*Neu4*^{-/-}, *Hexa*^{-/-}*GM2AP*^{-/-}, *GM2AP*^{-/-}*Neu4*^{-/-} and *Hexa*^{-/-}*GM2AP*^{-/-}*Neu4*^{-/-} mice. The test was performed for three times for each mouse after a training run that was done to teach mice how to stay and run on rotating rod. *Hexa*^{-/-} (n=4 for both ages), *GM2AP*^{-/-} (n=4 for 3-month-old, n=6 for 6-month-old group), *Hexa*^{-/-}*Neu4*^{-/-} (n=6 for 3-month-old, n=4 for 6-month-old group), *Hexa*^{-/-}*GM2AP*^{-/-} (n=4 for 3-month-old, n=8 for 6-month-old group, 2 of 8 didn't run on rotating rod in the test experiment), *GM2AP*^{-/-}*Neu4*^{-/-} (n=4 for both ages) and *Hexa*^{-/-}*GM2AP*^{-/-}*Neu4*^{-/-} (n=4 for both ages, 1 of 4 at the age of 3 months and 2 of 4 at the age of 6 months didn't run on rotating rod in the test experiment), mice show differences in motor coordination and possible memory deficit when compared with wild type (n=4 for 3-month-old, n=6 for 6-month-old group) and *Neu4*^{-/-} (n=4 for 3-month-old, n=5 for 6-month-old group) mice. (*p<0.05, ***p<0.001, ****p<0.0001) (p-values were determined by 2-way-Anova analysis via GraphPad. Data were reported as means ± SE.)

Thalamus is the region responsible for sending sensory information, including pain signals, to the cortex. It was shown that alterations in the thalamic region were associated with many different types of pain disorders⁶⁰. The hot plate test revealed that the accumulated gangliosides, especially when in thalamus region (Figure 3.20 and 3.24), might block the signaling pathway or the response to pain. Although the first response, the time of paw licking, was similar for all of the mice, the shaking time was significantly higher in the *Hexa*^{-/-}*GM2AP*^{-/-} mice (Figure 3.32A and B). The final response to the hot stimuli was jumping. The time of jumping was significantly lower in the *GM2AP* deficient single, double and triple mice compared to the wild type (Figure 3.32C), indicating that the deficient mice might have a reduced nociceptive sensitivity.

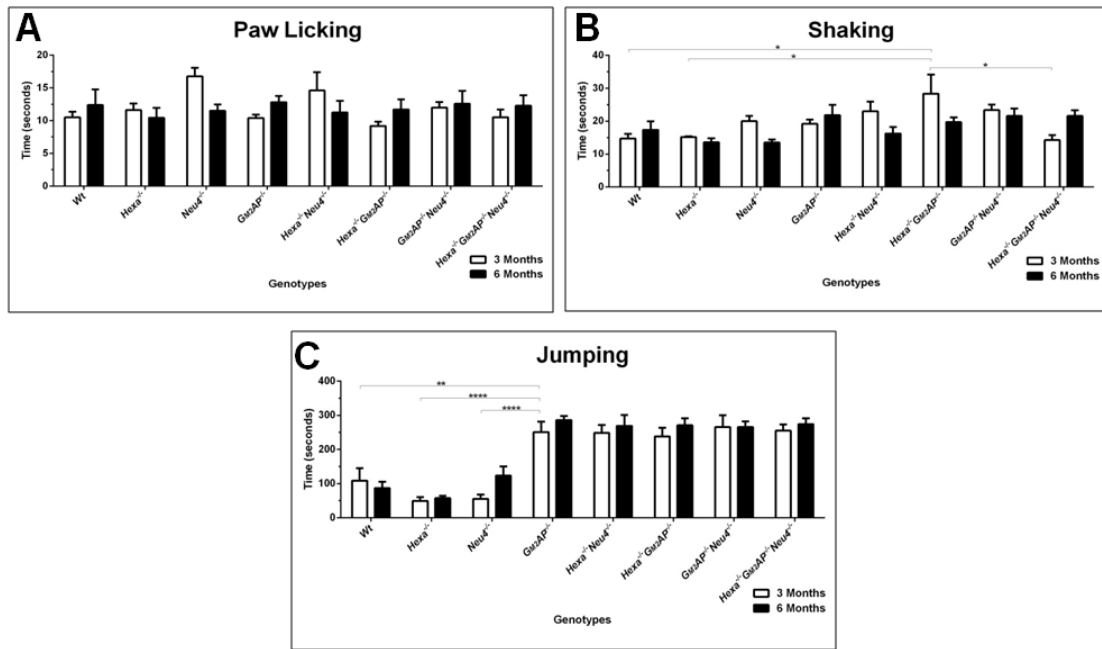


Figure 3.32. Paw licking (A), shaking (B), and jumping (C) times of 3- and 6-month-old *WT*, *Hexa*^{-/-}, *Neu4*^{-/-}, *G_{M2}AP*^{-/-}, *Hexa*^{-/-}*Neu4*^{-/-}, *Hexa*^{-/-}*G_{M2}AP*^{-/-}, *G_{M2}AP*^{-/-}*Neu4*^{-/-} and *Hexa*^{-/-}*G_{M2}AP*^{-/-}*Neu4*^{-/-} mice. During the experiment 300 seconds was set as cut-off time, those which did not jump were taken out and scored as 301s. There was no training for this experiment and each mouse was tested for one time due to the test feature. *G_{M2}AP*^{-/-} (n=4 for 3-month-old and n=6 for 6-month-old group), *Hexa*^{-/-}*Neu4*^{-/-} (n=4 for both ages), *Hexa*^{-/-}*G_{M2}AP*^{-/-} (n=4 for 3-month-old and n=6 for 6-month-old group), *G_{M2}AP*^{-/-}*Neu4*^{-/-} (n=4 for both ages), and *Hexa*^{-/-}*G_{M2}AP*^{-/-}*Neu4*^{-/-} (n=4 for 3-month-old and n=6 for 6-month-old group) mice showed a reduced nociceptive sensitivity and had a latency to jump from hot plate compared to wild type (n=4 for 3-month-old and n=5 for 6-month-old group), *Hexa*^{-/-} (n=4 for 3-month-old and n=6 for 6-month-old group), *Neu4*^{-/-} (n=4 for both ages). (*p<0.05, **p<0.005, ****p<0.0001) (p-values were determined by 2-way-Anova analysis via GraphPad. Data were reported as means ± SE.)

CHAPTER 4

DISCUSSION

Mice models are widely used for investigating human disease and biology due to genetic and physiological similarities between the species. Within the frame of this study, a possible cooperation of the sialidase *Neu4* and *G_{M2} activator protein* in the degradation of gangliosides was investigated taking advantage of the newly produced double and triple deficient mice models, by crossing the available *Hexa^{-/-}Neu4^{-/-}* and *GM2AP^{-/-}* mice. By this cross, *WT*, the *Hexa^{-/-}*, *Neu4^{-/-}*, *GM2AP^{-/-}*, *Hexa^{-/-}Neu4^{-/-}*, *Hexa^{-/-}GM2AP^{-/-}*, *GM2AP^{-/-}Neu4^{-/-}* and *Hexa^{-/-}GM2AP^{-/-}Neu4^{-/-}* mice were generated following the F2 generation by appropriate sibling in breeding. 3- and 6-month-old groups were studied for in order to evaluate the information regarding the age-dependent discrepancy on the metabolisms of mice.

After all of the brain samples were collected (8 different genotype, n=2-4 depending on the experiment), the biochemical analysis from the soft brain tissues were applied via three different ways as in the following: The analysis of brain gangliosides, the analysis of relative gene expression, and the analysis of enzyme activities. In other concept paraformaldehyde fixed brain tissues were used for immunohistochemical analysis. Brains of mice were also analyzed by imaging mass spectrometry to observe region specific distribution of gangliosides. Different then brain tissues, collected urines of mice were studied to reveal accumulation of free oligosaccharides. Lastly two different behavioral analyses were performed from each mouse to see the affect of ganglioside alteration on motor coordination and pain response.

The thin layer chromatography was used to analyze brain gangliosides depending on their chromatographic mobility and staining reactivity with the comparison of the standards⁶¹. The *G_{A2}* ganglioside is one of the 0-series gangliosides originating from the lactosylceramide (Figure 1.1). It accumulates in cells with the breakdown of ganglioside degradation pathway. An accumulation of the *G_{A2}* ganglioside was observed in two types of the *G_{M2}* gangliosidosis mice models: The *Hexb^{-/-}* mice had a higher concentration of the *G_{A2}* ganglioside in their brains compared to the *GM2AP^{-/-}* mice, while the *Hexa^{-/-}* mice had almost none⁴⁵. When we compared the

band intensities of G_{A2} ganglioside in the *WT*, *Hexa*^{-/-}, *Neu4*^{-/-}, *G_{M2}AP*^{-/-}, *Hexa*^{-/-}*Neu4*^{-/-}, *Hexa*^{-/-}*G_{M2}AP*^{-/-}, *G_{M2}AP*^{-/-}*Neu4*^{-/-} and *Hexa*^{-/-}*G_{M2}AP*^{-/-}*Neu4*^{-/-} mice, we notified that in both 3- and 6-month-old groups had a significant accumulation of the G_{A2} ganglioside in the *Hexa*^{-/-} mice brain, similar to the case of the *Hexa*^{-/-}*Neu4*^{-/-} mice, which was not detected in the *WT* and *Neu4*^{-/-} mice (Figure 3.6). While the accumulation level in the *G_{M2}AP*^{-/-} mice was similar to that of the *Hexa*^{-/-} mice for the 3-month-old group, an increase of three times was observed in the 6-month-old *G_{M2}AP*^{-/-} mice compared to the same aged *Hexa*^{-/-} mice. When the deficiencies of *Hexa*^{-/-} and *G_{M2}AP*^{-/-} combined in the double deficient mice model (*Hexa*^{-/-}*G_{M2}AP*^{-/-}), the accumulation of G_{A2} ganglioside was increased 1.8 time in the 3-month-old, and 1.5 time in the 6-month-old groups compared to the *G_{M2}AP*^{-/-} mice (Figure 3.6). *In vivo* approved that these two enzymes co-operate on the G_{M2} ganglioside degradation as also previously remarked *in vitro*²¹. It is therefore demonstrated for the first time in this study that the 3-month-old *Hexa*^{-/-}*G_{M2}AP*^{-/-}*Neu4*^{-/-} mice had a close level of the G_{A2} ganglioside which decreased at their 6th month for 0.78 times compared to the *Hexa*^{-/-}*G_{M2}AP*^{-/-} mice (Figure 3.6), while the *G_{M2}AP*^{-/-}*Neu4*^{-/-} mice had a slightly higher level of the G_{A2} ganglioside relative to the 3-month-old *G_{M2}AP*^{-/-} mice for 1.14 times, and 6-month-old mice for 1.15 times.

The lactosylceramide accumulation on lysosomal storage disorders was previously indicated not only in the sphingolipid activator protein deficient mice model⁶², but also in the Tay-Sachs disease model¹³. The analysis of lactosylceramide band intensities in these eight differently-genotyped mice demonstrated that there was not found an accumulation of this lipid in any of the mice at any ages (Figure 3.8A). Since the lactosylceramide does not have sialic acid residue in its formation (Figure 1.1), the sialidase *Neu4* cannot function on it. A similar level in different mice revealed that *G_{M2}AP* did not have a degradability effect on the lactosylceramide *in vivo*, either.

G_{M1} ganglioside is none of the a-series ganglioside mediating several physiological and pathological processes in cell⁶³. The concentration of G_{M1} ganglioside was significantly decreased in 3- and 6-month-old *Neu4*^{-/-} mice, and the 3-month-old *Hexa*^{-/-}*Neu4*^{-/-} mice compared to the *WT* mice (Figure 3.8B), as noted previously¹⁰. An accumulation or diminution was not observed in the other genotypes at any ages (Figure 3.8B).

G_{M2} ganglioside is the other a-series ganglioside synthesized from the G_{M3} ganglioside (Figure 1.1). It is accumulated in the G_{M2} gangliosidosis⁶⁴. The chromatographic analysis of the deficient mice brains in this study revealed an

increased level of the G_{M2} ganglioside accumulation in the *Hexa*^{-/-}*G_{M2}AP*^{-/-} mice compared to the *G_{M2}AP*^{-/-} mice at their 3 and 6 months (Figure 3.7). However, the G_{M2} ganglioside level was similar and did not change significantly in the *G_{M2}AP*^{-/-}*Neu4*^{-/-} mice compared to the *G_{M2}AP*^{-/-} mice, as well as in the *Hexa*^{-/-}*G_{M2}AP*^{-/-}*Neu4*^{-/-} mice compared to the *Hexa*^{-/-}*G_{M2}AP*^{-/-} mice.

Since the sialidase *Neu4* is responsible for the degradation of two sialic acids having an a-series ganglioside, the G_{D1a} ganglioside¹⁰, an increased level of G_{D1a} in the *Neu4*^{-/-} mice was compatible with the decreased level of G_{M1} ganglioside in the same mice group. In the other genotypes, a significant change was not observed again, which might imply that the sialidase *Neu4* functions on this ganglioside along with *G_{M2}AP* (Figure 3.8C). Two of the b-series gangliosides, G_{D1b} and G_{T1b}, being the major component of the myelin formation⁴ and known to improve the synaptic plasticity in the hippocampus region of brain⁶⁵, did not hold a varied intensity between different mice studied (Figure 3.9A and 3.9B) at both ages.

To date, more than fifty different lysosomal storage diseases have been identified to be rare inherited metabolic disorders caused by some defects in the lysosomal enzymes, cofactors or transport proteins as a result of the disruption in the lysosomal degradation pathway of biomolecules which can be classed according to the material accumulated^{29,30}. Deficiencies of lysosomal hydrolases or degradation related protein can lead to the accumulation of secondary intermediate metabolites from glycoprotein or glycolipid degradation pathways, including free oligosaccharides and glycoaminoacids, which may accumulate in urine³⁴. In galactosialidosis (an accumulation of oligosaccharides, glycoproteins and glycolipids), mucopolysaccharidosis (an accumulation of glycosaminoglycans) and mannosidosis (an accumulation of glycoproteins) diseases, the oligosaccharides increase as well, as a consequence of the enzyme defect, and it is excreted by the urine³¹. Urines of the *WT*, *Hexa*^{-/-}, *Neu4*^{-/-}, *G_{M2}AP*^{-/-}, *Hexa*^{-/-}*Neu4*^{-/-}, *Hexa*^{-/-}*G_{M2}AP*^{-/-}, *G_{M2}AP*^{-/-}*Neu4*^{-/-} and *Hexa*^{-/-}*G_{M2}AP*^{-/-}*Neu4*^{-/-} mice were studied by the thin layer chromatography in order to analyze the deficiency of different lysosomal enzymes or proteins affecting the degradation of oligosaccharides. Although an alteration can be observed on the chromatography (Figure 3.10), intensities of two bands only can be specifically measured by the ImageJ. Compared to the standard sugars/oligosaccharides loaded on the plate, these two bands are defined to be galactose and raffinose. While the galactose decreased in the *Hexa*^{-/-} and *Neu4*^{-/-} mice, it increased 1.67 times in the *Hexa*^{-/-}*G_{M2}AP*^{-/-}*Neu4*^{-/-} mice compared to

the *WT* mice (Figure 3.11A). The *G_{M2}AP^{-/-}Neu4^{-/-}* mice had a level of galactose 1.22 times more than that of the *G_{M2}AP^{-/-}* mice, which might be a result of the changed lysosomal environment in the double deficient mice. Raffinose is a trisaccharide composed of glucose, galactose and fructose molecules. The intensity of this oligosaccharide is lower in the *Hexa^{-/-}* and *Neu4^{-/-}* mice compared to the *WT*, as also noted in the galactose concentration (Figure 3.11B). The *G_{M2}AP^{-/-}* mice had a similar level with the *WT* mice, however, an additional deficiency of the *Hexa* or *Neu4* enzyme resulted in a lower level of raffinose in the *Hexa^{-/-}G_{M2}AP^{-/-}* and *G_{M2}AP^{-/-}Neu4^{-/-}* mice, respectively. Interestingly, in the results of the *Hexa^{-/-}Neu4^{-/-}* mice was a thick band formation between the raffinose and lactose, which could not be identified by the comparison to our standards (Figure 3.10). It was previously noted that the analysis of the excreted urinary oligosaccharides could provide information concerning the deficiency of enzyme, and could be utilized for the diagnosis depending on the accumulated types³⁶. Analysis of the urinary oligosaccharides in the *Hexa^{-/-}Neu4^{-/-}*, *Hexa^{-/-}G_{M2}AP^{-/-}*, *G_{M2}AP^{-/-}Neu4^{-/-}* and *Hexa^{-/-}G_{M2}AP^{-/-}Neu4^{-/-}* mice was performed for the first time in this study with chromatography. An altered pattern has been observed in the mice of concern, revealing that studying the urine with other sensitive methods like MALDI-TOF mass spectrometry³⁴ might provide more reliable results.

The relative gene expression analysis was applied in order to observe the deficiency of lysosomal enzymes/protein caused the changes in the expression level of the ganglioside synthesis and the degradation enzymes. The *Lactosylceramide synthase (B4Galt6)* gene expression levels were unaffected by the deficiency of different enzymes/protein (Figure 3.14A), where the concentration of LacCer did not change over all the mice analyzed with the chromatography (Figure 3.9A). The *N-acetylgalactosaminyl transferase 1 (Galgt1)* (Figure 3.14B) and *Galactosyl transferase (B3Galt4)* (Figure 3.15C) gene expressions did not change, either, indicating that the ganglioside synthesis pathway was not altered widely. There still were some changes in the level of two synthesis enzymes, namely *G_{M3}S* and *G_{D3}S*. The absence of *G_{M2}AP* may result in a lower level of the *G_{M3}* ganglioside. Since the *G_{M2}* ganglioside cannot be degraded, the *G_{M3}* synthase enzyme expression may increase up to 1.74 times in the *G_{M2}AP^{-/-}Neu4^{-/-}* mice compared to the *Neu4^{-/-}* mice (Figure 3.15A) to meet the need of cells. *G_{D3}S* was higher 1.67 times in 3-month-old *G_{M2}AP^{-/-}* mice compared to the *WT* mice. It was lower in the 6-month-old mice; whereas it reached to the same level with the *WT* mice (Figure 3.15D).

The sialidases were studied as their expressions were previously noted to be changed in the bypass mechanism observed in the Tay-Sachs mice model¹³ as well as in another lysosomal storage disease, the mucopolisaccharidosis type I (MPSI)⁵⁵. The sialidase *Neu1* is the lysosomal sialidase which had the strongest expression among the four sialidases,¹⁴ which exhibited a similar expression ratio for all of the genotypes in all ages, except a lower level in the 6-month-old *G_{M2}AP*^{-/-} mice compared to the *WT* mice (Figure 3.12A). This decrease was unexpected, since it was previously discovered that the 6-month-old *G_{M2}AP* deficient mice had a 1.7 times of an increase in the expression of the sialidase *Neu1* compared to the *WT*⁶⁶. Another study however, noted the expression level of the sialidase *Neu1* to be lower in MPSI model mice brains⁵⁵, indicating that the expression level could be affected by both of the ways in the lysosomal storage diseases. Sialidase *Neu2* is the cytosolic sialidase having an activity through the glycoproteins, oligosaccharides and gangliosides under a neutral pH *in vitro*¹⁴. The expression level of the sialidase *Neu2* was significantly altered among the deficient mice models and ages. Although the expression of the sialidase *Neu2* is approximately 10 times lower than that of the sialidase *Neu1*, changes in the expression ratio might affect the degradation levels of different molecules in cells. The 3-month-old *Hexa*^{-/-}*G_{M2}AP*^{-/-} mice brains exhibited a 4.48 times of an increase in the expression ratio of the sialidase *Neu2* compared to the same age group of the *Hexa*^{-/-} mice (Figure 3.12B). This difference was not conserved through the months passed, and both groups had a similar expression ratio at their 6 months. However, the *G_{M2}AP*^{-/-}*Neu4*^{-/-} and *G_{M2}AP*^{-/-} mice exhibited a similar expression pattern with the *Hexa*^{-/-}*G_{M2}AP*^{-/-} mice, and three of the groups had a higher expression ratio when they were 3 months old. It was significantly lower when they turned 6 months old (Figure 3.12B). This may be a quick response of the cells in order to clean the accumulated macromolecule in lysosomes of the deficient mice brains, and then coming back to the normal expression ratio since the sialidase enzyme was available from then on. On the other hand, an increase for 2.37 times was observed in the 6-month-old *Neu4*^{-/-} mice compared to 3 months of age counterparts (Figure 3.12B). This may be a clue for the sialidase *Neu2* substitution in the absence of *Neu4* to function on the altered ganglioside metabolism as previously suggested¹².

Sialidase *Neu3* is known to be a plasma-membrane associated sialidase where its function on the gangliosides was previously explained *in vitro*¹⁴ and *in vivo*¹³. The

expression level of the sialidase *Neu3* did not exhibit any changes between the genotypes and ages (Figure 3.12C).

Sialidase *Neu4* is the fourth sialidase known to construct two different forms, namely long and short, and found in two different subcellular locations, lysosome²⁵ and mitochondria²⁷. Restoration of normal morphological phenotype in the *Neu1* deficient sialidosis fibroblasts by the elimination of undigested substrates after the over expression of the sialidase *Neu4* revealed that *Neu4* is biologically active against a majority of endogenous substrates of the sialidase *Neu1* such as glycoproteins, oligosaccharides and sialylated glycolipids²⁵. Besides presenting an altered G_{D1a} and G_{M1} gangliosides level in the single deficiency of sialidase¹⁰, the epileptic seizures and rapid neuronal loss due to the G_{M2} ganglioside accumulation in the double deficient mice, *Hexa*^{-/-}*Neu4*^{-/-11} emphasizes the importance of the sialidase *Neu4* in the degradation of gangliosides. The expression profile for was performed for the *WT*, *Hexa*^{-/-}, *G_{M2AP}*^{-/-}, *Hexa*^{-/-}*G_{M2AP}*^{-/-} mice, and significant changes were observed only in the 6-month-old *G_{M2AP}*^{-/-} mice compared to the 3-month-old mice (Figure 3.12D). The decrease of 2.65 times may have resulted by the absence of *G_{M2AP}*, since they might have been co-operating. Considering all of the gene expression profiles for the sialidasases, it can be reasonable to think that there could not be so many alterations, regular increases or decreases correlated to the deficiencies. However, by the specific sialidase activity measured depending on the free fluorescent tag, cleaved by 4MU-NANA via the enzyme activity in brain tissue, it can be referred that there was an increase of 1.99 to 2.07 times in the activity of the sialidase in the 6-month-old *G_{M2AP}*^{-/-}*Neu4*^{-/-} and *Hexa*^{-/-}*G_{M2AP}*^{-/-}*Neu4*^{-/-} mice compared to the *Neu4*^{-/-} mice, respectively (Figure 3.16A). An increase of 2.73 times was noted in the 3-month-old *Hexa*^{-/-}*G_{M2AP}*^{-/-} mice as well, compared to the *Hexa*^{-/-} mice, similarly to the case of the sialidase *Neu2* in the expression level (Figure 3.12B), which refers to a higher sialidase activity due to the sialidase *Neu2*.

The intensities of both the G_{A2} and G_{M2} gangliosides differ in each genotype and age, however, their degradation enzymes, β-Hexosaminidase b (*Hexb*) and *G_{M2AP}* did not present any significant changes in the expression levels (Figure 3.13A and 3.13B). Although it was previously noted that the *Hexb* mRNA levels were higher for 1.4 to 1.3 times in the *Hexa*^{-/-} and *G_{M2AP}*^{-/-} mice, respectively, and the *G_{M2AP}* mRNA level increased for 1.5 times in the *Hexa*^{-/-} mice when 6 month old⁶⁶; our results did not prove any expression regulation over the mentioned genes in the absence of other lysosomal

degradation enzymes. Different from the unchanged expression ratio, activity of the Hexb enzyme was only slightly -1.1 times higher in the 3-month-old *Hexa*^{-/-}*Neu4*^{-/-} mice compared to the *Hexa*^{-/-} mice, and significantly - 2.88 to 2.95 times higher in the 6-month-old *Hexa*^{-/-}*G_{M2}AP*^{-/-}*Neu4*^{-/-} mice compared to the *Hexa*^{-/-}*Neu4*^{-/-} and *Hexa*^{-/-} mice, respectively (Figure 3.16B).

β-Galactosidase enzyme is responsible for the removal of galactose residue from different gangliosides such as G_{A1}, G_{M1} and G_{D1b} (Figure 1.2) in order to form simple ones via their degradation in lysosomes. Generally the expression level of this enzyme was stable or decreasing by age (Figure 3.13C). The decrease was observed in the 6-month-old *G_{M2}AP*^{-/-}, *Hexa*^{-/-}*G_{M2}AP*^{-/-} and *G_{M2}AP*^{-/-}*Neu4*^{-/-} mice compared to the 3-month-old group. Since the activity of this enzyme did not alter significantly between genotypes (Figure 3.16C), it may infer that the variances in the expression level did not correlate with the activity of the enzyme. Significant decrease was only seen in *G_{M2}AP*^{-/-} mice compared to *Hexa*^{-/-} mice at 3-month-old group (Figure 3.16C). Since there was reduced activity in the absence of *G_{M2}AP*, this may show possible *in vivo* involvement of *G_{M2}AP* in the degradation of G_{M1} with *β-Galactosidase*, which was shown previously *in vitro*²⁰. Unchanged enzyme activity in *Neu4* deficiency having double and triple mice could be the result of reduced level of G_{M1} ganglioside seen in the deficiency of sialidase *Neu4*.

β-Glucosidase is the enzyme which degrades the glucosylceramide in lysosomes (Figure 1.2). Its deficiency results in another lysosomal storage disorder, namely the Gaucher disease. It is known that most of the lysosomal diseases share a common biochemical and metabolic feature³¹, although different enzymes are affected in different diseases. Therefore, the analysis of this enzyme via our pathway may provide some information about the lysosomal conditions. Although the gene expression analysis was not performed for the mentioned enzyme, the activity measurement was realized in order to reveal if the changed lysosomal environment, depending on the accumulated gangliosides, to affect other lysosomal enzymes. Under the thin layer chromatography analysis of 3- and 6-month-old mice, we could not directly detect the glucosylceramide bands (Figure 3.3 and 3.5). Hence, we cannot confidently state the presence or absence of an accumulation of glucosylceramide. Nevertheless, the increments of *β-Glucosidase* activity in the *G_{M2}AP*^{-/-}, *Hexa*^{-/-}*G_{M2}AP*^{-/-}, *G_{M2}AP*^{-/-}*Neu4*^{-/-} and *Hexa*^{-/-}*G_{M2}AP*^{-/-}*Neu4*^{-/-} mice indirectly implied the presence of a lysosomal accumulation of glucosylceramide which needed to be cleaned by the enzyme activity.

In the 6-month-old $G_{M2}AP^{-/-}Neu4^{-/-}$ mice, the activity increased for 4.03 times compared to the $G_{M2}AP^{-/-}$ mice, which may be a hint for the possible responsibility of the sialidase *Neu4* over that deficiency (Figure 3.16D). The 3-month-old $Hexa^{-/-}G_{M2}AP^{-/-}Neu4^{-/-}$, $Hexa^{-/-}G_{M2}AP^{-/-}$ and $Hexa^{-/-}Neu4^{-/-}$ mice had enzyme activities 5.92, 5.67, and 2.97 times, respectively, compared to the $Hexa^{-/-}$ mice. The comparison between the $Hexa^{-/-}G_{M2}AP^{-/-}Neu4^{-/-}$ and $Hexa^{-/-}G_{M2}AP^{-/-}$ mice; and the comparison between the $Hexa^{-/-}Neu4^{-/-}$ and $Hexa^{-/-}$ mice revealed that the reason of higher levels of activity was the deficiency of the sialidase *Neu4*. It was also stated that Saposin C enhanced the β -*Glucosidase* enzyme activity¹⁶ (Figure 1.2). It can be referred that the accumulated molecules trigger Saposin C in the $Hexa^{-/-}G_{M2}AP^{-/-}Neu4^{-/-}$, $Hexa^{-/-}G_{M2}AP^{-/-}$ and $Hexa^{-/-}Neu4^{-/-}$ mice without $G_{M2}AP$ and sialidase *Neu4*, since it is available and active in the medium, activating also β -*Glucosidase* in order to clean the accumulated molecules.

Gangliosides are the major glycosphingolipids, highly enriched in neurons and mostly carrying neuron-specific physiological functions. Their distributions differ not only during the developmental stages⁵, but also in adult brains⁶⁷. The levels of G_{M2} ganglioside in the deficient mice were compared by the thin layer chromatography after the isolation of acidic gangliosides (Figure 3.7). This method provides information only regarding the concentration of ganglioside. In order to discover the region where the detected G_{M2} ganglioside accumulates, the immunohistochemical analysis was performed taking advantage of the immunofluorescent antibodies Lamp1 (red) and G_{M2} (green). Lamp1 highlighted in merged images the lysosomes and G_{M2} ganglioside detected in the mentioned regions, demonstrating that the accumulation was in lysosomes, as expected. Accumulation of the G_{M2} ganglioside in the 3- and 6-month-old $Hexa^{-/-}$, $G_{M2}AP^{-/-}$, $Hexa^{-/-}Neu4^{-/-}$, $Hexa^{-/-}G_{M2}AP^{-/-}$, $G_{M2}AP^{-/-}Neu4^{-/-}$ and $Hexa^{-/-}G_{M2}AP^{-/-}Neu4^{-/-}$ mice were detected to be at different levels at different regions. The 3-month-old $G_{M2}AP^{-/-}$ mice had a slightly higher degree of the G_{M2} ganglioside compared to the $Hexa^{-/-}$ mice in cortex (Figure 3.18), however, a similar degree in the hippocampus (Figure 3.19) and thalamus (Figure 3.20). In the 6-month-old $G_{M2}AP^{-/-}$ and $Hexa^{-/-}$ mice, an increased accumulation of G_{M2} for the both genotypes at the cortex (Figure 3.22), hippocampus (Figure 3.23) and thalamus (Figure 3.24) were consistent with the chromatography results (Figure 3.7). The 3-month-old $Hexa^{-/-}Neu4^{-/-}$ mice exhibited an accumulation level similar to that of the $G_{M2}AP^{-/-}$ mice, however, higher than the $Hexa^{-/-}$ mice in the cortex (Figure 3.18), hippocampus (Figure 3.19) and in thalamus (Figure 3.20). Although the exact situation was conserved at 6-month-old mice with a higher

accumulation, the specific subregions that had a G_{M2} accumulation in the thalamus were completely different in the $Hexa^{-/-}Neu4^{-/-}$ mice from the $G_{M2}AP^{-/-}$ mice (Figure 3.24). The 6-month-old $Hexa^{-/-}G_{M2}AP^{-/-}$, $G_{M2}AP^{-/-}Neu4^{-/-}$ and $Hexa^{-/-}G_{M2}AP^{-/-}Neu4^{-/-}$ mice had a higher amount of G_{M2} ganglioside than the single deficient and $Hexa^{-/-}Neu4^{-/-}$ mice for the cortex (Figure 3.22), hippocampus (Figure 3.23) and thalamus regions (Figure 3.24). There traced an obviously high accumulation in the thalamus of the 6-month-old $Hexa^{-/-}G_{M2}AP^{-/-}Neu4^{-/-}$ mice compared not only to the same genotyped 3-month-old mice, but also to their age counterparts (Figure 3.24). Level of Lamp1 changed between different deficient mice just like G_{M2} ganglioside, meaning that there was an increase in the number of lysosomes depending on the accumulation. More accumulation resulted in increased level of lysosomes as expected¹³.

Intensity analysis for immunohistochemical staining revealed that although 3-month-old group had similar G_{M2} ganglioside level, it was differently increased by age in all brains in the cortex (Figure 3.25), hippocampus (Figure 3.26) and thalamus (Figure 3.27). In the cortex region (Figure 3.25), $G_{M2}AP^{-/-}Neu4^{-/-}$ mice had a 1.3 times increase compared to $G_{M2}AP^{-/-}$ and $Hexa^{-/-}G_{M2}AP^{-/-}Neu4^{-/-}$ mice 1.2 times increase compared to $Hexa^{-/-}G_{M2}AP^{-/-}$ at the age of 6 months. In the hippocampus region (Figure 3.26), $G_{M2}AP^{-/-}Neu4^{-/-}$ mice had a 1.5 times increase compared to $G_{M2}AP^{-/-}$ and $Hexa^{-/-}G_{M2}AP^{-/-}Neu4^{-/-}$ mice 1.2 times increase compared to $Hexa^{-/-}G_{M2}AP^{-/-}$ at the age of 6 months. And in the thalamus region (Figure 3.27), $G_{M2}AP^{-/-}Neu4^{-/-}$ mice had a 2.6 times increase compared to $G_{M2}AP^{-/-}$ and $Hexa^{-/-}G_{M2}AP^{-/-}Neu4^{-/-}$ mice 8 times increase compared to $Hexa^{-/-}G_{M2}AP^{-/-}$ at the age of 6 months. All these comparisons showed that accumulation was increased in the additional deficiency of sialidase *Neu4* which means that sialidase *Neu4* and *G_{M2}AP* may work together and their coordination is more obvious when time passes.

In addition to the immunohistochemical analysis, the brains were analyzed with the imaging mass spectrometry method in the other perspective of sagittal sections. 36- and 38- carbon G_{M2} , G_{M1} and G_{D1a} gangliosides were detected in the 3-month-old $Hexa^{-/-}$, $Neu4^{-/-}$, $G_{M2}AP^{-/-}$, $Hexa^{-/-}Neu4^{-/-}$, $Hexa^{-/-}G_{M2}AP^{-/-}$, $G_{M2}AP^{-/-}Neu4^{-/-}$ and $Hexa^{-/-}G_{M2}AP^{-/-}Neu4^{-/-}$ mice. The MALDI-IMS analysis for these mice was performed for the first time in this study. The distributions of gangliosides were demonstrated throughout the brains and cerebellums. Although the accumulation of the G_{M2} ganglioside in hippocampus in sagittal sections was not obvious as how it was detected in coronal sections, an accumulation in the cortex and thalamus was observable (Figure 3.28). Likewise, the

cerebellum and hypothalamus were analyzed as well. The behavioral tests results could be explained in detail when observed the ganglioside distribution in these regions, since behavioral tests measure the motor coordination and pain sensitivity that are directly related to these brain regions. The $G_{M2}(d36:1)$ ganglioside accumulation in the cerebellum increased gradually among the $G_{M2}AP^{-/-}$, $Hexa^{-/-}G_{M2}AP^{-/-}$, and $Hexa^{-/-}G_{M2}AP^{-/-}Neu4^{-/-}$ mice with the addition of *Hexa* deficiency and *Hexa*, *Neu4* deficiency (Figure 3.28). Due to the accumulation in cerebellum, the $G_{M2}AP^{-/-}$ mice had a worse impaired motor coordination and balance compared to the *WT* and $Hexa^{-/-}$ mice as observed in rotarod (Figure 3.31), and as previously stated⁴⁵. In compatible with the accumulated G_{M2} ganglioside level in cerebellum (Figure 3.28), the $Hexa^{-/-}G_{M2}AP^{-/-}$ and $Hexa^{-/-}G_{M2}AP^{-/-}Neu4^{-/-}$ mice exhibited a worse motor coordination, while the $Hexa^{-/-}Neu4^{-/-}$ and $G_{M2}AP^{-/-}Neu4^{-/-}$ mice had a similar coordination with the $Hexa^{-/-}$ mice (Figure 3.31). It was revealed in the rotarod test that the $Hexa^{-/-}G_{M2}AP^{-/-}Neu4^{-/-}$ mice had a reduced balance and motor coordination capacity. One out of the four 3-month-old mice, and two out of the four 6-month-old mice could not stay still on the rotating rod in the test experiment. Although the triple deficient mice did not have an increased G_{M2} ganglioside level in the chromatographic analysis (Figure 3.7), the immunohistochemical and MALDI-IMS analyses inferred that the additional deficiency of *Neu4* in these mice might have caused a higher level of G_{M2} throughout the brain and cerebellum. Differently from the G_{M1} and G_{D1a} gangliosides, the G_{M2} ganglioside is not found in cells in high concentrations, constituting only 0.5% of total gangliosides or 0.08% of total brain lipids⁵². In this respect, the increase in the level of G_{M2} ganglioside in the brain and cerebellum might deleteriously affect different biological occurrences, more importantly than other gangliosides.

Thalamus is the formation responsible for the sensory information transmission such as pain signals⁶⁰, whereas hypothalamus is the region where the body temperature and hormonal releases are maintained⁶⁸. Since the gangliosides are known to function on temperature adaption²⁸, the hot plate test was applied in order to reveal the possible changes of the accumulation in the sensory neurons activities in the deficient mice. Higher ganglioside levels detected by the immunohistochemical and imaging mass spectrometric analysis in the $G_{M2}AP^{-/-}$, $Hexa^{-/-}Neu4^{-/-}$, $Hexa^{-/-}G_{M2}AP^{-/-}$, $G_{M2}AP^{-/-}Neu4^{-/-}$ and $Hexa^{-/-}G_{M2}AP^{-/-}Neu4^{-/-}$ mice compared to the *WT*, $Hexa^{-/-}$ and $Neu4^{-/-}$ mice led to a reduced sense capacity. Excluding the *WT*, $Hexa^{-/-}$ and $Neu4^{-/-}$ mice, the other deficient mice did not jump in the hot plate test (Figure 3.32), and could resist the 55°C

plate for 300 seconds. A similar behavior observed in the mentioned mice cannot be directly related to the G_{M2} ganglioside level (Figure 3.7). However, the total ganglioside alteration in each sample might be the reason for their low nociceptive sensitivity (Figure 3.32).

CHAPTER 5

CONCLUSION

In this study comparison between newly generated *Hexa*^{-/-}*G_{M2}AP*^{-/-}*Neu4*^{-/-}, *Hexa*^{-/-}*G_{M2}AP*^{-/-} and *G_{M2}AP*^{-/-}*Neu4*^{-/-} mice and the available *Neu4*^{-/-}, *Hexa*^{-/-}, *G_{M2}AP*^{-/-} and *Hexa*^{-/-}*Neu4*^{-/-} mice models was realized in a biochemical, molecular biological, immunohistochemical and imaging mass spectrometric manners, gaining the major part of the information regarding a quantitative level of gangliosides.

Comparative analyses of seven different deficient mice with the wild type and among each other provided an important contribution concerning the possible involvement of the G_{M2} activator protein as a cofactor of sialidase *Neu4* in the bypass mechanism in the Tay-Sachs mice, *in vivo*. Based on the increased G_{M2} ganglioside level in brain and cerebellum detected by the immunohistochemical and imaging mass spectrometric analysis, we speculate that the sialidase *Neu4* functions on the degradation of G_{M2} ganglioside with G_{M2} activator protein, *in vivo*.

This study showed an additional *in vivo* function of the sialidase *Neu4* in the degradation pathway of gangliosides and the metabolic bypass observed in Tay-Sachs mice. Understanding the biological role of the sialidase *Neu4* in ganglioside metabolism is of importance for the G_{M2} gangliosidosis, since it is regarded as a G_{M2} ganglioside degrading sialidase.

5.1. Future Studies

A detailed investigation about the brain tissues gangliosides and lipids is recommended to be performed by the mass spectrometry in order to reveal the entire primary and secondary alterations in the levels of every simple and complex ganglioside and lipid, if there might be any. The same procedure may be utilized for the analysis of urine samples in order to identify the oligosaccharides accumulated depending on the deficiency. Moreover, other tissues of double and triple deficient mice might be analyzed since the sialidase *Neu4* is also identified in kidney, spleen and liver in addition to brain¹⁴.

Gangliosides exhibit some functions on different metabolic pathways. G_{M1} ganglioside mediates several physiological and pathological processes in cell⁶³. It is an active molecule for the regulation of the signals in the plasma membrane^{63,69}, as well as that of the nuclear calcium metabolism in the nuclear membrane⁷⁰. On the one hand, the accumulated G_{M1} ganglioside cause a neurodegeneration resulted by the neuronal death upon the unfolded protein response in the *β-Galactosidase* deficient mice⁷¹. The G_{M1} ganglioside had a symptomatic and potentially disease-modifying effects when applied on the patients suffering from the Parkinson disease⁷².

G_{M2} ganglioside normally constitutes only 1–2% of the total gangliosides in adult brains⁷³. It was noted that the G_{M2} ganglioside holds some inhibitory roles over the insulin receptor in the plasma membrane⁷⁴, regulates the tumor cell migration by an interaction with the integrin⁷⁵, functions over the infection or inflammation signals, and involves in some other neurological diseases like those of Alzheimer, Parkinson and Huntington⁶⁵.

G_{D1} is the major component of the myelin formation⁴ and known to improve the synaptic plasticity in the hippocampus region of brain⁶⁵. Since there were alterations in the level of these gangliosides, all these metabolic pathways might be further investigated in these double and triple deficient mice models' brains to reveal how these pathways are affected and what functions the sialidase *Neu4* specifically holds.

Although the generated double and triple deficient mice are not a direct imitation for the human lysosomal storage disease, they still can be benefitted for the developments of drugs in order to diminish the G_{M2} accumulation. They can also be evaluated as models for the G_{M2} gangliosidosis. Therapeutical treatments might be applied on these mice in order to enhance the G_{M2} degradation which then might be utilized for human patients, as well.

REFERENCES

- (1) Carter, H. E.; Haines, W. J. *J. Biol. Chem.* 1947, 169 (1), 77–82.
- (2) Kolter, T.; Doering, T.; Wilkening, G.; Werth, N.; Sandhoff, K. *Biochem Soc Trans* 1999, 27 (4), 409–415.
- (3) Coet, T.; Suzuki, K.; Popko, B. *Trends Neurosci.* 1998, 21 (97), 126–130.
- (4) Olsen, A. S. B.; Færgeman, N. J. *Open Biol.* 2017, 7 (5), 170069.
- (5) Schengrund, C.-L. *Trends Biochem. Sci.* 2015, 40 (7), 397–406.
- (6) Xu, Y.-H.; Barnes, S.; Sun, Y.; Grabowski, G. A. *J. Lipid Res.* 2010, 51 (7), 1643–1675.
- (7) Sandhoff, K.; Harzer, K. *J. Neurosci.* 2013, 33 (25), 10195–10208.
- (8) Yu, R. K.; Tsai, Y.-T.; Ariga, T.; Yanagisawa, M. *J. Oleo Sci.* 2011, 60 (10), 537–544.
- (9) Julien, S.; Bobowski, M.; Steenackers, A.; Le Bourhis, X.; Delannoy, P. *Cells* 2013, 2 (4), 751–767.
- (10) Seyrantepe, V.; Canuel, M.; Carpentier, S.; Landry, K.; Durand, S.; Liang, F.; Zeng, J.; Caqueret, A.; Gravel, R. a.; Marchesini, S.; Zwingmann, C.; Michaud, J.; Morales, C. R.; Levade, T.; Pshezhetsky, A. V. *Hum. Mol. Genet.* 2008, 17 (11), 1556–1568.
- (11) Seyrantepe, V.; Lema, P.; Caqueret, A.; Dridi, L.; Bel Hadj, S.; Carpentier, S.; Boucher, F.; Levade, T.; Carmant, L.; Gravel, R. A.; Hamel, E.; Vachon, P.; Di Cristo, G.; Michaud, J. L.; Morales, C. R.; Pshezhetsky, A. V. *PLoS Genet.* 2010, 6 (9).
- (12) Timur, Z. K.; Akyildiz Demir, S.; Marsching, C.; Sandhoff, R.; Seyrantepe, V. *Mol. Genet. Metab. Reports* 2015, 4, 72–82.
- (13) Seyrantepe, V.; Akyildiz, S.; Timur, Z. K.; Gerichten, J. Von; Marsching, C.; Erdemli, E.; Oztas, E.; Takahashi, K.; Yamaguchi, K.; Ates, N.; Dönmez, B.; Dalkara, T.; Erich, K.; Hopf, C. *Exp. Neurol.* 2017, 299 (July 2017), 26–41.

- (14) Miyagi, T.; Yamaguchi, K. *Glycobiology* 2012, 22 (7), 880–896.
- (15) Fürst, W.; Sandhoff, K. *Biochim. Biophys. Acta - Lipids Lipid Metab.* 1992, 1126 (1), 1–16.
- (16) Kolter, T.; Sandhoff, K. *FEBS Lett.* 2010, 584 (9), 1700–1712.
- (17) Shimada, Y.; Li, Y.-T.; Li, S.-C. *J. Lipid Res.* 2003, 44, 342–348.
- (18) Wu, Y. Y.; Lockyer, J. M.; Sugiyama, E.; Pavlova, N. V.; Li, Y. T.; Li, S. C. *J. Biol. Chem.* 1994, 269 (23), 16276–16283.
- (19) Li, S.-C. C.; Li, Y.-T. T.; Moriya, S.; Miyagi, T. *Biochem. J.* 2001, 360, 233–237.
- (20) Wilkening, G.; Linke, T.; Uhlhorn-Dierks, G.; Sandhoff, K. *J. Biol. Chem.* 2000, 275 (46), 35814–35819.
- (21) Werth, N.; Schuette, C. G.; Wilkening, G.; Lemm, T.; Sandhoff, K. *J. Biol. Chem.* 2001, 276 (16), 12685–12690.
- (22) Mundel, T. M.; Heid, H. W.; Mahuran, D. J.; Kriz, W.; Mundel, P. *J. Am. Soc. Nephrol.* 1999, 10, 435–443.
- (23) Saito, M.; Fronda, C. L.; Yu, R. K. *J. Neurochem.* 2002, 66 (5), 2205–2208.
- (24) Miyagi, T.; Tsuiki, S. *J. Biol. Chem.* 1985, 260, 6710–6716.
- (25) Seyrantepe, V.; Landry, K.; Trudel, S.; Hassan, J. A.; Morales, C. R.; Pshezhetsky, A. V. *J. Biol. Chem.* 2004, 279 (35), 37021–37029.
- (26) Miyagi, T. *Seikagaku.* 1990, 62 (12), 1506–1512.
- (27) Yamaguchi, K.; Hata, K.; Koseki, K.; Shiozaki, K.; Akita, H.; Wada, T.; Moriya, S.; Miyagi, T. *Biochem. J.* 2005, 390 (Pt 1), 85–93.
- (28) Plomp, J. J.; Willison, H. J. *J. Physiol.* 2009, 587, 3979–3999.
- (29) Neufeld, E. F. *Annu. Rev. Biochem.* 1991, 60, 257–280.

- (30) Winchester, B. *Biochem. Soc.* 2000, 28, 50–54.
- (31) Wraith, J. E. *Paediatr. Child Health (Oxford)*. 2002, 21, 76–79.
- (32) Conzelmann, E.; Sandhoff, K. *Dev. Neurosci.* 1983, 6 (1), 58–71.
- (33) Terry, R. D.; Weiss, M. J. *Neuropathol. Exp. Neurol.* 1963, 22, 18–55.
- (34) Xia, B.; Asif, G.; Arthur, L.; Pervaiz, M. A.; Li, X.; Liu, R.; Cummings, R. D.; He, M. *Clin. Chem.* 2013, 59 (9), 1357–1368.
- (35) Bonesso, L.; Piraud, M.; Caruba, C.; Van Obberghen, E.; Mengual, R.; Hinault, C. *Orphanet J. Rare Dis.* 2014, 9 (1).
- (36) de Geest, N.; Bonten, E.; Mann, L.; de Sousa-Hitzler, J.; Hahn, C.; d’Azzo, A. *Hum. Mol. Genet.* 2002, 11 (12), 1455–1464.
- (37) Schröder M, Schnabel D, Suzuki K, S. K. *FEBS Lett.* 1991, 290 (1), 1–3.
- (38) van Echten, G.; Sandhoff, K. *J. Neurochem.* 1989, 52 (1), 207–214.
- (39) Triggs-Raine, B.; Mahuran, D. J.; Gravel, R. A. *Adv. Genet.* 2001, 44, 199–224.
- (40) Phaneuf, D.; Wakamatsu, N.; Huang, J. Q.; Borowski, A.; Peterson, A. C.; Fortunato, S. R.; Ritter, G.; Igdoura, S. a.; Morales, C. R.; Benoit, G.; Akerman, B. R.; Leclerc, D.; Hanai, N.; Marth, J. D.; Trasler, J. M.; Gravel, R. a. *Hum. Mol. Genet.* 1996, 5 (1), 1–14.
- (41) Mahuran, D. J. *Biochim. Biophys. Acta - Lipids Lipid Metab.* 1998, 1393, 1–18.
- (42) Conzelmann, E.; Sandhoff, K. *Proc. Natl. Acad. Sci. U. S. A.* 1978, 75 (8), 3979–3983.
- (43) Yamanaka, S.; Johnson, M. D.; Grinberg, A.; Westphal, H.; Crawley, J. N.; Taniike, M.; Suzuki, K.; Proia, R. L. *Proc. Natl. Acad. Sci. U. S. A.* 1994, 91 (October), 9975–9979.

- (44) Cohen-Tannoudji, M.; Marchand, P.; Akli, S.; Sheardown, S. A.; Puech, J. P.; Kress, C.; Gressens, P.; Nassogne, M. C.; Beccari, T.; Muggleton-Harris, A. L. *Mamm. Genome* 1995, 6 (12), 844–849.
- (45) Liu, Y.; Hoffmann, A.; Grinberg, A.; Westphal, H.; McDonald, M. P.; Miller, K. M.; Crawley, J. N.; Sandhoff, K.; Suzuki, K.; Proia, R. L. *Proc. Natl. Acad. Sci. U. S. A.* 1997, 94 (15), 8138–8143.
- (46) Sango, K.; McDonald, M. P.; Crawley, J. N.; Mack, M. L.; Tifft, C. J.; Skop, E.; Starr, C. M.; Hoffmann, A.; Sandhoff, K.; Suzuki, K.; Proia, R. L. *Nat. Genet.* 1996, 14 (3), 348–352.
- (47) Sango, K.; Yamanaka, S.; Hoffmann, A.; Okuda, Y.; Grinberg, A.; Westphal, H.; McDonald, M. P.; Crawley, J. N.; Sandhoff, K.; Suzuki, K.; Proia, R. L. *Nat. Genet.* 1995, 11 (2), 170–176.
- (48) Pan, X.; De Aragão, C. D. B. P.; Velasco-Martin, J. P.; Priestman, D. A.; Wu, H. Y.; Takahashi, K.; Yamaguchi, K.; Sturiale, L.; Garozzo, D.; Platt, F. M.; Lamarche-Vane, N.; Morales, C. R.; Miyagi, T.; Pshezhetsky, A. V. *FASEB J.* 2017, 31 (8), 3467–3483.
- (49) Pekmezci, Z. K. Brain lipid profiling of triply mouse model with the deficiencies of sialidase Neu1, Neu4 and β -hexosaminidase a enzymes, İzmir Institute of Technology, 2011.
- (50) Mann, B.; Loh, L. N.; Gao, G.; Tuomanen, E. *Bio-protocol* 2016, 6 (23).
- (51) Sidman, R. L.; Kosaras, B.; Misra, B.; Senft, S. High Resolution Mouse Brain Atlas <http://www.hms.harvard.edu/research/brain/atlas.html> (accessed Oct 27, 2017).
- (52) Woods, A. S.; Colsch, B.; Jackson, S. N.; Post, J.; Baldwin, K.; Roux, A.; Hoffer, B.; Cox, B. M.; Hoffer, M.; Rubovitch, V.; Pick, C. G.; Schultz, J. A.; Balaban, C. *ACS Chem. Neurosci.* 2013, 4 (4), 594–600.
- (53) Yu, R. K.; Ledeen, R. W. *Biochim. Biophys. Acta (BBA)/Lipids Lipid Metab.* 1972, 280, 356–364.
- (54) Shiozaki, K.; Koseki, K.; Yamaguchi, K.; Shiozaki, M.; Narimatsu, H.; Miyagi, T. *J. Biol. Chem.* 2009, 284 (32), 21157–21164.
- (55) Kreutz, F.; Petry, F. dos S.; Camassola, M.; Schein, V.; Guma, F. C. R.; Nardi, N. B.; Trindade, V. M. T. *Gene* 2013, 527 (1), 109–114.

- (56) Nakamura, K.; Koike, M.; Kuwana, Y.; Kjuragi, K.; Igarashi, S.; Hasegawa, M.; Hanai, N. 1994, 3–6.
- (57) Chen, Y.; Allegood, J.; Liu, Y.; Wang, E.; Cachón-González, B.; Cox, T. M.; Merrill, A. H.; Sullards, M. C. *Anal. Chem.* 2008, 80 (8), 2780–2788.
- (58) Ribeiro-Resende, V. T.; Gomes, T. A.; De Lima, S.; Nascimento-Lima, M.; Bargas-Rega, M.; Santiago, M. F.; De Melo Reis, R. A.; De Mello, F. G. *PLoS One* 2014, 9 (10), 1–12.
- (59) Schestatsky, P.; Nascimento, O. J. M. *Arq. Neuropsiquiatr.* 2009, 67 (June), 741–749.
- (60) Huh, Y.; Cho, J. *PLoS One* 2015, 10 (6).
- (61) Scandroglio, F.; Loberto, N.; Valsecchi, M.; Chigorno, V.; Prinetti, A.; Sonnino, S. *Glycoconj. J.* 2009, 26 (8), 961–973.
- (62) Fujita, N.; Suzuki, K.; Vanier, M. T.; Popko, B.; Maeda, N.; Klein, A.; Henseler, M.; Sandhoff, K.; Nakayasu, H.; Suzuki, K. *Hum. Mol. Genet.* 1996, 5 (6), 711–725.
- (63) Ohmi, Y.; Tajima, O.; Ohkawa, Y.; Mori, A.; Sugiura, Y.; Furukawa, K.; Furukawa, K. *Proc. Natl. Acad. Sci.* 2009, 106 (52), 22405–22410.
- (64) Yamanaka, S.; Johnson, M. D.; Grinberg, A.; Westphal, H.; Crawley, J. N.; Taniike, M.; Suzuki, K.; Proia, R. L. *Proc. Natl. Acad. Sci.* 1994, 91 (21), 9975–9979.
- (65) Palmano, K.; Rowan, A.; Guillermo, R.; Guan, J.; McJarrow, P. *Nutrients.* May 22, 2015, pp 3891–3913.
- (66) Potratz, A.; Hüttler, S.; Bierfreund, U.; Proia, R. L.; Suzuki, K.; Sandhoff, K. *Biochim. Biophys. Acta - Mol. Basis Dis.* 2000, 1502, 391–397.
- (67) Vajn, K.; Viljetić, B.; Degmečić, I. V.; Schnaar, R. L.; Heffer, M. *PLoS One* 2013, 8 (9).
- (68) Piomboni, P.; Governini, L.; Gori, M.; Puggioni, E.; Costantino-Ceccarini, E.; Luddi, A. *Front. Endocrinol. (Lausanne).* 2014, 5 (JAN).
- (69) Ohmi, Y.; Tajima, O.; Ohkawa, Y.; Yamauchi, Y.; Sugiura, Y.; Furukawa, K.; Furukawa, K. *J. Neurochem.* 2011, 116 (5), 926–935.

- (70) Ledeen, R.; Wu, G. *Journal of neurochemistry*. Blackwell Publishing Ltd November 1, 2007, pp 126–134.
- (71) Tessitore, A.; Martin, M. D. P.; Sano, R.; Ma, Y.; Mann, L.; Ingrassia, A.; Laywell, E. D.; Steindler, D. a.; Hendershot, L. M.; D’Azzo, A. *Mol. Cell* 2004, 15, 753–766.
- (72) Schneider, J. S.; Gollomp, S. M.; Sendek, S.; Colcher, A.; Cambi, F.; Du, W. J. *Neurol. Sci.* 2013, 324, 140–148.
- (73) Walkley, S. U.; Siegel, D. A.; Dobrenis, K. *Neurochem. Res.* 1995, 20 (11), 1287–1299.
- (74) Vainio, S.; Heino, S.; Månsson, J.-E.; Fredman, P.; Kuismanen, E.; Vaarala, O.; Ikonen, E. *EMBO Rep.* 2002, 3 (1), 95–100.
- (75) Kundu, M.; Mahata, B.; Banerjee, A.; Chakraborty, S.; Debnath, S.; Sinha Ray, S.; Ghosh, Z.; Biswas, K. *BBA - Mol. Cell Res.* 2016, 1863, 1472–1489.

VITA

Zehra Kevser Timur

Date and Place of Birth: 1987 Bursa

E-mail: zehrapekmezci@gmail.com

Education

Ph.D. Molecular Biology and Genetics

2012-2017 Izmir Institute of Technology,
Molecular Biology and Genetics Department, Izmir, Turkey

MSc. Molecular Biology and Genetics

2009-2011 Izmir Institute of Technology,
Molecular Biology and Genetics Department, Izmir, Turkey

BSc. Molecular Biology and Genetics

2005 – 2009 Halic University,
Molecular Biology and Genetics Department, Istanbul, Turkey

Teaching and Professional Experience

Research assistant

2010 – 2017 Izmir Institute of Technology,
Molecular Biology and Genetics Department, Izmir, Turkey

Publications

Seyrantepe V, Demir SA, Timur ZK, Von Gerichten J, Marsching C, Erdemli E, Oztas E, Takahashi K, Yamaguchi K, Ates N, Demir BD, Dalkara T, Erich K, Hopf C, Sandhoff R, Miyagi T. “Sialidase Neu3 facilitates GM2 degradation and bypass in mouse model of Tay-Sachs disease.” *Exp Neurol*. 2017 Sep. doi: 10.1016/j.expneurol.2017.09.012.

Timur ZK, Demir SA, Seyrantepe V. “Lysosomal Cathepsin A Plays a Significant Role in the Processing of Endogenous Bioactive Peptides.” *Front Mol Biosci*. 2016 Oct. 3:68. doi:10.3389/fmolb.2016.00068

Z.K. Timur, S. Akyildiz Demir, C. Marsching, R. Sandhoff, V. Seyrantepe. “Neuraminidase-1 contributes significantly to the degradation of neuronal B-series gangliosides but not to the bypass of the catabolic block in Tay–Sachs mouse models.” *Mol Genet Metab Rep*. 2015 Aug 72–82. doi: 10.1016/j.ymgmr.2015.07.004.